CSIRO ENERGY
www.csiro.au

CSF Roadmap: Appendix

Review of the Current Status of Solar Thermochemical Fuels Production Technologies

ARENA Project Solar Hybrid Fuels (3-A018)

Jim Edwards, Jim Hinkley, Robbie McNaughton

9 March 2016

CSIRO Energy

Citation

Edwards J, Hinkley J and McNaughton R (2016) Review of the current status of solar thermochemical fuels production technologies. CSIRO, Australia.

Copyright

Important disclaimer

Preface

This technical appendix is a companion document to the final report of the CSF Roadmap Study.

Contents

Figures

Acknowledgments

This project is supported by the Australian Government through the Australian Renewable Energy Agency.

The project team was able to draw on the expertise of many of the leading researchers in the field, including the following international experts:

- Dr Christian Sattler, German Aerospace Research Centre (DLR)
- Professor Aldo Steinfeld, ETH Zurich, Switzerland
- Dr Anton Meier, Paul Scherrer Institut (PSI), Switzerland
- Professor Ellen Stechel, Arizona State University, USA
- Professor Tatsuya Kodama, Niigata University, Japan
- Dr Stephanie Trottier, Alberta Innovates Technology Futures, Canada
- Dr Michael Epstein, (formerly) Weizmann Institute of Science, Israel

1 Introduction

In the context of this report, the primary solar fuels are hydrogen (H_2) and synthesis gas, or syngas. Syngas is a mixture of H_2 and carbon monoxide (CO) that can be further processed into a wide range of liquid fuels and chemicals.

The technologies for the production of these solar fuels can be categorised as follows:

- **Hybrid solar–fossil fuel technologies**
  - reforming of methane-containing gases with steam and/or CO_2
  - thermal cracking of methane to produce H_2 and carbon
  - gasification of coal and heavy petroleum residues (e.g. petroleum coke)
- **Purely renewable energy-based solar fuels technologies**
  - gasification of sustainable biomass with steam or supercritical water
  - two-step metal oxide/redox cycles for H_2O and/or CO_2 splitting
  - sulfur-based thermochemical cycles for H_2O splitting
  - high-temperature steam and CO_2 electrolysis.

In all three hybrid routes, as well as in biomass gasification, the primary reactions are highly endothermic (heat consuming). The necessary reaction heat is supplied by concentrated solar thermal energy.

Concentrated solar thermal energy also supplies the reaction heat for the high-temperature endothermic steps of the metal oxide/redox and sulfur-based cycles: metal oxide reduction in the former, and sulfuric acid decomposition in the latter.

Solar energy can supply both the electricity and heat requirements for the high-temperature electrolysis of both steam and CO_2, making this a truly renewable energy route to hydrogen and/or syngas.

This report briefly reviews the current state-of-the-art of these technologies for solar fuel production. It also describes the key technical issues and challenges that must be addressed as part of future research, development and demonstration to make each option potentially commercially viable.

2 Solar thermal reforming of methane with steam and/or CO_2

2.1 Thermochemistry and equilibrium

Steam reforming of methane, as shown in Reaction 1, is widely used to produce hydrogen for industrial uses (primarily in hydrocracking and hydrotreatment of hydrocarbons in oil refining) and ammonia. It is also used to produce syngas for the production of methanol and liquid fuels and waxes by Fischer–Tropsch synthesis:

$$CH_4 + H_2O \leftrightarrow CO + 3H_2 \; \Delta H^0_{298K} = +206 \; kJ/mol \quad (1)$$

Methane can also be reformed using CO_2 in place of steam, by Reaction 2, often referred to as dry reforming:

$$CH_4 + CO_2 \leftrightarrow 2CO + 2H_2 \; \Delta H^0_{298K} = +246 \; kJ/mol \quad (2)$$

Depending on the reformer operating conditions, the mildly exothermic (heat-producing) water gas shift (WGS) Reaction 3 will also occur to some extent. This reaction is also employed in a separate step, together with CO_2 removal, when hydrogen rather than syngas is the required product:

$$CO + H_2O \leftrightarrow CO_2 + H_2 \; \Delta H^0_{298K} = -41 \; kJ/mol \quad (3)$$

The undesired formation of carbon during methane reforming can occur via the following reactions:

$$CH_4 \leftrightarrow C_{(s)} + 2H_2 \; \Delta H^0_{298K} = +75 \; kJ/mol \quad (4)$$

$$2CO \leftrightarrow C_{(s)} + CO_2 \; \Delta H^0_{298K} = -173 \; kJ/mol \quad (5)$$

$$CO + H_2 \leftrightarrow C_{(s)} + H_2O_{(g)} \; \Delta H^0_{298K} = -131 \; kJ/mol \quad (6)$$

Both reforming reactions 1 and 2 are strongly endothermic (heat consuming), and require the presence of a catalyst to proceed to any significant extent. Both reforming reactions are equilibrium-limited, with methane conversion increasing with temperature (Figure 1) and decreasing with pressure (Figure 2). In conventional reforming reactors, the reaction temperature likely needs to be above about 800 °C.

If solar energy is used to provide this heat, the maximum degrees of enhancement of the input methane energy by embodied solar energy in the syngas (ignoring the effect of the WGS Reaction 3) are 27.9% (Reaction 1) and 27.5 % (Reaction 2) on a higher heating value (HHV) basis. The corresponding maximum values on a lower heating value (LHV) basis are 25.4% (Reaction 1) and 30.6% (Reaction 2).

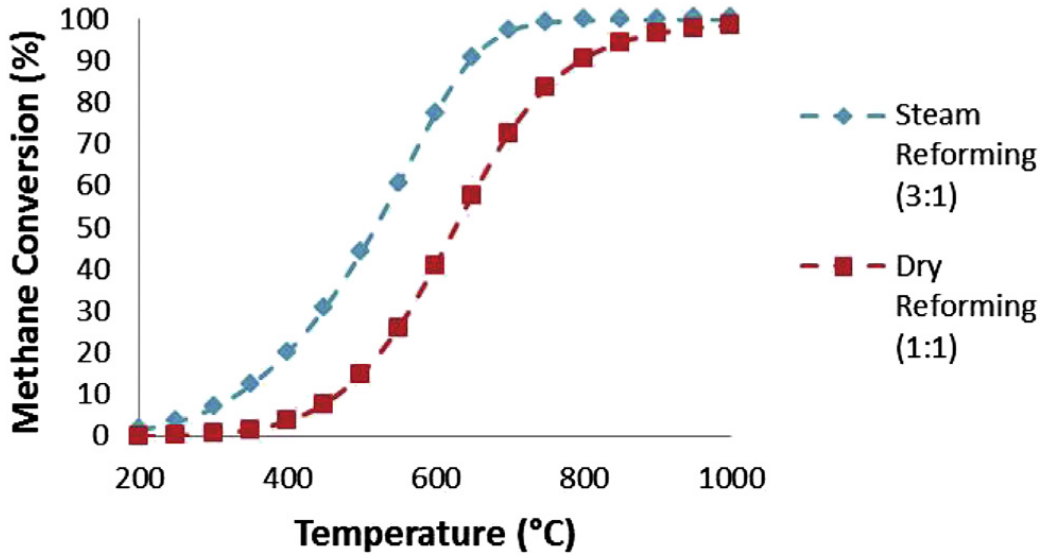

Figure 1: Effect of temperature on the equilibrium methane conversion for steam reforming (H_2O/CH_4 molar ratio 3/1) and dry reforming (CO_2/CH_4 molar ratio 1/1)

Source: (Sheu, Mokheimer et al. 2015)

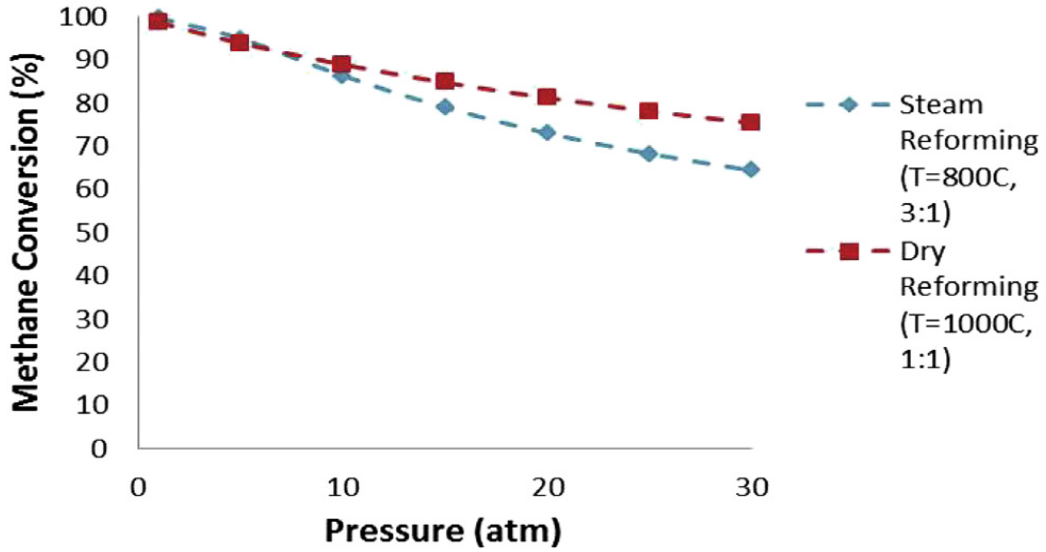

Figure 2: Effect of pressure on the equilibrium methane conversion for steam reforming at 800 °C (H_2O/CH_4 molar ratio 3/1) and dry reforming at 1000 °C (CO_2/CH_4 molar ratio 1/1)

Source: (Sheu, Mokheimer et al. 2015)

The past 25 years or so have seen extensive research and development efforts from more than 20 organisations and research groups worldwide on the solar reforming of methane in all three modes: steam, mixed (H_2O/CO_2) and dry (CO_2). This work has been comprehensively reviewed in three recent publications (Sheu, Mokheimer et al. 2015; Agrafiotis, von Storch et al. 2014; Simakov, Wright et al. 2015). Readers are referred to these publications for information on work overseas, while Australian research in this area by CSIRO is summarised below.

2.2 CSIRO research

Key workers: R. Benito, R. McNaughton, J. Hinkley, M. Dolan, Y. Sun, J. Edwards, G. Hart W. Stein et al.

Period of publications: 1998–2015

Main areas of activity:

- CSIRO has been studying this process since the 1990s: initially on a parabolic dish, while subsequently using a heliostat field and tower. Inside a cavity-based tubular reactor, steam and methane are contacted with a conventional reforming catalyst inside a tubular coil that is externally irradiated. The reactor has an inner and outer tube, with the incoming water passing through the inner tube to preheat and vapourise it before it is mixed with methane or natural gas and passed through the catalyst bed (Figure 3, left). Figure 3 (right) shows the 200-kW_{th} reactor prior to its installation in the receiver. Figure 4 (left) shows the reformer suspended from the receiver frame and Figure 4 (right) shows the reactor operating on-sun at the CSIRO Energy Centre in Newcastle, Australia.
- CSIRO has recently completed a project involving the design, construction and operation of a low-temperature membrane reforming reactor. Via the continuous removal of hydrogen from the product gas, the reactor can operate at temperatures as low as 550–600 ^{o}C, enabling it to be linked with conventional thermal storage (e.g. molten nitrate salt). The hydrogen-permeable membranes were developed and supplied by the Colorado School of Mines. They are based on metal alloys with palladium as a reference, and are supported on sintered metal tubes with a ceramic coating to provide a smooth surface. A test rig was developed to provide proof of concept and allow integration with the CSIRO solar thermal energy storage facility at Newcastle.
- Laboratory-scale supporting research has focused on developing new catalyst formulations capable of conducting mixed (H_2O/CO_2) and dry (CO_2) reforming under carbon-free conditions, in recognition of Australia's high demand for liquid transport fuels and large reserves of natural and coal seam gases containing variable levels of CO_2.

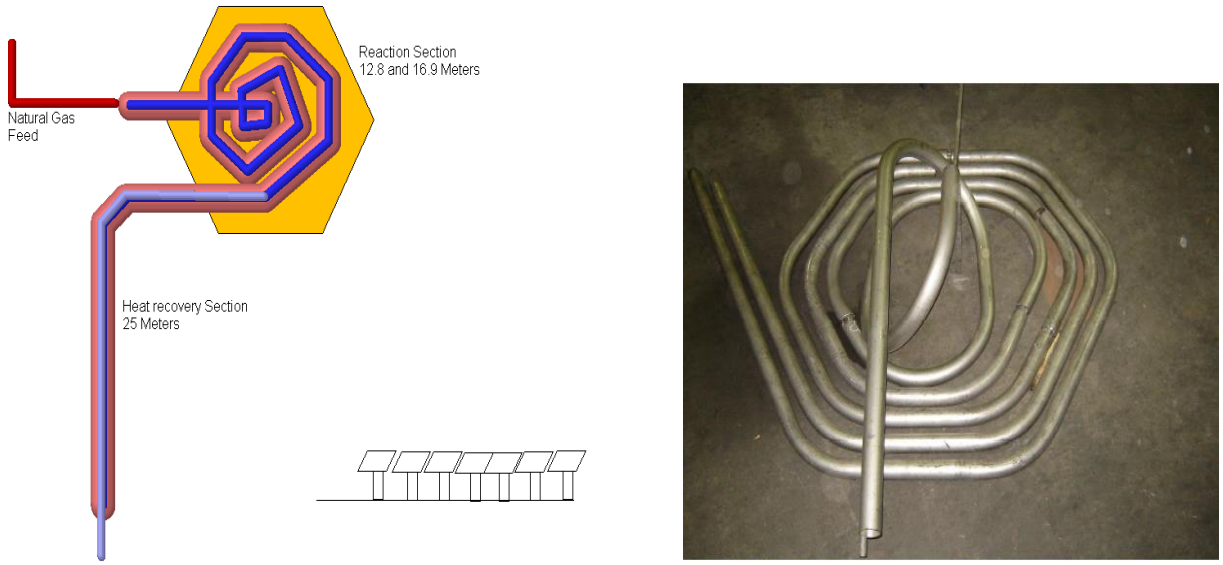

Figure 3: Schematic of the CSIRO 200-kWth reformer (left) and the reactor prior to its installation inside the receiver (right)

Figure 4: The 200-kWth steam reformer with the fabricated coils suspended from the receiver frame (left) and the reformer on-sun at the CSIRO Energy Centre, Newcastle, Australia (right)

Key results:

- CSIRO has successfully demonstrated the technology on a dish at 25-kW_{th} scale and using a heliostat field and tower at both 25-kW_{th} and 200-kW_{th} scales.
- The 200-kW_{th} reactor was operated using natural gas in a stable manner (Figure 5) (CSIRO in-house data) for long periods under variable insolation, over a wide range of operating conditions (steam/carbon molar ratio 3.2–5.7, reactor outlet temperature 920–1100 K, pressure 6.3–10.2 bar (abs) and natural gas feed rate 1.9–11.6 kg/h). It gave carbon-free carbon conversion, approaching equilibrium levels under all conditions (Figure 6) (CSIRO in-house data), and the degree of LHV solar enhancement was up to 23% (Figure 7) (CSIRO in-house data). In some cases, the product gas remained exposed to the catalyst in the outlet section of the reactor at lower temperatures. This was due to lower solar flux at this point and resulted in an increased contribution from the WGS reaction (Reaction 3). While this reaction assists in the production of hydrogen, it is mildly exothermic and therefore reduces the LHV energy content of the syngas. If the intent is to store solar energy for combustion processes, this loss of embedded solar energy is undesirable. It also increases the H_2/CO ratio, making it less suitable for liquid fuel synthesis.
- The indirect reformer was operated using pressurised air as the heat-transfer fluid, with a thermal input of 600 kW at 850 °C. Dry reforming was used rather than steam reforming, because of concerns that the system might not be able to generate sufficient steam to prevent carbon formation.
- A range of catalyst formulations of the generic composition $NiMg_3AlM_{0.2}O_x$ (M=Ce, Y, Gd) were prepared, characterised and tested in a fixed-bed micro-reactor. They were shown to have high activity and stability under carbon-free conditions, making them a viable option for mixed or dry reforming reactors driven by solar energy (Sun, Collins et al. 2013).
- For the low-temperature membrane reformer, several bifunctional catalysts formulated from Ni and Cu active components and a La_2O_3-Cr_2O_3 inert support were prepared, and their activity for steam reforming (Reaction 1) and WGS (Reaction 3) was evaluated at 550 °C. The test catalysts exhibited higher activity for both reactions than the corresponding commercial catalysts.
- The low-temperature membrane reformer prototype operated well in the laboratory with a commercial catalyst, giving good methane conversion (70%) and high hydrogen yield (95%) at 540 °C and demonstrating proof of concept. However, when integrated with CSIRO's Newcastle

energy storage system using CO_2 as the heat-transfer fluid, the reformer experienced membrane fractures and catalyst deactivation.

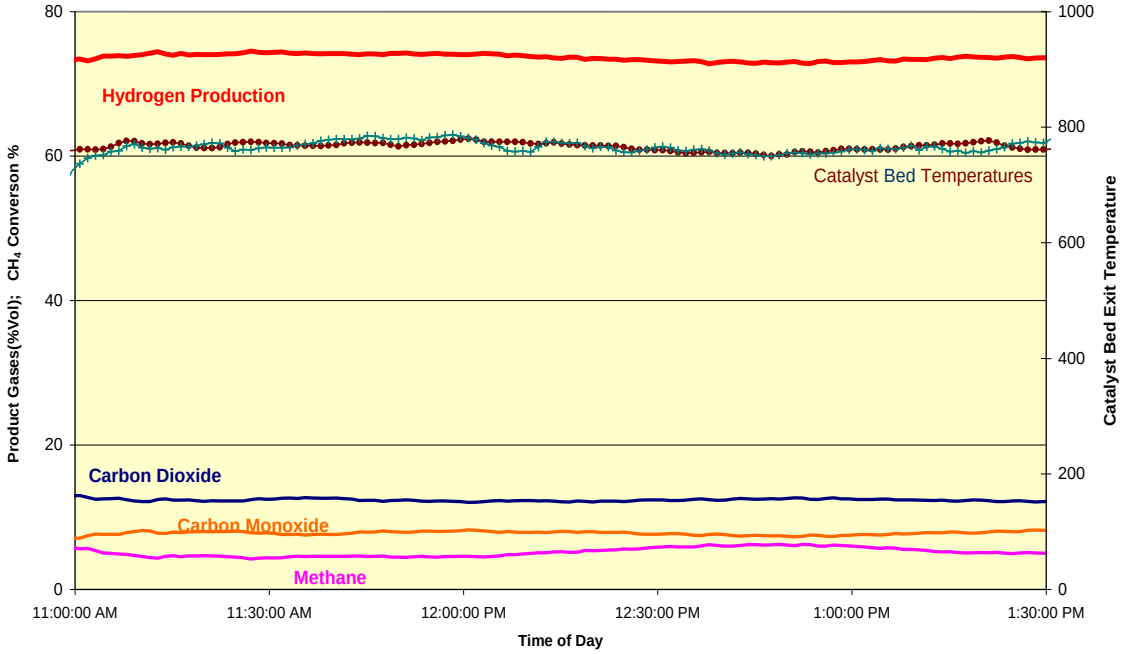

Figure 5: Illustrative stable operation of the CSIRO 200-kW_{th} solar reformer

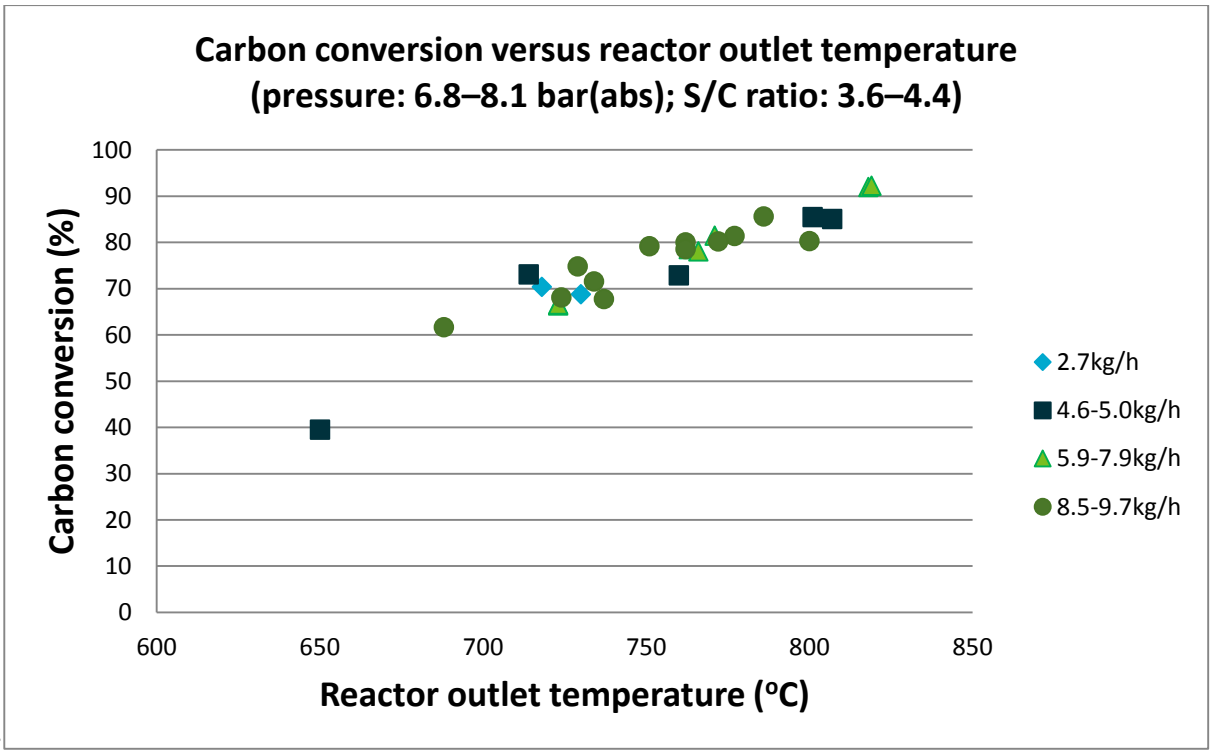

Figure 6: Carbon conversion versus reactor outlet temperature for the CSIRO 200-kW_{th} reformer at various natural gas feed rates

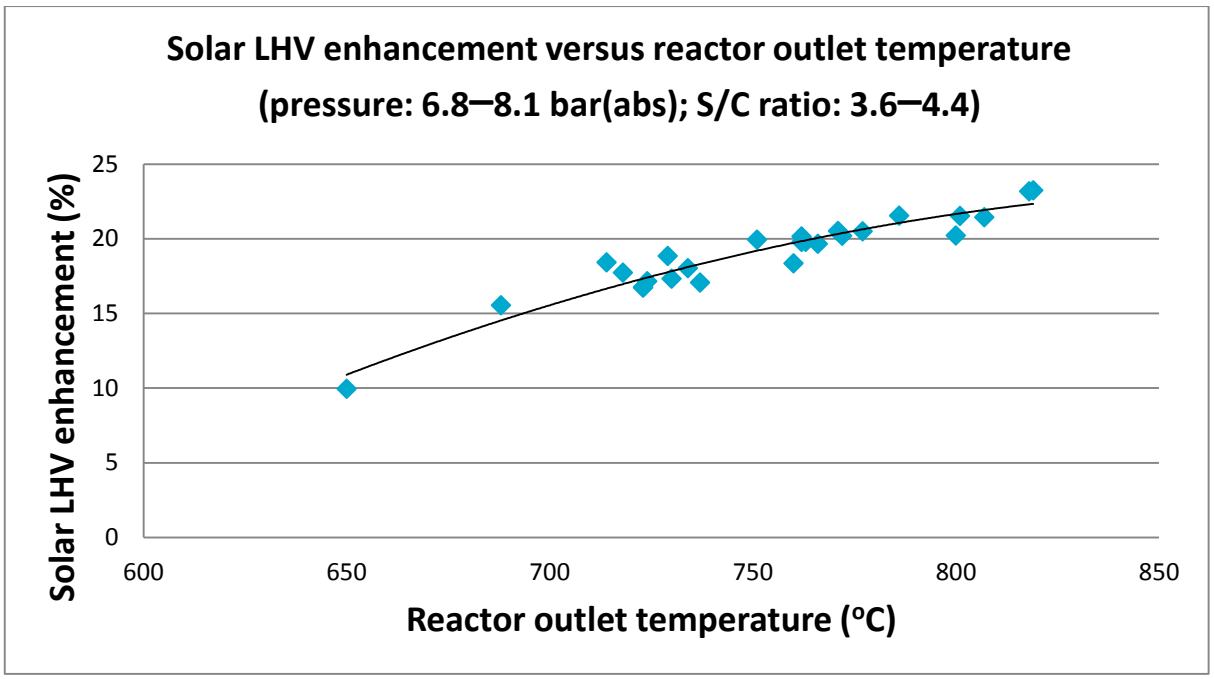

Figure 7: Solar lower heating value (LHV) enhancement versus reactor outlet temperature for the CSIRO 200-kW_{th} reformer

2.3 Issues and challenges for solar reforming of methane

- Industrial reforming of methane is used to produce more than 95% of the world's hydrogen, and is therefore an extremely mature technology. Large commercial reformers produce more than 200,000 Nm^3/h of hydrogen in a single train. Solar methane reforming is perhaps the most widely studied solar thermochemical option, with extensive on-sun experience in Australia and overseas using a variety of reactors with solar inputs from 25–600 kW_{th}. Steam reforming has been more widely investigated than either mixed or CO_2 reforming. Steam reforming can also use commercially available catalysts, whereas mixed and CO_2 reforming require some measure of catalyst development, which has only been done at the laboratory and small pilot-plant scales. Solar-driven steam reforming is therefore considered to be closer to commercialisation than the other two modes.
- Carbon deposition on the reactor's internal surfaces and catalyst is a potential issue with all three modes of reforming. This is particularly the case for dry reforming and mixed steam/CO_2 reforming, which will be required to produce a syngas with the necessary H_2/CO molar ratio for production of liquid fuels (~2/1). In the case of steam reforming, carbon deposition is avoided by operating with higher than stoichiometric steam/carbon molar ratios: around 2.5:1 or 3.5:1. This results in a significant amount of unreacted steam, which has considerable enthalpy through phase change from water to steam and sensible heating to the reaction temperature. While heat recovery is crucial for efficient capture of solar energy in chemical form, rather than as sensible heat, it is generally not possible to usefully recover all of the latent heat released by the condensation of the surplus steam. This imposes a significant energy penalty on the process. Therefore, new active catalysts capable of operating at lower steam/carbon ratios are required to improve commercial viability. In the case of dry reforming, which has an even greater carbon-formation potential than steam reforming, CSIRO and other groups are developing new catalysts to enable the reaction to be conducted under carbon-free conditions.

- Thermodynamic analysis of steam, mixed and dry reforming has established operating conditions (temperature, pressure and ($H_2O + CO_2$)/CH_4 ratio) under which carbon formation is not possible (Sun, Ritchie et al. 2011; Sun and Edwards 2015). The challenge is to develop reactor and control systems that enable operation under these conditions, given the daily start-up and shutdown of solar-driven applications. The durability of both reactor construction materials and catalysts under thermal cycling conditions needs to be confirmed through longer-term testing under real solar conditions.
- The reaction temperature is close to the limit for alloy steels, which are the only suitable materials for pressurised tubular receivers. The temperature is also too high for integration with current generation thermal storage technology (molten nitrate salts).
- Membrane reactors are being developed to shift the equilibrium and enable the reaction to be conducted at lower temperatures that are more compatible with thermal storage options. The membranes remove hydrogen, forcing the reforming reaction to the right. This also requires the development of new catalysts with good activity at lower temperatures and without carbon deposition. Reducing the receiver temperature will improve the efficiency of energy collection, while integration with thermal storage will enable continuous operation. Note that membrane reformers are only suitable for hydrogen production, rather than syngas production, because hydrogen production relies on the in-situ conversion of CO to hydrogen.
- Volumetric reactors require a window that can withstand the 10–15 bar pressure within the reactor. The window must be made of high-transmissivity materials to avoid being heated up. The German Aerospace Research Centre (DLR) has developed a domed window from silica glass, but the design is limited to an aperture of approximately 600 mm. Scale-up to larger reactor sizes is problematic, although it may be possible to have multiple reactors on a single tower.
- Thermal cycling between reaction and ambient temperatures is an issue specific to all solar thermochemical applications. This affects the operation and control of the process, as well as the selection of construction materials to avoid corrosion and thermal stress problems arising from thermal cycling. In the longer term, many of these problems could be overcome by high-temperature thermal storage systems that enable around-the-clock operation under controlled conditions using solar energy. The development of such systems is being addressed by CSIRO and others.

3 Solar thermal cracking of methane

3.1 Thermochemistry and equilibrium

The basic reaction is:

$$CH_4 \rightarrow C + 2H_2 \; \Delta H^0_{298K} = +75.6 \; kJ/mol \tag{7}$$

Methane conversion is favoured by high temperature and low pressure, the effects of which on the equilibrium methane conversion are shown in Figure 8.

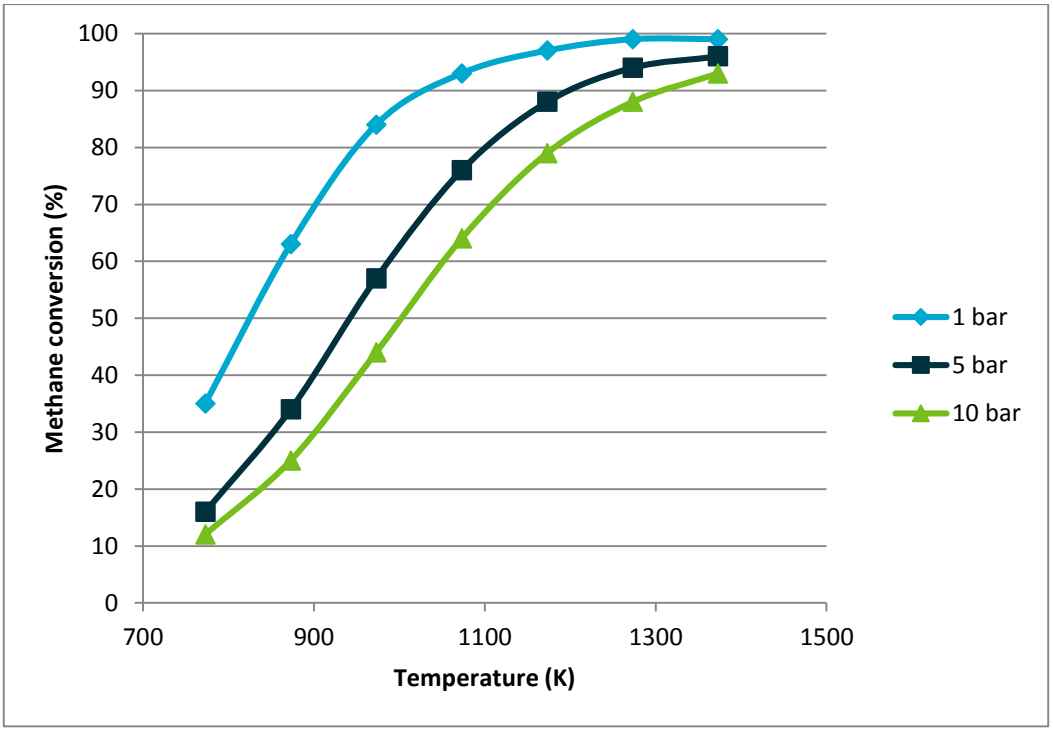

Figure 8: Equilibrium methane conversion as a function of temperature and pressure

Since the chemistry is based on the formation of intermediate radicals, other by-products can be formed depending on the reaction conditions. These include acetylene (C_2H_2) and undesirable poly-aromatic hydrocarbons (PAHs).

3.2 Major research and development activities

3.2.1 Weizmann Institute of Science (WIS), Israel

Key workers: A. Kogan, M. Kogan et al.

Period of publications: 2002–2007

Main area(s) of activity:

- The use of a tornado flow reactor to prevent hot co-product carbon from coming into contact with the quartz window, while minimising the auxiliary gas 'curtain' required to achieve this and thereby reducing energy losses.

Key results:

- Cold model testing of various tornado flow configurations demonstrated the technical feasibility of the concept, as well as determining the optimum design for the hot flow reactor (Kogan and Kogan 2002). A laboratory-scale hot flow reactor was subsequently operated in an unseeded mode under real solar conditions, but carbon deposits on reactor wall and exit pipe were major problems. The maximum methane conversion reported was 28% at 1320 K (Kogan and Kogan 2003).
- After room-temperature simulation tests of a seeded solar reactor (Kogan, Kogan et al. 2004), the reactor was operated under real solar conditions with carbon black seeding. A seeding mass loading of 0.1 g/m^3 of irradiated gas successfully improved heat transfer (and hence methane conversion) and eliminated carbon deposition on the reactor walls (Kogan, Kogan et al. 2005).
- A computational fluid dynamics model of the confined tornado flow configuration was developed and applied to verify the experimental data during the above investigations (Kogan, Israeli et al. 2007).

3.2.2 University of Colorado/National Renewable Energy Laboratory (NREL), United States

Key workers: J. Dahl, A. Lewandowski, A. Weimer et al., University of Colorado; P. Spath and W. Amos, NREL

Period of publications: 2002–2004

Main areas of activity:

- Using a fluid wall graphite aerosol flow reactor (10-kW solar input using NREL solar furnace) to study the effect of reactor wall temperature and residence time on methane conversion.
- Developing a kinetic model for methane cracking in this type of reactor to study the sensitivity of the methane decomposition process to three parameters: flow rate of carbon particles in the feed, carbon particle radius and reactor wall temperature.
- Supporting techno-economic studies by NREL, using data from the aerosol reactor to investigate the effect on the hydrogen cost of key process operating and economic parameters and co-product carbon black price.

Key results:

- Methane conversion of ~90% was obtained at a reactor wall temperature of 2133 K (9 kW solar power level) and residence time of 0.01 s. At 1923 K (6-kW power level), methane conversion decreased to 35%. As expected, the highest methane conversions were obtained with carbon black particles in the feed gas (Dahl, Buechler et al. 2004).
- The kinetic model study showed that high reactor wall temperatures must be maintained to achieve essentially complete methane conversion. In addition, micron-sized carbon black particles (the actual flow rate is not critical) must be fed to the reactor to increase the heat transfer to the gas phase (Dahl, Weimer et al. 2004).
- The NREL techno-economic evaluation (Spath and Amos 2003) showed that a per-pass methane conversion of 70% is preferred to 90%, because the methane feed rate can be increased significantly to achieve 70% conversion versus 90% at a specific reaction temperature. This increased the hydrogen production rate, and since the unconverted methane was ultimately recycled, it was not lost to the process. The evaluation also highlighted the effect of the carbon black price on that of hydrogen.

3.2.3 PROMES (Processes, Materials and Solar Energy Laboratory) – CNRS (National Centre for Scientific Research), France

Key workers: S. Abanades, G. Flamant et al.

Period of publications: 2005–2014

Main areas of activity:

- Development of a reactor in which concentrated radiation from a solar furnace is absorbed by a graphite nozzle and transferred to methane inside the nozzle. The reactor was operated to determine the influence on methane conversion of solar power input, graphite nozzle geometries, temperature, gas flow rate and composition (CH_4/argon). Argon was added to prevent deposition of carbon particles on the windows, and to provide an inert atmosphere to prevent oxidation of the graphite tube.
- Studies of methane cracking in a 1-kW, indirectly heated tubular reactor.
- Development of a kinetic model for a tubular solar methane cracking reactor in which the reaction zone is modelled by three plug-flow reactors in series, representing the preheating, isothermal and cooling zones of the reactor.

Key results:

- A range of nozzle geometries were investigated with a view of maximising the rate of wall-to-gas heat transfer. With the optimum nozzle geometry, the maximum methane conversion was around 95% at 1700 K (Abanades and Flamant 2005). Substantial quantities of acetylene were formed under certain operating conditions, but this was minimised by increasing the residence time (Abanades and Flamant 2008).
- The maximum methane conversion in the 1-kW tubular reactor was 75%, and appeared to be limited by the small size of the tube (10 mm diameter) and its ability to absorb the concentrated radiation (Abanades and Flamant 2008).

- The kinetic model predicted the rate of evolution of gas species as a function of residence time. It was claimed to give good agreement with experimental results obtained from a 10-kW solar multi-tubular reactor, and showed the importance of both residence time and temperature in achieving high methane conversion (Rodat, Abanades et al. 2009).

3.2.4 ETH (Swiss Federal Institute of Technology)/Paul Scherrer Institute, Switzerland

Key workers: A. Steinfeld, A.Meier, D. Hirsch et al.

Period of publications: 1999–2010

Main areas of activity:

- Initial work involved investigating catalytic methane cracking for the production of filamentous carbon (Steinfeld, Kirillov et al. 1997; Meier, Kirillov et al. 1999), but was then redirected to non-catalytic methane cracking for hydrogen and nanocarbon production.
- Operation of a 5-kW solar chemical reactor that featured a vortex flow of methane within a cavity receiver. The reactor was laden with carbon particles that served simultaneously as radiant absorbers and nucleation sites for the heterogeneous decomposition reaction. The reactor was operated in a solar furnace with flux intensities exceeding 3500 kW/m^2. This type of reactor was selected because vortex-flow and cyclone reactors maximise the transfer of heat to gas flows laden with particles. In solar applications, the quartz window is actively cooled and kept clean of carbon particles by an auxiliary gas flow injected at the window and aperture planes.

Key results:

- Although kinetic modelling of the vortex-flow reactor indicated that a residence time of only 0.3 s was required for 90% conversion at 1500 K (Trommer, Hirsch et al. 2004), a maximum methane conversion of only 67% was obtained experimentally at 1600 K, 1 bar and a residence time of 10 s. This was probably as a result of severe heat-transfer limitations within the solar reactor compared with those assumed in the modelling studies (Hirsch and Steinfeld 2004).
- A reactor model was developed and validated using a 10-kW solar prototype and applied to optimise the design and estimate the performance of a 10-MW tubular reactor/solar tower system. Complete methane conversion was predicted for a flow of 0.7 kg/s and outlet temperature of 1870 K (Maag, Rodat et al. 2010).

3.2.5 Alberta Innovates – Technology Futures, Canada

Key workers: D. Paxman, S. Trottier et al.

Period of publications: 2014

Key activities:

- Investigation of methane cracking in a molten medium (see

- Figure 9) in an effort to improve the efficiency of the process and facilitate collection of the carbon. The molten medium would improve heat transfer to the reaction gas, potentially catalyse the reaction, serve to trap the product carbon and limit the transient effects of solar energy.

Key results:

- The concept has been investigated at the laboratory scale under non-solar conditions. A 50-kW_{th} scale solar receiver reactor was proposed to be designed and built for solar testing. Tin (Sn) was chosen as the molten medium because it has a low melting point, is less toxic than possible alternatives such as lead, and has a low vapour pressure (Paxman, Trottier et al. 2014).

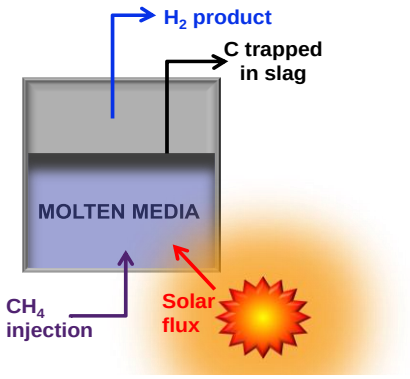

Figure 9: Schematic of solar molten media methane cracking reactor concept of Alberta Innovates Technology Futures

3.2.6 Pilot-scale methane cracking project (SOLHYCARB), European Union

Project partners: CNRS/ETH/ Paul Scherrer Institut (PSI)/WIS/DLR/Aerosol and Particle Technology Laboratory (APTL, Greece)

Period of publications: 2006–2010

Key activities:

- Design, construction and testing of a 10-kW, directly heated tornado solar reactor and two indirectly heated tubular reactors of 10 and 50-kW_{th} scales.
- Development of a heat-transfer model to simulate a multi-tubular methane cracking reactor located in a cavity receiver.
- Characterisation of the properties of the co-product carbon black produced in the 50-kW_{th} pilot-scale reactor.
- Flow sheet development and design of the complete 10-MW_{th} solar methane cracking process.

Key results (Flamant 2010)**:**

- All three solar reactors were operated successfully, with the 50-kW_{th} reactor having methane conversions of 72–100% at temperatures between 1600 and 1930 K.
- The performance of the carbon black approached that of commercial carbons in a range of applications.
- A residence time of around 100 ms was required to avoid PAH formation.

- Economics were strongly dependent on the value of the carbon black.

3.3 Issues and challenges for solar methane cracking

- High process temperatures and residence times are required for the high conversion of methane to hydrogen, to avoid unwanted by-products (e.g. PAHs) and to generate high-quality, marketable carbon. For indirectly heated reactors, the reactor walls must be heated to very high temperature (>2000 K) to ensure the gas is at the required temperature. This results in significant stresses on the construction materials used, especially due to thermal cycling.
- Efficient heating of the gas is challenging in both direct and indirect 'traditional' reactor designs, because they either rely on injected solid carbon or reactor walls to absorb radiation and heat the gas. Molten bath methane cracking should improve this via bubbling the reactant gas through heated liquid media.
- The formation of a solid carbon co-product poses serious challenges in removing/recovering the carbon from the reactor, and preventing it from coming into contact with the quartz window when using windowed cavity reactors.
- The process is significantly less attractive without the co-production of high-value, marketable carbon (hydrogen cost is dependent on the price obtained for the carbon). As such, the process must reliably produce a uniform carbon product with significant market demand. A method to efficiently collect carbon from the process must also be developed. Further optimisation of this process is required to make it commercially viable.
- However, if the carbon is to be sequestered, in-house work by CSIRO has shown that the use of a cheap, disposable catalyst can dramatically reduce the decomposition temperature to around 1100 K and still obtain high per-pass (essentially equilibrium) methane conversion in a fluidised-bed reactor, with a large amount of carbon produced before the catalyst is deactivated. This option requires further assessment in the Australian context, particularly for a possible future scenario in which carbon emissions carry a real cost penalty.

4 Solar thermal pyrolysis/gasification of biomass with steam or supercritical water

4.1 Background

If biomass is derived from a truly renewable, sustainable source, then gasifying it using solar thermal energy to provide the reaction enthalpy is a potentially attractive means of producing emission-free syngas. As with solarised coal gasification, using solar energy as the heat source increases both the yield and quality of the syngas, since no internal combustion processes are required.

The organic component of biomass contains carbon, hydrogen, oxygen, nitrogen and sulfur. Ignoring the relatively small amounts of nitrogen and sulfur, the general highly endothermic steam gasification reaction can be written thus:

$$C_xH_yO_z + (x-z)H_2O \rightarrow \left(\left(\frac{y}{2}\right) + x - z\right)H_2 + xCO \quad (8)$$

In addition to steam, supercritical water gasification can use solar energy at moderate temperatures (700–900 K) to produce syngas from wet organic matter, such as certain types of biomass and waste materials. Supercritical water gasification is claimed by some to offer other advantages over conventional gasification, such as high solubility of organic matter in supercritical water, high reaction efficiency with high H_2 selectivity, no formation of tar or coke, and no need to separate the water or dry the feed stock before gasification.

Compared with other solar fuels options, gasification of biomass materials has received only moderate attention, with some of this work briefly summarised below.

4.2 Major investigators and projects

4.2.1 The University of Minnesota, United States

Key workers: B. Hathaway, J. Davidson, D. Kittleson et al.

Period of publications: 2011–2014

Main areas of activity:

- Kinetics study of solar pyrolysis and gasification of biomass in molten salt.
- Development of a molten salt reactor for solar gasification of biomass.
- The roles of storage and hybridisation in solar gasification of biomass.

Key results:

- The study compared the reaction kinetics of pyrolysis and gasification of cellulose from 1124–1235 K in an electric furnace, in an inert environment as well as in a bath of a ternary eutectic

blend of lithium, potassium and sodium carbonates. Arrhenius rate expressions were derived from the experimental data supported by a simulation model of heat and mass transfer. The molten salt increased the rate of pyrolysis by 74% and the gasification rates by more than an order of magnitude, while giving product gas compositions nearer to the thermodynamic equilibrium values. The results were claimed as providing justification for the use of carbonate salts as both a catalyst and heat-transfer medium for solar gasification of biomass (Hathaway, Davidson et al. 2011).

- A prototype 3-kW_{th} concentric tube solar reactor was designed and constructed to gasify biomass. The molten salt is contained in the annulus to which the reactants are fed. It serves as a catalyst, ensures effective heat transfer for the reaction, and also provides short-term thermal storage for steady operation during solar transients (Hathaway, Kittelson et al. 2014). Performance data from this reactor do not yet appear to have been published.
- The impacts of thermal storage and degree of hybridisation on the efficiency, specific yield of syngas and variation in the output of a solarised biomass gasification facility were explored through parametric simulations of a generalised 100-MW_{th} solar receiver facility. The biomass properties are assumed to be an average of 32 common species of United States biomass. Nominal syngas yield rates from 1.5–50 tonnes/h are considered, along with molten carbonate storage volumes from 200–6500 m^3. A high annual solar fraction (95%), defined as the percentage of the total gasification heat requirement met by solar, results in a maximum thermal efficiency of 79% and a specific syngas yield of 139 GJ/hectare of biomass crop. Low solar fractions (10%) for highly hybridised facilities reduce the thermal efficiency to 72% and specific syngas yield to 88 GJ/hectare (Hathaway, Kittelson et al. 2014).

4.2.2 ETH/PSI (Switzerland)

Key workers: M. Kruesi, T. Melchior, A. Steinfeld et al.

Period of publications: 2014–2015

Main areas of activity:

- Steam gasification of bagasse in a laboratory-scale combined drop-tube and fixed-bed reactor.
- Solar-driven gasification of beechwood charcoal in a 3-kW solar tubular absorber/reactor, and development of a process simulation model to evaluate the thermal performance for scaled-up reactors to gasify the same material.
- Kinetic investigation of steam gasification of charcoal under direct, high-flux irradiation.

Key results:

- A two-zone solar reactor concept was developed for the steam gasification of biomass. The concept was designed to provide pyrolysis and gasification systems for high carbon conversion to syngas, while suppressing the formation of tar and gaseous hydrocarbons. It achieves this by having a down-flow reactor with an upper drop-tube zone, in which a high radiative heat flux to the dispersed particles results in rapid pyrolysis. In the lower trickle-bed zone, a structured packing provides the residence time and temperature required for char gasification and decomposition of the pyrolysis products.

- Laboratory-scale experiments of the two-zone reactor concept for the steam gasification of bagasse, which used an electric furnace at reactor temperatures of 1073–1573 K and feed rate of 0.48 g/min, yielded a high-quality syngas (H_2/CO = 1.6 and CO_2/CO = 0.31 molar ratios) with an energy upgrade factor (ratio of LHV of syngas over that of the feed) of 1.12. Theoretical energetic upgrade factors of up to 1.26, along with the treatment of wet feed stock and the elimination of the air separation unit, were claimed to support the potential benefits of solar-driven over autothermal gasification of biomass (Kruesi, Jovanovic et al. 2013).
- Experiments were subsequently conducted in a high-flux solar simulator to demonstrate the technical feasibility of using solar energy to provide the heat for the two-zone reactor concept (Kruesi, Jovanovic et al. 2014).
- The reaction kinetics of steam gasification of activated charcoal pellets were investigated in a quartz tubular reactor, which contained a fluidised bed of material directly exposed to an external source of concentrated radiation. Rate laws were formulated based on elementary reaction mechanisms describing reversible adsorption/desorption processes and irreversible surface chemistry. Assuming plug-flow conditions, the rate constants were computed by matching theoretical and experimental results, and their temperature dependence as determined by imposing an Arrhenius-type rate law. High-quality syngas containing an equimolar mixture of H_2 and CO, and less than 5% CO_2, was produced at temperatures above 1400 K (Müller, Zedtwitz et al. 2003).
- A reactor model that coupled radiative, convective and conduction heat transfer to the chemical kinetics was prepared and validated by comparing its output with experimentally measured temperatures and carbon conversion for beechwood charcoal. The simulation model was further applied to evaluate the thermal performance of 100-kW and 1-MW scaled-up multi-tubular absorber/reactors, yielding a theoretical maximum solar-to-chemical energy conversion efficiency of 39% and 50%, respectively. Major sources of irreversibility were associated with re-radiation losses through the cavity's aperture (Melchior, Perkins et al. 2009).

4.2.3 NREL/University of Colorado, United States

Key workers: P. Lichty, C. Bingham, A. Weimer et al.

Period of publications: 2010–2011

Key activity:

Biomass gasification in a multi-tubular solar reactor.

Key results:

- Flash pyrolysis of biomass was studied in a cavity multi-tube reactor using NREL's high-flux solar furnace. Biomass conversions as high as 58% were achieved in initial tests at temperatures of around 1273 K. Gaseous product yields were maximised, while that of condensable tars was minimised (Lichty, Perkins et al. 2010).
- Sundrop Fuels (United States) have reportedly collaborated with the University of Colorado to construct a 1-MW solar tower pilot plant with a solar biomass gasifier based on the indirectly irradiated, entrained-flow reactor concept (Piatkowski, Wieckert et al. 2011).

4.2.4 WIS, Israel

Key workers: M. Epstein, R. Adinberg, D. Zveglisky, J. Karni

Period of publications: 2004–2013

Main areas of activity:

- Pyrolysis and gasification of rice husks.
- Solar gasification of biomass in molten salt.

Key results:

- Direct combustion of rice husks is problematic, because of their chemical composition. The experimental results of two alternative conversion methods were compared: fast pyrolysis of rice husks dispersed in a medium of molten salts, and gasification under supercritical water conditions.
- The results of chemical analysis of the products obtained with the above methods were compared with the results of pyrolysis of rice husks under direct heating conditions. A substantial increase in carbon conversion was observed when using the alternative methods, along with a simultaneous decrease in the amount of silica in the fixed solid residue. As the silica skeleton of the rice husk collapses, the 'blocking' effect it has on the conversion of carbon-containing compounds is significantly reduced. In both methods, the conversion of organic matter was 80–86%. The only products were gases, comprising mainly H_2, CO and CO_2.
- Possible 'beam-down' molten salt reactors that can use concentrated solar energy for these two processes were presented and discussed (Zvegilsky, Adinberg et al. 2012).
- A concept was proposed for a molten carbonate salt reactor in which biomass could be converted to syngas using solar energy. Assessments of a commercial plant are claimed to show that a system could be developed in which the pyrolysis/gasification of biomass particles in a molten salt medium could be conducted around the clock, using the molten salt as both an in-situ heat storage medium and a catalyst (Adinberg, Epstein et al. 2004).

4.2.5 PROMES-CNRS, France

Key workers: K. Zeng, D. Gauthier, G. Flamant et al.

Period of publications: 2014–2015

Main area of activity:

- High-temperature flash pyrolysis of wood in a laboratory-scale solar reactor.

Key results:

- The pyrolysis of beechwood sawdust pellets in a crucible located at the vertical axis of a 1.5-kW solar furnace was investigated at 873–1473 K using heating rates of 5–100 K/sec. The product gas yield, which increased from 28 to 48% with increasing temperature and heating rate, largely came from tar decomposition. In the solar reactor, heating rate played a more important role

than temperature in determining product yield (Zeng, Gauthier et al. 2014). Gas yield decreased when the sweep gas (argon) over the crucible increased, due to a drop in the temperature of the hot zone in the solar reactor: a condition not favourable for gas formation from tar cracking (Zeng, Flamant et al. 2015).

4.2.6 Niigata University, Japan

Key workers: T. Kodama, N. Gokon et al.

Main activity:

- Simultaneous biomass gasification and tar reforming in a catalytic, fixed-bed reactor.

Key results:

- Steam gasification of cedar wood/bark and catalytic reforming of the tar component in the product gas were simultaneously performed in a laboratory-scale fixed-bed reactor at 873–1073 K. The reactor was operated under conditions claimed by the researchers to simulate the use of solar energy for this purpose. Light (fuel) gases, mostly H_2 and CO, were produced from the reforming of tar in biomass gasification by using limonite and dolomite as catalysts. Hydrogen yields increased with temperature in the range of 923–1073 K, because the WGS reaction was promoted by the catalyst. The yield of hydrogen gas increased by about 160% when using a mixed catalyst of limonite and dolomite compared with using limonite only.

4.2.7 University of Wyoming, United States

Key workers: S. Kenasari, Y. Zheng

Main activity:

- Development of a model to simulate the rapid pyrolysis of biomass pellets using solar energy.

Key results:

- A numerical simulation model developed for the rapid pyrolysis of cylindrical biomass pellets was used to predict product distribution and rate of mass loss of oak and pine pellets under various solar heat fluxes. The inclusion of secondary reactions (e.g. tar cracking) was important in determining the product distribution of gases, vapours and char, especially when the pyrolysis time was relatively long. The model was successfully validated by comparing simulations to various sets of experimental data from the literature (Kenarsari and Zheng 2014).

4.2.8 Norwegian University of Science and Technology, Norway

Main activity:

- Process evaluation for producing methanol through solar-driven biomass gasification.

Key results:

- Process simulation studies were conducted on a wood-to-methanol concept using concentrated solar energy to drive the process. High-temperature heat for gasification was obtained from a solar concentrating tower/molten salt system, while the H_2 required for the reverse WGS step (to convert CO_2 generated during fuel production back to CO) is produced by water electrolysis driven by concentrating solar power. The results were compared with those of a conventional biomass gasification process using biomass as the energy source and without the reverse WGS. For a given production of methanol, the new conversion concept required only 33% of the biomass input and 38% of the total land area required by the conventional process, while still exhibiting a CO_2-neutral fuel cycle (Hertwich and Zhang 2009).

  Note: A major limitation of this analysis is its assumption that a molten salt system (e.g. LiF-NaF-KF) could be developed to provide heat at the 970–1170 K temperature level required for the efficient gasification of wood.

4.2.9 The Australian National University, Australia

Key workers: L. Watson, J. Pye et al.

Main activity:

- Modelling studies of solar-powered supercritical water biomass gasifier.

Key results:

- A detailed simulation model was developed and used to design a tubular solar supercritical water gasification reactor. The model incorporates a directly irradiated solar receiver/reactor operating at conditions of 28 MPa and 873–973 K. An initial heat exchange unit preheats the biomass using the waste heat (steam) assumed to be available from a downstream Fischer–Tropsch process, which is not included in this analysis. An intermediate heat exchange unit recovers the waste heat prior to biomass gasification. Under the ideal assumptions applied, the predicted thermal efficiency of the reactor was 53%, excluding the thermal and optical losses associated with the solar receiver and heliostat field (Watson, Pye et al. 2012).

4.3 Challenged and opportunities for solarised pyrolysis/gasification of biomass

- Biomass is a low-grade material compared with coal, particularly the higher-rank bituminous and sub-bituminous coals. For example, biomass derived from wood has high oxygen levels (40–45 wt% dry ash-free) and a low energy content (17–18.5 MJ/kg dry basis). The ashes contain significant amounts of alkali and alkaline earth metals, making the use of quartz-windowed solar reactors problematic. The presence of chlorides is also a potential corrosion issue for metal surfaces.
- The particle shape factor (e.g. length/diameter ratio) and moisture content of some types of biomass, such as grasses and wood barks, can pose serious challenges in feeding them into the gasification reactor at a steady rate.
- The gasification of certain biomass and waste materials using supercritical water is potentially attractive for solar applications, since it enables a very significant reduction in temperature.

5 Solar gasification of coal and petroleum derivatives (petroleum coke and vacuum residue)

5.1 Basic chemistry and potential advantages of solar gasification

The solar steam gasification of coal and other carbonaceous materials to produce high-quality syngas is a potentially attractive industrial process. It is represented by the simplified net stoichiometric reaction (neglecting the relatively small amounts of sulfur and nitrogen in the coal):

$$C_xH_yO_z + (x-z)H_2O \rightarrow \left(\left(\frac{y}{2}\right) + x - z\right)H_2 + xCO \quad (9)$$

An important, highly endothermic reaction occurring during coal and other carbonaceous feed stocks gasification is the steam/carbon reaction:

$$C + H_2O \rightarrow H_2 + CO \; \Delta H^0_{298K} = +131 kJ/mol \quad (10)$$

Depending on the operating conditions, components such as tars and other volatile organics may also be formed, especially when using coal.

In conventional autothermal gasification, about 35% of the feed stock is combusted internally with pure O_2 to supply the high-temperature heat for this highly endothermic reaction. This inherently decreases the hydrogen and CO yield, and contaminates the gas with significant amounts of CO_2.

Using solar energy to provide the reaction heat offers the following benefits over conventional autothermal gasification:

- A higher yield of syngas (H_2 and CO) is produced, since no portion of the feed is combusted for process heat.
- Contamination of the syngas with combustion by-products (mainly CO_2) is avoided, consequently reducing costly downstream gas cleaning and separation requirements.
- The need for an air separation plant is eliminated, since steam is the gasifying agent.
- Intermittent solar energy can be stored in a transportable chemical form.
- No portion of the feed stock is combusted for process heat, and so the chemical energy content of the feed can be upgraded by up to 33%.

Several studies have simulated the solarised gasification of coal, including Second Law analyses and evaluation of energy conversion efficiency and CO_2 mitigation potential. Different reactor concepts have also been proposed for this application, including directly irradiated fluidised-bed, molten salt pool, vortex-flow, indirectly irradiated packed-bed, and particle flow reactors. Of these reactor types, several have been tested for the gasification of coal and other carbonaceous feed stocks at the laboratory and pilot-plant scale under real or simulated solar conditions.

5.2 Major investigators and projects

5.2.1 ETH/PSI, Switzerland

Key workers: A. Z'Graggen, P. Haueter, P. Von Zedtwitz, C. Wieckert, A. Steinfeld et al.

Period of publications: 2003–2013

Main areas of activity:

- Thermodynamic analysis to evaluate the energy conversion efficiency and CO_2 mitigation potential of solar steam gasification of coal and petroleum coke.
- Reactor design, testing and modelling of the solar steam gasification of petroleum coke.
- Numerical and experimental studies of gas–particle radiative heat transfer in a fluidised-bed reactor for the solar steam gasification of coal.
- Solar steam gasification of coal, petroleum coke and petroleum-derived vacuum residue in a 5-kW vortex-flow reactor.
- Reactor modelling, optimisation and scale-up for solar steam gasification of carbonaceous materials.
- Experimental investigation of a batch packed-bed solar reactor for steam gasification of coal and other carbonaceous materials.
- Heat and mass transfer analysis of a suspension of reacting particles undergoing steam gasification.

Key results:

- Thermodynamic analysis shows that solar steam gasification of coal or petroleum coke, followed by either a syngas-fuelled 55% efficient combined cycle or by a hydrogen-fuelled 65% efficient fuel cell, can halve the specific CO_2 emissions of a coal-fired 35% efficient Rankine cycle (von Zedtwitz and Steinfeld 2003). Subsequent laboratory-scale experiments with petroleum coke in a fluidised-bed reactor, directly exposed to concentrated thermal radiation at 1350–1550 K, showed that a syngas with approximately equal molar ratios of H_2 and CO and less than 5 mol% CO_2 could be produced (Trommer, Noembrini et al. 2005).
- Low-volatile, high fixed-carbon feedstocks are best suited for solar gasification, since they lead to the largest upgrade of their calorific value (Piatkowski, Wieckert et al. 2011).
- A vortex-flow reactor was operated for the steam gasification of petroleum coke with a solar furnace power input of 3.3–3.6 kW. It achieved 87% conversion of petroleum coke and 69% conversion of steam. The nominal residence time was ~1 s and the temperature range was 1300–1800 K. The solar energy conversion efficiency, defined as the portion of solar energy input absorbed as both chemical energy and sensible heat, was 17–20%, with the solar-to-chemical energy efficiency reported as 9% (Z'Graggen, Haueter et al. 2007).
- The same reactor was used to steam gasify a petroleum vacuum residue at around 1500 K, but conversion was only around 33–50% (Z'Graggen, Haueter et al. 2008).
- A heat and mass transfer model was applied to simulate the performance of the 5-kW vortex-flow reactor and its scaled-up version of 300 kW solar input. Complete reaction was predicted for initial particle sizes of 2–7 and 11–35 μm at residence times of 1.4 and 9.7 s and peak

temperatures of 2046 and 1818 K for the 5 and 300-kW reactors, respectively. For the 300-kW reactor, a solar-to-chemical energy conversion efficiency of 24% was predicted for a petroleum coke feed rate of 44 kg/h (Z'Graggen and Steinfeld 2008).

- The above model was able to predict the actual performance of the 5-kW vortex-flow reactor, in terms of average temperature, carbon and steam conversions, and gas composition at the reactor outlet (Z'Graggen and Steinfeld 2008).
- Coal and a range of other carbonaceous and waste materials were successfully steam gasified in both 5 and 150-kW batch packed-bed solar reactors, where the fuel value was upgraded by a factor of 1.26 (Piatkowski, Wieckert et al. 2009; Wieckert, Obrist et al. 2013).
- A heat-transfer model was developed and used to analyse the performance of a conceptual 10-MW gasification reactor mounted on a solar tower. For an optimised reactor geometry and a desired outlet temperature of 1500 K, a solar-to-chemical energy conversion of 37% was predicted for 1500-suns concentration (Maag and Steinfeld 2010).

5.2.2 Niigata University, Japan

Key workers: T. Kodama, N. Gokon et al.

Period of publications: 2002–2012

Main areas of activity:

- Evaluation of solar reactors using internally circulating fluidised beds of coal or coal coke particles for solar gasification of these materials (Figure 10). These types of reactor can be combined with beam-down optics.
- Side-irradiated CO_2 gasification of Australian black coal using an internally circulating fluidised-bed reactor located a 3-kW solar furnace simulator.
- CO_2 gasification of cokes in an upward-facing fluidised-bed reactor using a 3-kW solar furnace simulator.

Key results:

- For the CO_2 gasification of an Australian bituminous coal, the solar-to-chemical conversion increased with increasing energy-flux density of irradiation, to a maximum of 8% at an average flux density of 830 kW/m^2 and a fluidisation velocity of 37–49 times the minimum. (Kodama 2002).
- A laboratory-scale reactor was fabricated and evaluated using a 3-kW solar simulator. The feedstock was an Australian coal coke and the gasifying agent was CO_2. A 10–15% energy conversion from solar to chemical fuels (mainly CO) was obtained in the laboratory-scale experiments (Kodama 2010). A 50 to 80-kW solar reactor will be tested at the Miyazaki 100-kW beam-down solar concentrating facility.
- For the CO_2 gasification of cokes, an internally circulating fluidised-bed reactor (Figure 10) with a draft tube (i.e. a spouted-bed reactor) was superior to the conventional fluidised-bed reactor in terms its gasification rate, carbon conversion and solar-to-chemical energy efficiency (Gokon, Hatamachi et al. 2012).

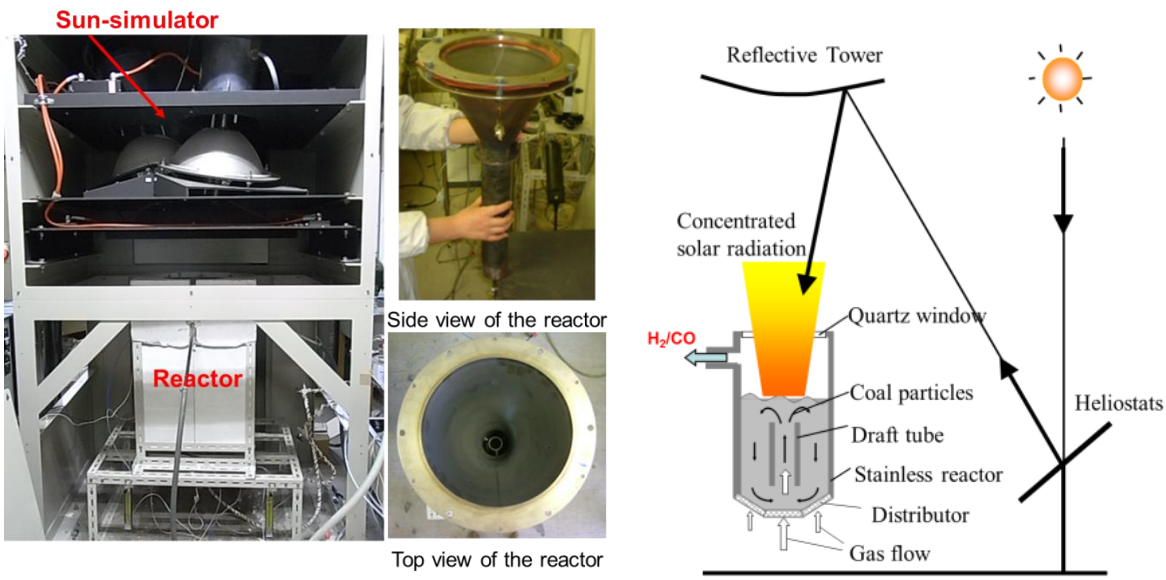

Figure 10: Concept of solar gasifier with internally fluidised beds of coal particles (right) and laboratory-scale performance test of the reactor using sun-simulator (left)

5.2.3 The University of Minnesota, United States

Key workers: Ng and Lipinski

Period of publications: 2012

Main areas of activity:

- A thermodynamic analysis was conducted for the solarised steam and CO_2 gasification of peat, lignite, bituminous coal and anthracite to produce a syngas for subsequent conversion to liquid fuels via the Fischer–Tropsch synthesis.

Key results:

- Results showed that replacement of a conventional coal gasification/Fischer–Tropsch process with a process based on solarised gasification reduces specific CO_2 emissions by at least 39%, with CO_2 gasification of bituminous coal being the best option (Ng and Lipinski 2012).

5.2.4 The University of Adelaide, Australia

Key workers: Gou, Saw, van Eyk and Kaniyal

Period of publications: 2013-2015

Main areas of activity:

- Techno-economic assessments for a range of solar hybrid coal and coal/biomass-to-liquid fuels process concepts, based on Australian coals and insolation conditions (Guo, Saw et al. 2015) (Guo, van Eyk et al. 2015) (Kaniyal, Van Eyk et al. 2013) (Kaniyal, Eyk et al. 2013).

Key results:

- One study (Saw, Kaniyal et al. 2015) consisted of a techno-economic assessment of a coal-to-liquid (CTL) fuels process integrated with a solar-hybridised, oxygen-blown, vortex-flow gasifier operated at atmospheric pressure (referred to as SCTL) compared with that of a reference, non-

solar, pressurised entrained-flow gasifier (CTL). Conceptual plants sited at Woomera (South Australia) and Geraldton (Western Australia) were considered in this study. Both cases included CO_2 capture, liquefaction and sequestration and storage of syngas to allow for variation in throughput of the intermediate process unit to be maintained within normal operational ranges throughout the day. This required syngas storage of 3.75 and 5.33 hours for the Geraldton and Woomera sites, respectively.

- In comparison with the conventional process, the SCTL concept reduced the input coal by 18% for a given Fischer–Tropsch liquids output. With the addition of solar energy to the CTL plant, CO_2 production can be reduced by 26%.
- For the production of 1500 barrels per day of Fischer–Tropsch liquids, the fixed capital investment for the SCTL plant was estimated at around $467–493 million, depending on the solar site and the type of coal. In comparison, the conventional CTL plant would cost around $377–384 million if both plants were constructed in the year 2020. The levelised cost of fuel (LCOF) for the CTL plants was estimated to be $40–41/GJ LHV compared with $46–49/GJ LHV for the SCTL plants. The LCOF for both plants was very sensitive to capital investment, load factor and cost of carbon capture and sequestration, while the LCOF for the SCTL plant is also very sensitive to the cost of syngas storage.

5.3 Pilot-scale solar gasification projects

The solarised gasification of carbonaceous materials has been investigated at the pilot-plant scale in the SOLSYN and SYNPET projects, which are briefly summarised below.

5.3.1 SOLSYN Project

Project partners: ETH, PSI and HOLCIM (a cement manufacturing company)

Period of publications: 2006–2012

Main areas of activity:

- High-temperature solar process heat is applied to produce high-quality syngas for substituting fossil fuels in a cement kiln. Compared to conventional autothermal gasification, the solar-driven process delivers a higher syngas output of better quality and lower CO_2 intensity. This is because no portion of the low-grade carbonaceous feedstock is combusted, and its energy content is solar-upgraded. There were two phases to this project:
  - **Phase 1:** Following an initial pre-feasibility study of the solar steam gasification process, experiments were conducted on a range of carbonaceous feed stocks in a high-flux solar facility at PSI.
  - **Phase 2**: Design, construction and operation of a 150-kW_{th} packed-bed solar gasification pilot plant installed at the Plataforma Solar de Almería (PSA) and operated in batch mode.

Key results:

- Laboratory-scale conversion of miscellaneous carbonaceous feed stocks using a two-cavity solar reactor (Figure 11, left) was successfully demonstrated.

- Solar gasification was experimentally demonstrated in a pilot plant with 150-kW_{th} radiative power input using a packed-bed solar reactor operated in batch mode (Figure 11, right). Nine different carbonaceous feed stocks were gasified in the PSA pilot plant**.** The materials were characterised by their wide range of volatiles, ash, fixed carbon, moisture content and elemental composition (Wieckert, Obrist et al. 2013).
- The calorific value of the produced syngas was upgraded by a factor of up to 1.3. The solar-to-fuel energy conversion efficiency (defined as the ratio of the heating value of the fuel produced to the solar and feedstock energy inputs) varied between 22 and 35%, depending on the feedstock used (Wieckert, Frommherz et al. 2007; Wieckert, Obrist et al. 2013) .
- The project partners claim that the SOLSYN solar reactor concept is scalable to an industrial application (MW_{th}) and can, in general, accept bulk carbonaceous feedstock of any shape and size without prior processing.

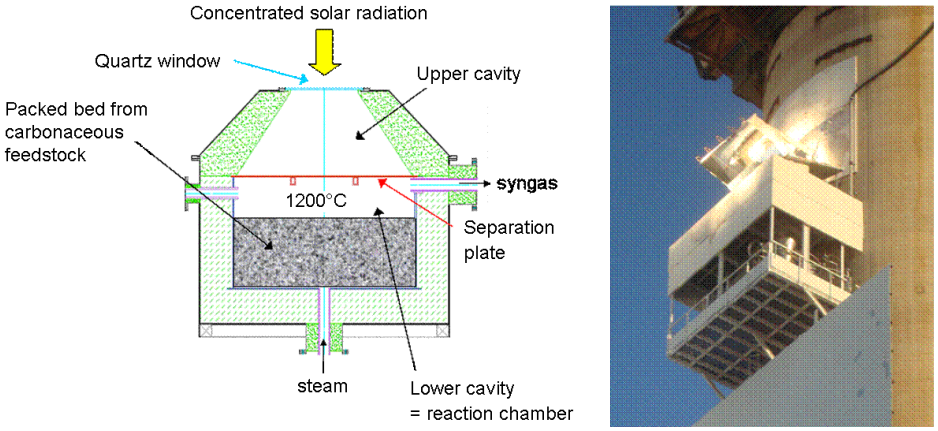

Figure 11: Schematic of SOLSYN two-cavity, beam-down reactor (left) and installation of 150-kWth SOLSYN reactor on solar tower at PSA (right)

5.3.2 SYNPET Project

Project partners: Petroleos de Venezuela (PDVSA), ETH and the CIEMAT

Period of publications: 2002–2010

Main areas of activity:

- Thermodynamic and kinetic modelling of the key reactions associated with the steam gasification of Venezuelan petroleum coke to select optimum reaction conditions (e.g. temperature, particle sizes, contact times) for gasification tests under real solar conditions.
- Scale-up of a 5-kW_{th} solar reactor (Figure 12, left) tested in Zurich to the design and construction of the main components of a 500-kW quartz-windowed cavity system, with slurry feeding, that was installed and tested on the PSA solar tower (Figure 12, right).

Key results:

- The modelling and kinetics study predicted that 100% carbon conversion is obtained at peak temperatures of 1820 K, yielding high-quality syngas with a calorific content that has been solar-upgraded by 19% over that of the petcoke gasified (Z'Graggen and Steinfeld 2009).
- The results from the 500-kW_{th} facility at PSA showed that the use of direct absorption receivers allows production of a gas with essentially no CO_2 emissions at lower temperatures than indirect

absorption tubular reactors. This was a result of the direct irradiation of the reactants providing a more effective way to transfer heat directly to the reaction sites, improving both the kinetics and heat-transfer processes required to supply the reaction heat (Vidal, Denk et al. 2010).

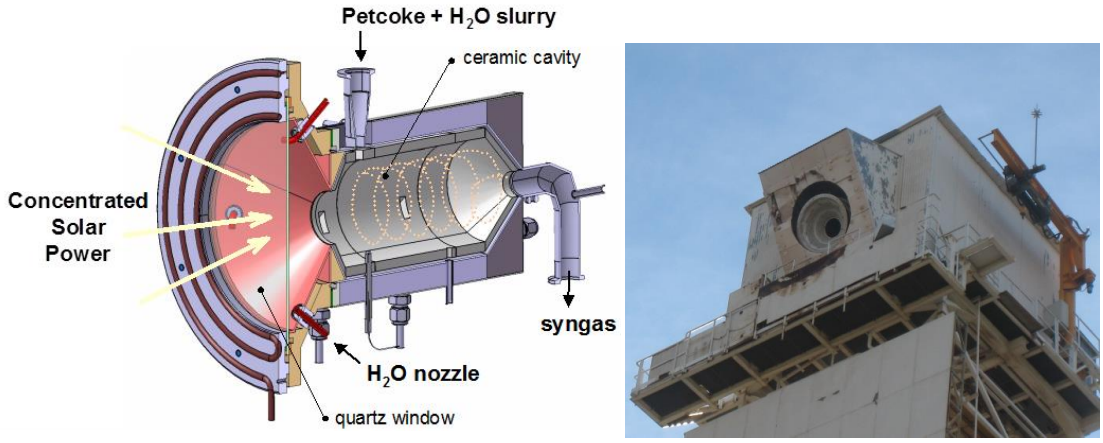

Figure 12: Schematic of the 5-kW_{th} SYNPET vortex-flow reactor at PSI (left) and the 500 kW_{th} SYNPET reactor mounted on top of the solar tower at PSA (right)

5.4 Issues and challenges for solar gasification of coal and carbonaceous materials

- As with other solar–fossil fuel hybrid systems, the principal performance indicators of the solar gasification process are the solar-to-fuel energy conversion efficiency, η, and the energetic upgrade factor, U. The different values of η and U obtained for the various feedstock materials are due to their heterogeneous morphological properties (particle size, porosity and specific surface area) and their different initial moisture, volatiles and fixed-carbon contents (Wieckert, Frommherz et al. 2007). These differences strongly affect heat-transfer rates, reaction kinetics and enthalpy changes, which in turn influence the extent of the reactions and the composition of the syngas.
- Many of the issues and challenges for solar-driven gasification are common across all of the carbonaceous feed stocks, including biomass materials. These include feeding solids or slurries into the gasification zone, and removing solids (ash and unconverted carbon) from the reactor in a controlled manner.
- In windowed volumetric receiver/reactors (e.g. vortex-flow reactors), further problems involve keeping the quartz window clean and transparent. Of particular concern are alkali metals, which are present to a significant extent in Australian brown coals and biomass. At high temperatures, alkali metal compounds will react with the quartz glass, rapidly rendering the window translucent or opaque.
- Ash melting/slagging must be avoided to prevent these materials sticking to any cooler parts of the reactor. Australian black coals generally have significantly higher ash fusion temperatures than coals from the northern hemisphere, which should be advantageous in solar gasification.

6 Metal oxide/redox cycles for hydrogen and syngas from H_20 and CO_2 splitting

Two-step reaction cycles are the simplest, multi-step, thermochemical H_2O and CO_2-splitting methods. They may be classified into one of the following three types of reactions:

Oxide type

$$XO \rightarrow X + \frac{1}{2}O_2 \quad (11)$$

$$X + H_2O \rightarrow XO + H_2 \quad (12)$$

Hydride type

$$XH_2 \rightarrow X + H_2 \quad (13)$$

$$X + H_2O \rightarrow XH_2 + \frac{1}{2}O_2 \quad (14)$$

Hydroxide type

$$2XOH \rightarrow 2X + H_2O + \frac{1}{2}O_2 \quad (15)$$

$$2X + 2H_2O \rightarrow 2XOH + H_2 \quad (16)$$

Thermodynamic analysis shows that for the first two cycle types, feasible two-step cycles cannot be found at metal oxide reduction or metal hydride decomposition temperatures below 1400 K. The minimum number of reaction steps for thermochemical cycles operating between 298 and 1000 K is three, as inferred from the required entropy change. However, by raising the temperature limit, the thermochemical constraints for chemical compounds to form via two-step cycles are less stringent.

Two-step, thermochemical water splitting by a metal oxide redox pair represents the first type of cycle (oxide type), which is called the metal oxide (redox) cycle or process. When this cycle is used for CO_2 splitting, the relevant reactions are:

$$XO \rightarrow X + \frac{1}{2}O_2 \quad (17)$$

$$X + CO_2 \rightarrow XO + CO \quad (18)$$

Overall, the net reactions are:

$$2H_2O + 572kJ/mol \rightarrow 2H_2 + O_2 \quad (19)$$

$$CO_2 + 283kJ/mol \rightarrow CO + \frac{1}{2}O_2 \quad (20)$$

A solar thermochemical liquid fuels system based on these highly endothermic splitting reactions needs a source of CO_2 and water, a suitable metal oxide working material (not consumed), a solar

receiver/reactor in which the reduction and reoxidation reactions take place, and a fuel-processing unit that converts the produced H_2 and CO into 'drop-in', qualified liquid transport fuels (gasoline, aviation jet fuel and diesel).

The metal oxide/redox approach to water splitting, and to a lesser extent, CO_2 splitting, has been extensively investigated over the past 15 years, with numerous publications and reviews completed by more than 30 research institutions worldwide (e.g Agrofiotis, Roeb et al. 2015; Kodama and Gokon 2007, Roeb, Neises et al. 2012; Romero and Steinfeld 2012; Smestad and Steinfeld 2012; Xiao, Wu et al. 2012).

In Australia, the only previous significant work on this option was a collaborative project between the Australian National University (ANU), Tokyo Institute of Technology and Niigata University (Japan). The work demonstrated the high-temperature thermal decomposition of zinc ferrite ($ZnFe_2O_4$) using the ANU's 15-kW dish concentrator (Kaneko, Kodama et al. 2004). More recently, work has commenced on improving redox materials/cycles within the ARENA-supported Australian Solar Thermal Energy Research Institute. The ANU has also begun developing new redox material structures that promise fast, efficient production of H_2 and CO from H_2O and CO_2 splitting, respectively. The project includes modelling/predictive studies, materials development and testing at the 1-kW scale in the new ANU solar simulator.

The following sections summarise major overseas research activities, achievements and key issues and challenges that need to be addressed to make the metal oxide/redox approach a viable means of both renewable hydrogen and syngas production. Metal oxide/redox systems can be further characterised into either volatile or non-volatile oxide cycles, which are now discussed in turn.

6.1 Volatile metal oxide cycles

Since the temperatures required for thermal reduction are very high, they can in some cases exceed the boiling point of the reduced species. In such cases, they are referred to as volatile metal oxide cycles. Those that have been investigated include the ZnO/Zn, SnO_2/SnO, GeO_2/GeO and CdO/Cd cycles. The ZnO/Zn cycle is by far the most investigated; work on it is briefly discussed below, followed by a brief mention of the tin-based SnO_2/SnO cycle.

Zinc (melting point 692 K; normal boiling point 1180 K) is relatively non-toxic, cheap and a potentially attractive energy vector.

The first step in the cycle is the thermal dissociation of ZnO to gaseous Zn and oxygen using solar process heat at temperatures exceeding 2000 K:

$$ZnO \rightarrow Zn + \frac{1}{2}O_2 \quad (21)$$

After quenching, the second, non-solar step is the exothermic reaction of Zn with H_2O and/or CO_2 to generate H_2 and/or CO:

$$Zn + H_2O \rightarrow ZnO + H_2 \quad (22)$$

$$Zn + CO_2 \rightarrow ZnO + CO \quad (23)$$

$$Zn + H_2O + CO_2 \rightarrow ZnO + H_2 + CO \quad (24)$$

Alternatively, Zn can be reacted with air in a Zn–air battery to produce electricity (as demonstrated in the SOLZINC project):

$$Zn + air \rightarrow ZnO + electricity \quad (25)$$

In all cases, ZnO is recycled to the first step, thus closing the cycle.

6.1.1 Carbothermic reduction route

The metal oxide reduction temperature can be significantly reduced by using carbonaceous materials as reducing agents. This also solves the problem of product Zn/O_2 recombination on cooling. Such materials can be derived from fossil fuels (e.g. coal, natural gas, coal bed methane) or possibly from renewable sources such as biochar and biogas.

When coal or coke/char (for simplicity, assumed here to be carbon) is used, the metal oxide reduction reaction can be represented as:

$$M_xO_y + yC \rightarrow xM + yCO \quad (26)$$

When methane is used, the metal oxide reduction reaction can be represented as:

$$M_xO_y + yCH_4 \rightarrow xM + y(2H_2 + CO) \quad (27)$$

In the case of ZnO, the reduction temperature can be reduced to around 1400–1500 K. If the methane or carbon is derived from a renewable resource, this is still a purely renewable option. However, if the reductant is derived from fossil fuels, then this becomes a hybrid concept.

Following the technical demonstration of the ZnO decomposition reaction with a 10-kW_{th} solar reactor prototype, a 100-kW_{th} solar pilot plant was designed, fabricated and experimentally tested at the large-scale solar concentrating facility of PROMES-CNRS in Odeillo, France. The test was part of the Solar2Zinc project, a project conducted by the Paul Scherrer Institute (PSI) and ETHZ with the financial support of the Swiss Federal Office of Energy.

The solar reactor and peripheral components are shown schematically in Figure 13. The experimental campaign involved more than 60 hours of on-sun testing at the 1-MW solar furnace, with each experiment lasting between three and nine hours. The reactor cavity lining exhibited good mechanical and thermal stability, and did not show any visible degradation at the end of the campaign.

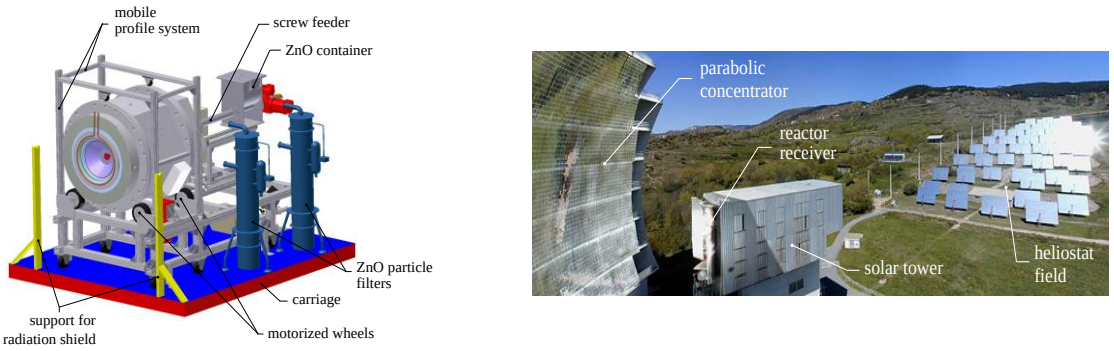

Figure 13: 3D layout of the 100-kW$_{th}$ solar pilot plant for thermal dissociation of ZnO (left), and view of large solar furnace of PROMES-CNRS in Odeillo, France (right)

The technical feasibility of using Zn to split both H_2O and CO_2 separately and simultaneously has been demonstrated in the laboratory (Loutzenhiser, Galvez et al. 2010; Loutzenhiser, Meier et al. 2010; Loutzenhiser, Stamatiou et al. 2011). The emphasis of this work has been on measuring the reaction kinetics and how they are influenced by factors such as temperature (700–1000 K), Zn particle size and conversion level. The use of aerosol reactors with sub-micron Zn particles in a flow of oxidant (H_2O, CO_2 or H_2O/CO_2) has received particular attention for this purpose.

The EU project SOLZINC was led by PSI in collaboration with ETH, PROMES-CNRS (France), the WIS (Israel), and industrial partners ScanArc Plasma Systems AB (Switzerland) and ZOXY Energy Systems AG (Germany).

In the project, a 300-kWth solar chemical pilot plant for the production of Zn by carbothermic reduction of ZnO was experimentally demonstrated in a beam-down solar tower concentrating facility at the WIS (Wieckert, Frommherz et al. 2007). The solar chemical reactor features two cavities (Figure 14). The upper cavity functions as the solar absorber, while the lower cavity is the reaction chamber, which contains a ZnO/C packed bed, was batch-operated at 1273–1473 K and yielded 50 kg/h of 95%-purity Zn.

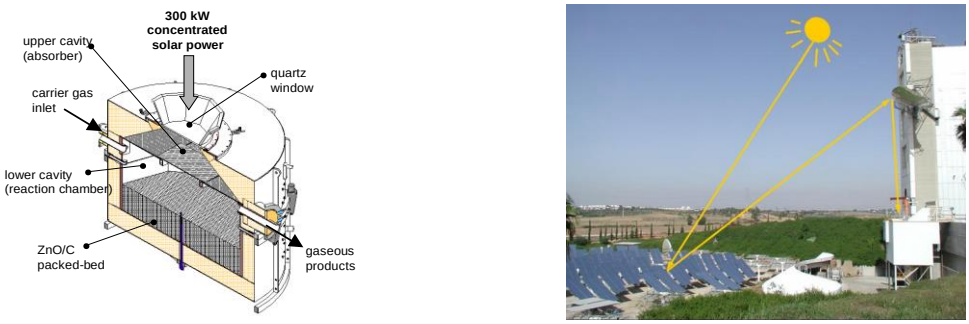

Figure 14: Two-cavity solar reactor concept for the carbothermal reduction of ZnO (left), and beam-down solar facility of the Weizmann Institute of Science in Rehovot, Israel (right)

6.1.2 SnO_2/SnO cycle

This cycle was originally proposed and studied in the laboratory by PROMES-CNRS. It involves the high-temperature (~1900 K) decomposition of SnO_2 to SnO (normal boiling point 1800 K) and O_2. Following quenching and O_2 removal, the reaction continues with either H_2O (800–900 K) or CO_2 (1100 K) to produce hydrogen or syngas to complete the cycle (Charvin, Abanades et al. 2011).

This cycle faces the same recombination problems encountered with the ZnO/Zn cycle, with the product from the reduction step consisting of a mixture of SnO and SnO_2. Advantages claimed for this cycle over the ZnO/Zn cycle include:

- lower reduction temperature (1900 K cf. >2000 K)
- less dependence of SnO_2 dissociation rate on quenching rate, since its reactivity with O_2 is less than Zn with O_2 in the quench zone (Chambon, Abanades et al. 2010)
- higher H_2 yield in the hydrolysis step, although the kinetics of this reaction are slower than in the Zn/ZnO cycle (Leveque, Abanades et al. 2014).

However, the reactivity of SnO for H_2O splitting is much greater than for CO_2 splitting, making the simultaneous H_2O/CO_2-splitting process for syngas production impractical (Leveque, Abanades et al. 2014).

The SnO_2 decomposition step has not been tested under real solar conditions to date.

6.1.3 Issues and challenges for the volatile metal oxide cycle (exemplified by the ZnO/Zn cycle)

- This cycle has major technical challenges centred on both the extremely high temperatures (2100–2300 K) required for the reduction step, and the undesired back reaction (Zn to ZnO) that occurs when the products (Zn and O_2) are cooled. Since zinc vapour readily combines with oxygen over a wide temperature range on cooling, high zinc yields can only be obtained by fast quenching and dilution of the product mixture with large amounts of inert gas. Such steps will be detrimental to the cycle's overall energy efficiency.
- The water and CO_2-splitting steps take place at around 700–1000 K, but experiments have shown the kinetics of these reactions to be slow. Both the water and CO_2-splitting reactions produce ZnO, which can have a serious detrimental effect on the per-cycle Zn conversion, due to the blinding/mass transfer limitations it imposes on this part of the overall process.
- The use of an inert gas (argon) reduces the operating temperature to around 2000 K, but separating a large amount of argon from the oxygen is problematic and expensive. Finding construction materials that can withstand these very high temperatures in the presence of oxygen is extremely challenging. In any commercial application of this process, the inert gas would most likely be N_2 from an air separation unit.
- The target conversions of ZnO to recovered Zn set by the United States Department of Energy of 70% (2015) and 85% (2025) have not been met, with the best reported to date for the 100-kW reactor being less than 50%. Even if these targets were reached, the economics of this option are still considered to be questionable (Perret 2011).

- An economic and policy analysis of hydrogen production by the ZnO/Zn cycle ((Haltiwanger, Davidson et al. 2010) suggests that it will not be economically competitive with conventional steam-methane reforming until around 2032 at the earliest, and only if all the demanding technical challenges outlined above are solved.
- Integrated operation of the complete cycle under real solar conditions has not yet been reported.
- In the Solar2Zinc project, operational experience has pointed to further research and development needs, and is guiding the development of an industrial solar chemical plant for the production of H_2 and syngas (Villasmil, Brkic et al. 2014). Major research challenges include efficient quenching of the gaseous products Zn and O_2, to prevent their recombination; aerodynamic protection of the transparent window, to avoid deposition of condensing products; and thermally and chemically stable, high-temperature materials for the solar reactor cavity walls.
- The solar carbothermic ZnO/Zn cycle using charcoal for reducing ZnO may be a viable medium-term option for CO_2-neutral production of electricity, hydrogen or syngas. Based on the experimental results of the 300-kWth solar chemical pilot plant, a conceptual design of a 5-MW_{th} demonstration plant and a 30-MW_{th} commercial plant was developed (Epstein, Olalde et al. 2008). In the SOLZINC project, the measured energy conversion efficiency (i.e. the ratio of the reaction enthalpy change to the solar power input) was 30%.
- For the thermal dissociation of ZnO (Solar2Zinc project), thermodynamic analysis indicates that the solar-to-fuel energy conversion efficiency, defined as the heating value of the fuel produced divided by the total energy input to the cycle, can exceed 30% (Loutzenhiser and Steinfeld 2011).

6.2 Non-volatile metal oxide cycles

Non-volatile metal oxide cycles produce hydrogen and/or syngas from CO_2 and water via the following general reactions:

$$\frac{1}{\delta}MO_{x,solid} \xrightarrow{heat} \frac{1}{\delta}MO_{x-\delta,solid} + \frac{1}{2}O_2 \tag{28}$$

$$\frac{1}{\delta}MO_{x-\delta} + CO_2 \rightarrow \frac{1}{\delta}MO_x + CO \tag{29}$$

$$\frac{1}{\delta}MO_{x-\delta} + H_2O \rightarrow \frac{1}{\delta}MO_x + H_2 \tag{30}$$

In essence, the reduction reaction results in a partially reduced oxide. The parameter ð represents the degree of reduction, non-stoichiometry or the reversible oxygen storage capacity respectively. Cycles based on iron oxides/ferrites, ceria, perovskites and cobalt ferrite/hercynites are among those that have been most widely investigated to date, and are now briefly reviewed in turn.

6.2.1 Iron-based metal oxide cycles

The original iron-based cycle (Nakamura 1977) involves the thermal reduction of magnetite (Fe_3O_4) to wustite (FeO) and O_2, followed by the reaction of FeO with H_2O and/or CO_2 to produce H_2/syngas and Fe_3O_4 to complete the cycle. The endothermic reduction step, driven by solar energy, requires a very high temperature (2300 K for complete reduction) and is complicated by the melting points of FeO (1650 K) and Fe_3O_4 (1870 K) being below this temperature.

Research efforts have been directed at ways to reduce the temperature and avoiding the melting point issue, while retaining the strong reduction and oxygen transfer capability potential of iron. In this context, ferrites (generic formula MFe_2O_4, where M = Mn, Ni, Zn, Co, etc.) have been extensively investigated.

A series of ferrites, prepared by a range of techniques, have been studied thermodynamically and experimentally: initially for water splitting. The preparation techniques have included:

- co-precipitation (Ishihara, Kaneko et al. 2008)
- oxidation of aqueous suspensions of Fe (II) hydroxide in metal salts solutions (Kodama, Kondoh et al. 2005; Kodama, Gokon et al. 2008)
- sol-gel (Bhosale, Shende et al. 2012)
- atomic layer deposition (Scheffe, Allendorf et al. 2011)
- combustion synthesis (Agrafiotis, Pagkoura et al. 2012)
- aerosol spray pyrolysis (Loentzou, Agrafiotis et al. 2008).

Comparative testing of various ferrite powders in the laboratory has identified the temperature ranges recommended for cyclic operation, as well as the effects of key process parameters on H_2 and O_2 yields (Frenso, Fernandez-Saavedro et al. 2009; Fresno, Yoshida et al. 2010). Their reduction temperatures are still very high (1600–1700 K), and sintering of the material is still a serious issue. Attempts to tackle this problem have included supporting the redox material on high-temperature-stabilised zirconia ZrO_2 (Kodama, Nakamuro et al. 2004; Scheffe, McDaniel et al. 2013; Gokon, Takahashi et al. 2009).

Work on iron oxides and ferrites has recently been extended to CO_2-splitting, either separately or simultaneously with H_2O-splitting. Sandia National Laboratory investigated H_2O and CO_2 splitting using iron oxide/yttria-stabilised zirconia (Fe_2O_3/YSZ) materials via temperature-programmed reduction/oxidation. The experiments were performed in a thermogravimetric analyser (TGA) between 1673 K (H_2O splitting) and 1373 K (CO_2 splitting), and using in-situ high-temperature X-ray diffraction (Coker, Ambrosini et al. 2011; Coker, Ohlhausen et al. 2012). Both splitting modes were demonstrated over multiple temperature cycles. They also reported that Fe ions dissolved within the YSZ lattice are more 'redox active', leading to higher O_2 yields and higher H_2 and/or CO yields during the subsequent oxidation step.

ETH/PSI has also performed comparative TGA studies on simultaneous H_2O and CO_2 splitting over Zn and FeO (Stamatiou, Loutzenhiser et al. 2010). They reported that during the interface diffusion-controlled regime for both Zn and FeO, there were higher reaction rates with H_2O than with CO_2. As expected, there was a strong dependency between the molar H_2O/CO_2 ratio in the feed and the H_2/CO molar ratio in the product gas over the temperature ranges investigated.

PROMES-CNRS studied the co-splitting of H_2O and CO_2 over FeO, which was produced by the solar thermal reduction of Fe_3O_4 in a TGA. They also found that H_2 production was favoured over CO production, with the H_2O-splitting reaction being responsible for more than 80% of the total FeO conversion back to Fe_3O_4 (Abanades and Villafan-Vidales 2011).

Research at the Aerosol and Particle Technology Laboratory of the Centre for Research and Technology Hellas in Greece showed that both H_2O and CO_2 splitting could be conducted over a Ni-ferrite to give a product with a H_2/CO molar ratio of 1.4. The group claimed that the two splitting reactions proceeded at nearly the same rate, indicating a similar mechanism at the particular experimental conditions employed (Lorentzou, Karagiannakis et al. 2014). Note that this is contrary to the results found above for FeO.

Various research groups have used TGA experimental data, as well as gas product compositions from mass spectrometers coupled to a range of test rigs, to develop kinetic models for the reduction and oxidation reactions (Go, Son et al. 2008; Kostoglou, Lorentzou et al. 2014). Work has indicated that oxidation of ferrites by both H_2O and CO_2 is much more rapid than their thermal reduction, resulting in less time for completion. Interestingly, the results of some research groups cannot be described by a single rate-governing process throughout the duration of the experiments. To explain this behaviour, the participation in the reaction of perhaps more than one 'population' of oxygen storage sites (Kostoglou, Lorentzou et al. 2014) or Fe ions (Scheffe, McDaniel et al. 2013) has been suggested.

In terms of materials composition, the current consensus is that among the many ferrites prepared and tested for this application, those containing Zn exhibit Zn-volatilisation problems, while those containing Mn are not stable at high temperatures (Frenso, Fernandez-Saavedro et al. 2009; Frenso, Fernandez-Saavedro et al. 2010; Agrafiotis, Pagkoura et al. 2012). This leaves only $NiFe_2O_4$ and $CoFe_2O_4$ (and their combined stoichiometries, e.g. $Ni_{0.5}Co_{0.5}Fe_2O_4$) as potentially the most suitable ferrites for operation under the challenging conditions required for solar H_2O and/or CO_2-splitting applications.

An energy flow analysis of an idealised version of the Fe_3O_4/FeO cycle is presented in Section 6.3.1 to illustrate the importance of key operating parameters, such as the extent of reduction and recuperation of high level sensible heat, on the overall cycle thermal efficiency.

6.2.2 Ceria cycle

The capacity of cerium oxides (Ce_2O_3/CeO_2) to store and release O_2 under varying reduction/oxidation atmospheres has been applied for decades in automobile catalytic convertor technology. However, it was not until 2006 that a research group from PROMES proposed the investigation of a cycle based on this feature of cerium for solar-driven H_2O and/or CO_2 splitting. The group demonstrated the reduction of CeO_2 to Ce_2O_3 and O_2 in a laboratory-scale solar reactor, followed by oxidation of the Ce_2O_3 back to CeO_2 with steam to produce H_2 (Abanades and Flamant 2006). However, the reduction step was conducted at pressures of 100–200 mbar and temperatures higher than 2220 K, where the CeO_2 was in the molten state.

To avoid the CeO_2 melting problem, a research group at the California Institute of Technology (Caltech) proposed a non-stoichiometric cycle, to become known as the ceria cycle, involving the following reactions (Chueh and Haile 2009):

$$CeO_2 \rightarrow CeO_{2-\delta} + (2-\delta)O_2\ (>1773K) \quad (31)$$

$$CeO_{2-\delta} + \delta H_2O \rightarrow CeO_2 + \delta H_2\ (900-1300K) \quad (32)$$

$$CeO_{2-\delta} + \delta CO_2 \rightarrow CeO_2 + \delta CO\ (900-1300K) \quad (33)$$

Since then, the ceria cycle has perhaps become the most widely investigated for this solar thermochemical application. Work has been largely motivated by the following desirable characteristics of the ceria system:

- CeO_2 can be reduced to a significant degree of non-stoichiometry without any phase changes while retaining a cubic fluorite structure.
- The cycle is capable of faster hydrogen and syngas production kinetics and high selectivity during the oxidation step.
- Ceria has high thermal stability, and maintains its oxygen transfer capability over repeated cycling between reduction and oxidation largely due to its fluorite-type structure. However, the reduction step occurs at temperatures not lower than 1773 K, even when the O_2 partial pressure is as low as 10^{-5} atm (Chueh, Falter et al. 2010).

Work on the ceria cycle has been conducted primarily in the following areas:

- Thermodynamic analyses to examine the effect of key process parameters on overall cycle performance. These parameters include the
  - temperatures of both the reduction and oxidation steps
  - degree of non-stoichiometry
  - use of sweep gas versus vacuum generation to reduce the O_2 partial pressure during reduction
  - isothermal versus temperature swing operation between reduction and oxidation
  - effect of sensible heat recuperation on overall cycle thermal efficiency.
- The use of metal dopants to reduce the reduction temperature while increasing both the degree of reduction (non-stoichiometry) and thermal stability/cyclability.
- Kinetics studies of the reduction and H_2O and/or CO_2-splitting steps over a variety of Ce-based materials.
- The development of support structures/substrates on which the ceria is deposited, for use in practical reactor systems in which there is efficient heat and mass transfer to maximise the performance of the cycle under real solar conditions.
- Performance testing of the reduction and oxidation steps using laboratory and pilot-scale reactors integrated with concentrated solar energy.

A few key points arising from the large amount research on this cycle are briefly discussed below.

In their initial work, the Caltech group reported a higher activation energy for CO_2 splitting than for H_2O splitting. They also calculated the thermodynamic cycle efficiency for using the cycle to prepare syngas with a 2/1 H_2/CO molar ratio. Assuming a value of 0.05 for the oxygen non-stoichiometry, ð, after reduction and cycling between 1073 and 1773 K, they reported a calculated efficiency of 13.2%. Assuming a 50% recovery of the available sensible heat, the efficiency increased to 22.9% (Chueh and Haile 2009). A more detailed discussion on the thermal efficiency

of the ceria cycle, and the key factors affecting this important parameter, is presented in Section 6.3.2.

Much of the research into improved ceria-based redox materials has aimed to decrease the reduction temperature, as well as increase the reversible oxygen storage capacity or non-stoichiometry. In the fluorite structure, certain metallic ions (Hf, Sm, Zr, Ti, Sn and Y) can partially substitute for ceria while maintaining the desired structural properties. In addition, partial incorporation of Zr increases the reduction rate as well as the rates of CO and H_2 production.

The PROMES research group investigated the addition of various metal dopants to ceria in an effort to reduce the reduction temperature (Le Gal, Abanades et al. 2011; Le Gal and Abanades 2011). While this was met with some success, it introduced instability problems that reduced the ceria's cyclability.

Both the efficiency and cycling rates between reduction and oxidation are limited by the poor heat transfer characteristics of ceria: particularly by the inability to get heat into the bulk of the ceria, where much of the reaction (both reduction and oxidation) needs to occur. A range of metal oxide structures and supports have been investigated, including:

- monolithic vertical pins and textured plates (Furler, Scheffe et al. 2012)
- foams (Gokon, Kodama et al. 2011)
- 3D ordered porous structure honeycombs (Venstrom, Petkovich et al. 2012)
- felts (Furler, Scheffe et al. 2012)
- monolithic- and lattice-type structures (Chueh, Falter et al. 2010).

Microporous (µm) structures, such as monoliths or felts, displayed rapid oxidation kinetics due to their high surface areas. However, they are limited by their heat-transfer rates, because of opacity to incident solar radiation. This leads to undesired temperature gradients across the structure (Chueh, Falter et al. 2010; Furler, Scheffe et al. 2012).

In an effort to overcome this structural limitation, ETH/PSI developed reticulated porous ceramic (foam-type) structures made of ceria with dual-scale porosities in the mm and µm size range. The larger void size range, with a mean diameter of 2.5 mm and a voidage of 0.76–0.82, enables volumetric absorption of concentrated solar radiation for efficient heat transfer to the reaction sites during reduction. The smaller void size range within the struts, with mean diameter of 10 µm and strut porosity of 0–0.4, increases the specific surface area for faster chemical kinetics during oxidation. CO_2-splitting experiments were conducted from 873–1273 K, and CO production rates were up to ten times higher for samples with 0.44 strut porosity than for samples with non-porous struts (Furler, Scheffe et al. 2014).

6.2.3 Perovskites cycle

While the ceria cycle has become the benchmark for the non-volatile metal oxide cycles, recent efforts have concentrated on finding new redox materials capable of decreasing the reduction temperature while increasing both the per-cycle H_2/CO yields and thermal stability. Non-stoichiometric perovskites have been identified, principally by research groups at ETH/PSI and Sandia National Laboratories (SNL), as being potentially superior to ceria in all of these respects.

Earlier work at the Chemical Process Engineering Research Institute, Thessalonika (Greece) demonstrated the technical feasibility of using non-stoichiometric perovskites (SrxLa1-x MnyAl1-yO3 (x=0.4 or 0.6; y=0.4 or 0.6) for H_2O splitting (Evdou, Zaspils et al. 2008). Since then, researchers at SNL reported that $LaAlO_3$ doped with Mn and Sr ($La_{0.6}Sr_{0.4}MnO_{3-\delta}$ perovskite) will efficiently split both H_2O and CO_2. Moreover, the H_2 and CO_2 yields are respectively nine and six times greater than those produced from ceria when reduced at 1623 K and reoxidised at 1273 K. The temperature at which O_2 begins to evolve from the perovskite is around 300 K lower than that for ceria. The materials also exhibited good thermal stability, maintaining their redox activity over 80 CO_2-splitting cycles (McDaniel, Miller et al. 2013).

Thermodynamic analysis by ETH/PSI for cycles based on similar perovskite materials has highlighted the effect of temperature and reduction/oxidation thermodynamics on overall cycle efficiency (Scheffe, Weibel et al. 2013). At a reduction temperature of 1800 K and oxidation temperature of 1000 K, the theoretical efficiency of the perovskite cycle (16%) is lower than that of ceria (22%). However, if the reduction temperature is reduced to 1600 K, while still maintaining an oxidation temperature of 1000 K, the efficiency of the perovskite cycle (17%) is now greater than that for ceria (13%). This is largely due to the greater degree of reduction of the perovskite at the lower temperature, and its lower sensible heat penalty (due to its higher specific heat) in cycling between reduction and oxidation.

Chinese researchers have tested perovskites of the type $La_xA_{1-x}Fe_yB_{1-y}O_3$ (A = Sr, Ce, B = Co, Mn; $0 \leq x, y \leq 1$) dispersed in three different commercial support materials (ZrO_2, Al_2O_3 and SiO_2) for the CO_2-splitting reaction. The type of support induced great differences in reaction performance, with a 25 wt% SiO_2 support giving the highest activity (Jiang, Zhou et al. 2014).

6.2.4 Cobalt ferrite/hercynite cycle

A mixed cobalt ferrite-hercynite system ($CoFe_2O_4/FeAl_2O_4$) has been proposed by the University of Colorado (United States) as a potential redox cycle (Scheffe, Li et al. 2010). The hercynite is produced due to the reaction between $CoFe_2O_4$ and its support material, Al_2O_3. The overall reactions for H_2O-splitting can be summarised as:

$$Reduction: CoFe_2O_4 + 3Al_2O_3 \rightarrow CoAl_2O_4 + 2FeAl_2O_4 + \frac{1}{2} O_2 \quad (34)$$

$$H_2O\ Splitting: CoAl_2O_4 + 2FeAl_2O_4 + H_2O \rightarrow CoFe_2O_4 + 3Al_2O_3 + H_2 \quad (35)$$

These reactions could be cycled between 1473 K (reduction) and 1273 (H_2O-splitting) under stable conditions.

The work was extended to CO_2 splitting thus:

$$RCoAl_2O_4 + 2FeAl_2O_4 + CO_2 \rightarrow CoFe_2O_4 + 3Al_2O_3 + CO \quad (36)$$

Under a total pressure of 75–600 torr, appreciable amounts of CO were produced after reduction at 1633 K: approximately 100–150 K lower than for ceria.

The research group demonstrated that the hercynite cycle can produce H_2 at 1273 K when reduced at 1473 K, with conversions between 14.2 and 18.7% achieved. However, the oxidation of $FeAl_2O_4$ in the presence of steam is less favourable than that for FeO under the same conditions.

The group also demonstrated in the laboratory that this cycle could conduct isothermal water splitting, albeit at the somewhat higher temperature of 1623 K, thereby avoiding the need to cycle between reduction temperature and a lower water-splitting temperature (Muhich, Evanko et al. 2013). They claim that this has the potential to avoid the thermal and time losses that occur in temperature swing operation, due to the frequent heating and cooling of the metal oxide.

In view of its potential advantages, the hercynite cycle warrants further investigation.

6.2.5 Reactors investigated for non-volatile metal oxide cycles

Besides the development of active metal oxides, the design and performance testing under real solar conditions of efficient and low-cost reactors is an essential step in the commercialisation of the thermochemical cycles. The reactors investigated to date can be classified into two generic categories, depending on the form of the redox material in the reactor: non-structured and structured. The first category includes the traditional fixed-bed, moving-bed, entrained-flow and fluidised-bed reactors. The second category consists of structured systems, such as honeycomb foam and membrane reactors. In all cases, the reactor design must meet the chemical requirements for carrying out the redox reactions as well as provide effective heat transfer and recuperation to maximise the overall thermal efficiency of the process.

A range of reactor designs have been constructed and tested at the laboratory and pilot-scale for direct on-sun application. In general, the main challenges to be faced are re-radiation, convection and conduction losses through the aperture and the walls, respectively. The very high temperatures required for reduction of metal oxides pose severe challenges for heat retention and use. Addressing these challenges will require both lower-temperature materials, and more efficient reactor designs that minimise re-radiation losses and allow for high radiation capture.

A brief description of the main reactor types developed and tested for the non-volatile metal oxide cycles follows.

Fixed-bed reactor

A 2-cm diameter, quartz glass, fixed-bed reactor containing a mixture of ferrite and alumina particles was operated at the focus of a solar furnace at PSI (Tamaura, Steinfeld et al. 1995). During reduction, argon was passed through the fixed bed, and a mixture of argon and steam was added afterwards. Both O_2 and H_2 were detected. Even though this was the first reported solar-aided production of hydrogen from ferrites below their melting point, this type of reactor was not pursued further: presumably due to the high bed temperature gradients developed within the fixed bed of redox material.

Moving fixed-bed reactor

This reactor concept has been proposed by SNL, and the Bucknell and Arizona state universities (Ermanoski, Siegel et al. 2013). A schematic of its operating principle is shown in Figure 15. The redox particles, in their oxidised state, are transported by a vertical screw conveyor with a rotating casing to the top of the reactor. Here, concentrated solar radiation enters through a quartz window and partly reduces the particles, with the O_2 pumped away from the reaction chamber. The basic idea is that of effective heat recuperation, since the packed bed of reduced particles

moves downwards via a connecting tube in a counter-current flow, with the oxidised particles moving upwards and being preheated. The whole reactor consists of three sections: a thermal reduction chamber at the top, a recuperator (solid-solid heat exchanger) in the middle, and a fuel production chamber at the bottom where the cooled particles are exposed to H_2O and/or CO_2. The cycle is completed by the oxidised particles being returned to the reduction zone via the recuperator/elevator.

Advantages claimed are spatial separation of pressures, temperatures and reaction products, solid-solid sensible heat recovery, and continuous on-sun operation. Vacuum pumping of the thermal reduction part of the cycle, made possible by the pressure separation in the particular reactor design, is claimed to have a decisive efficiency advantage over inert gas sweeping.

Solar-to-fuel efficiencies for syngas production of 30% have been reported for process simulations based on this concept, with ceria as the redox material. However, the concept has yet to be demonstrated experimentally at any scale.

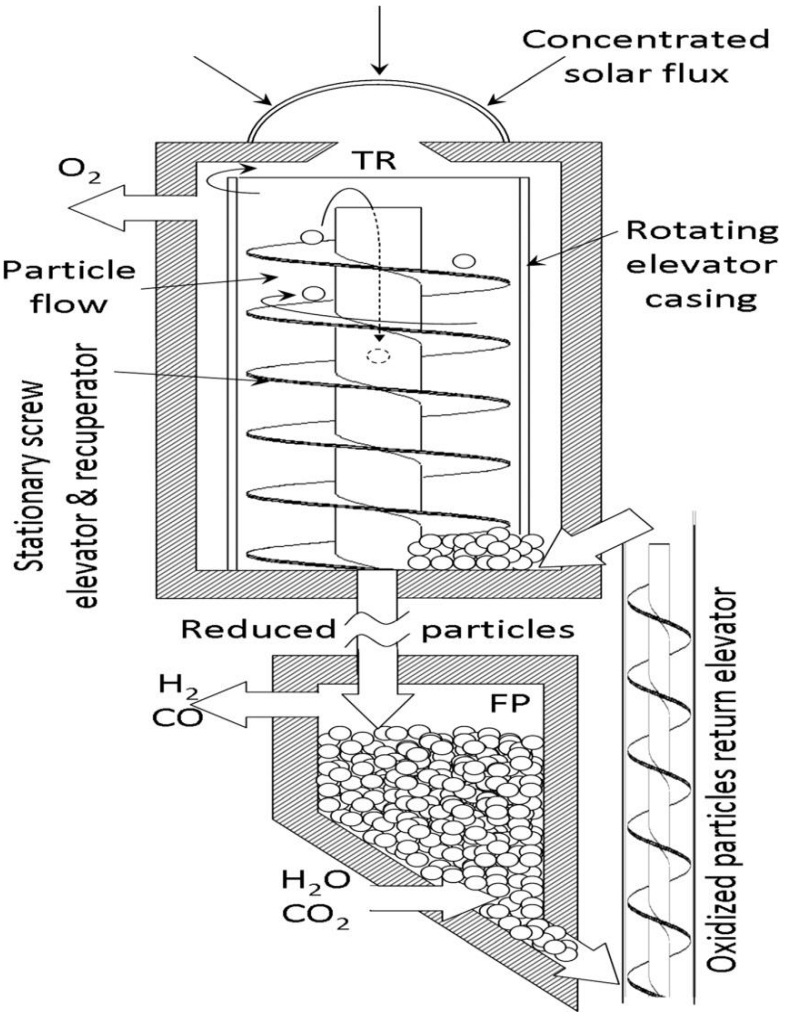

Figure 15: Schematic of the moving particle packed-bed reactor. FP = fuel production chamber; TR = thermal reduction chamber

Source: (Ermanoski, Siegel et al. 2013)

Fluidised-bed reactor

This type of reactor can, in principle, overcome the limitations of the fixed-bed reactor by improving heat transfer and minimising temperature gradients within the bed of redox particles.

The research group at Niigata University, Japan, has combined a laboratory-scale fluidised or spouted-bed reactor with a beam-down solar concentrating system to study the reduction of ferrites. In this system (

Figure 16), the redox particles are circulated through an internal tube and exposed to concentrated radiation from a 6-kW solar simulator entering through a quartz window at the top. The idea is that internal circulation will, among other things, minimise sintering and agglomeration and therefore reduce deactivation.

A range of ferrites (unsupported $NiFe_2O_4$ and supported $NiFe_2O_4/ZrO_2$), and more recently, ceria, were investigated for the reduction step. The surface of the spouted-bed reached 1773–1873 K and 1373–1523 K in the annular region. Approximately 35–40% of the supported Ni-ferrite ($NiFe_2O_4/ZrO_2$) was converted to the reduced state, and subsequently completely reoxidised with steam at 1373 K without any significant sintering or agglomeration.

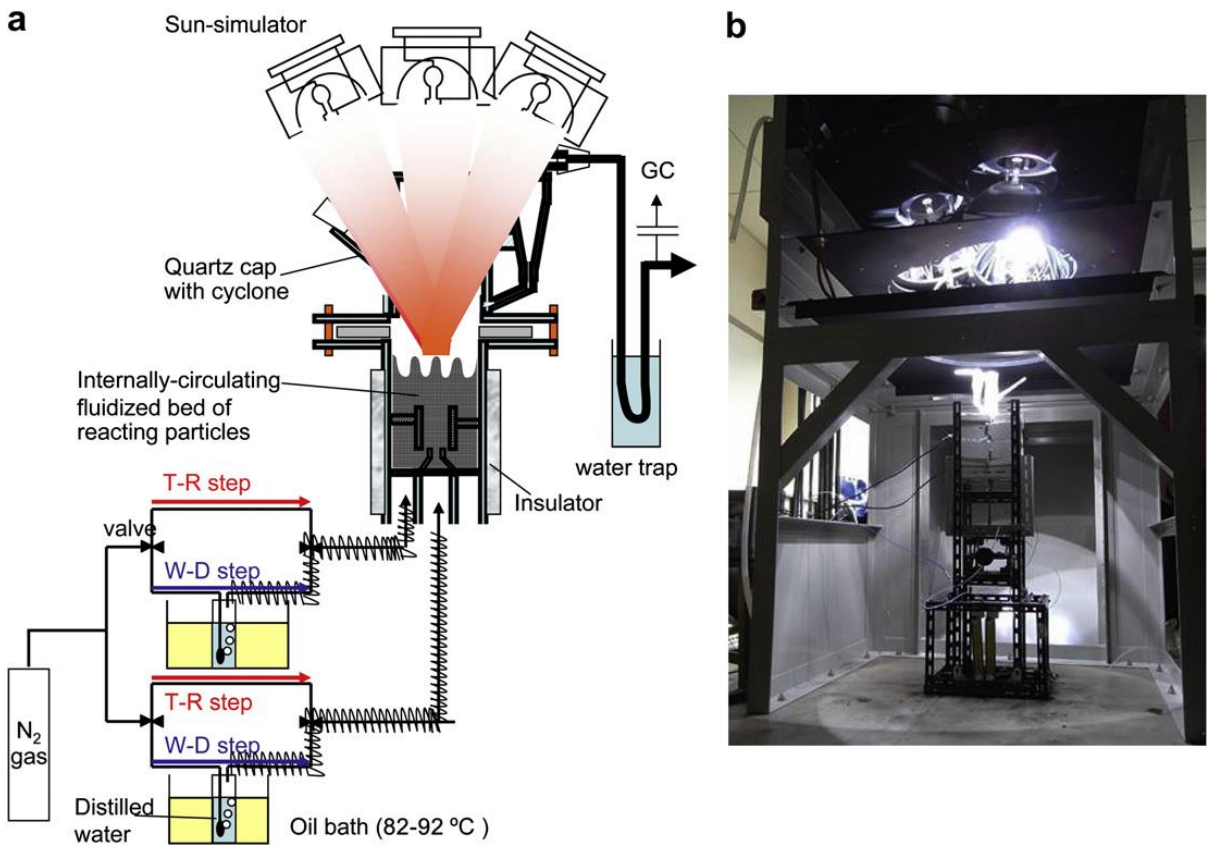

Figure 16: (a) Schematic of the Niigata University successive two-step, water-splitting, internally circulating fluidised-bed reactor for $Ni_2Fe_2O_4$ and CeO_2 metal oxide cycles; (b) photograph of the reactor being irradiated using the solar simulator

Source: (Gokon, Mataga et al. 2011)

Structured, directly irradiated receiver/reactors with no moving parts

Reactors in this category have employed honeycomb and ceramic foam redox materials coated on support structures, and subsequently, foams constructed entirely of redox material to maximise reversible oxygen storage capacity per unit mass.

Reactors based on ceramic monolithic honeycombs

The use of porous systems for thermochemical cycles was first proposed by workers from Caltech and PSI/ETH (Chueh, Falter et al. 2010). This reactor (Figure 17) consisted of a monolithic porous CeO_2 layer with a dual function: second wall and redox material. The reactant was directly exposed to the high-flux irradiation from a quartz window, reaching a maximum temperature of 1920 K in the centre of the reactor at 3.6-kWth power input. This configuration promoted heat transfer though the metal oxide due to high volumetric absorption, where the geometry achieved multiple internal reflections and thus reduced re-radiation losses. Both H_2O splitting and thermal reduction were demonstrated sequentially in the same reactor.

The main advantages claimed of this reactor are its simplicity, robustness and stability. However, a technical disadvantage comes from the poor thermal conductivity of CeO_2, which only allows the reaction to occur in the first few millimetres of the reticulated foam. Also, some sublimation of CeO_2 was observed after working for eight hours, resulting in deposition in the compound parabolic concentrator that was installed to reduce the radiative losses through the aperture. This reduced the radiative power input, and subsequently the fuel yield.

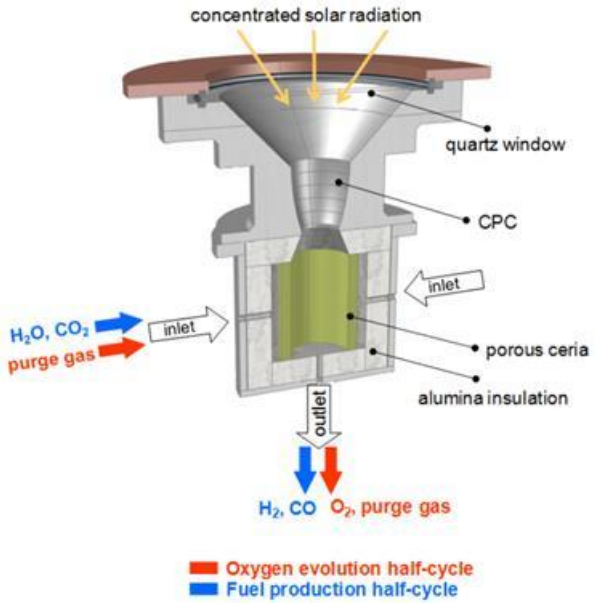

Figure 17: Porous monolithic reactor used to study the ceria cycle

Source: (Chueh, Falter et al. 2010)

Perhaps the best examples of this type of reactor are those developed and tested in the HYDROSOL I and II projects. These are based on the incorporation of active redox powders as coatings on multi-channelled monolithic honeycomb structures. The system was designed to demonstrate continuous operation of the reduction and H_2O-splitting steps, without the need to transfer the redox material between the two stages. This was achieved with a modular, dual-chamber, fixed honeycomb structure shown schematically in Figure 18. One module splits water while the other reduces the redox material, and the two modules are then switched to

achieve overall cyclic operation. Temperature control is achieved by adjusting the solar flux via partitioning the solar field, providing two 'switchable' focal points.

In this manner, H_2O splitting and thermal reduction were conducted simultaneously with a volumetric honeycomb structure of ferrites deposited on silconised SiC. The first prototype was a 10-kW_{th} reactor, which was tested at the DLR solar furnace to demonstrate proof of concept for quasi-continuous H_2 production (Roeb, Neises et al. 2009). The concept was then scaled up to a 100-kW_{th} unit, which was mounted on the PSA solar tower. While operation of this unit demonstrated proof of concept, with steam conversion of up to 30% obtained, the redox material suffered deactivation problems, largely through sintering (Roeb, Sack et al. 2011).

Following on from this work, the HYDROSOL 3D project involved further development of redox materials into absorber/monolithic structures, in an attempt to overcome the sintering problems and develop porous structures consisting entirely of redox material. It also included the detailed design of the complete process, with all of the balance of plant and secondary concentrator at the 1-MW_{th} scale having the capability of being integrated within a solar tower.

The 1-MW_{th} plant design study, which included detailed process simulation and exergy analyses, showed that the main exergy losses were associated with the solar receiver/reactor, as expected. The main objective for the new design was to increase efficiency by minimising re-radiation losses. A hemispherical absorber shape combined with a secondary concentrator was found to be the most suitable reactor design, promising at least 25% lower thermal losses than previous reactor designs (Houaijia, Sattler et al. 2013).

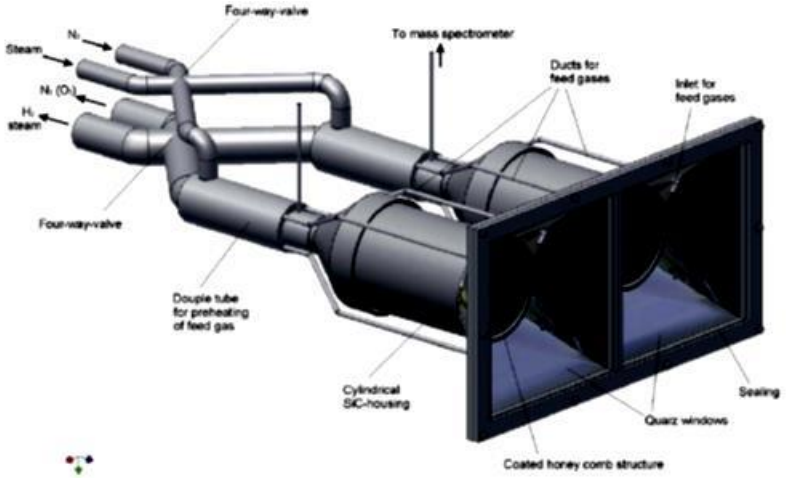

Figure 18: HYDROSOL II Project honeycomb reactor with dual cavities using ferrite-based redox materials

Reactors based on ceramic foams

Initial tests using ceramic foams containing ferrites or ceria supported on MgO/partially stabilised zirconia were conducted at Niigata University (Figure 19) in an attempt to reduce sintering and deactivation, with limited success (Kawakami, Myojin et al. 2014). Following this, the research group at ETH/PSI, in collaboration with Caltech, developed a reactor using a ceria foam. Tests with a reticulated porous ceria foam made entirely of ceria involved reduction at 1873 K in a solar furnace, followed by H_2O splitting at 1173 K. As expected with this material, the H_2O-splitting reaction was much faster than the reduction reaction (Chueh, Falter et al. 2010).

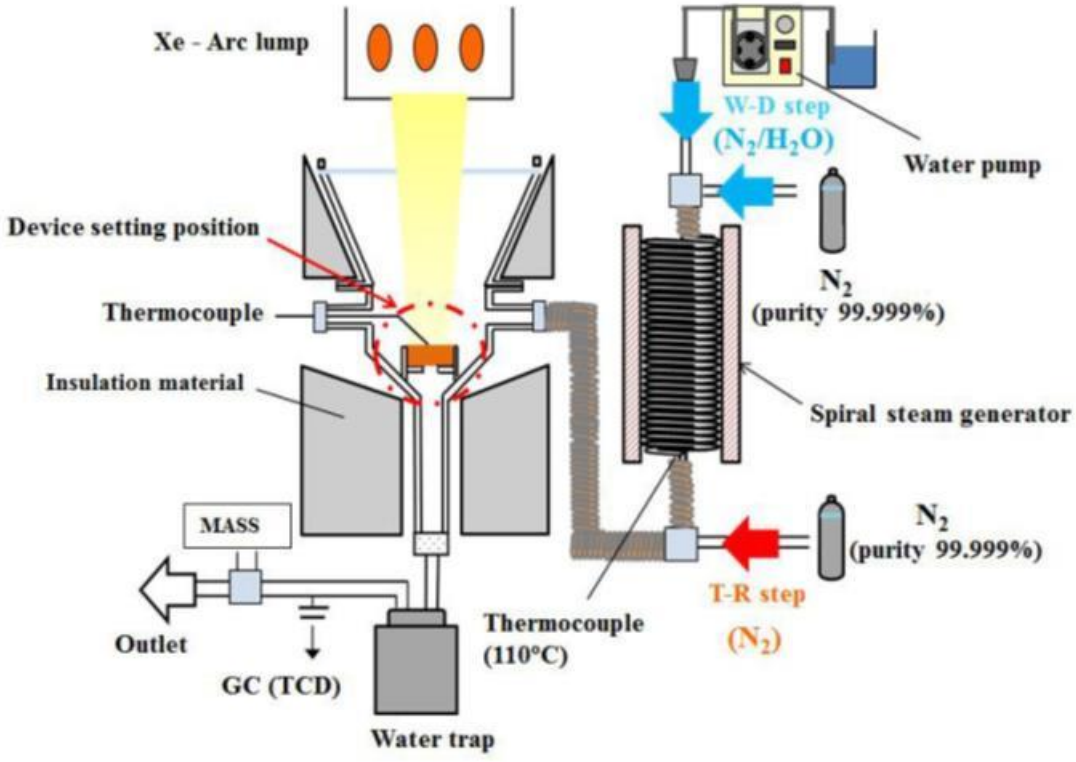

Figure 19: Ceramic foam reactor used by Niigata University to study the $NiFe_2O_4$ and ceria redox cycles

Source: (Kawakami, Myojin et al. 2014))

Structured, directly irradiated receiver/reactors with moving parts

CR5 metal redox reactor

In 2006, the research group at SNL developed the concept of a rotating reactor, referred to as the 'counter-rotating-ring receiver/reactor/recuperator', or CR5 (Diver, Miller et al. 2008). It features a stack of counter-rotating rings with thin fins along the perimeter, which contain the ferrite reactant supported on a refractory material. On the front side of the reactor, which is exposed to the aperture, the metal oxide fin is heated by the concentrated solar radiation under vacuum conditions to remove the released O_2. The stack rotates 180° to the off-solar side, where the steam reoxidises the reduced material, producing H_2 (Figure 20). The configuration of the CR5 facilitates the removal of the product gases, and the isolated reaction zones allow the separation of the solid and gaseous products. Previous analyses suggest that thermal efficiencies of about 50% are possible with this configuration. However, under experimental conditions, the solar-to-fuel efficiency fell to 1.5%. This result was mainly attributed to very high re-radiation losses through the aperture, and some parasitic energy losses from pumping and inert gas flow.

Much of the on-sun testing with the CR5 reactor was performed with four and eight-ring units, using thin ceria fins attached to a zirconia-based carrier that is in turn attached to a metal hub. These units demonstrated proof of concept for CO_2 splitting over short runs on-sun. However, when the scaled-up version containing 22 rings was tested, operation ceased shortly after start-up when several of the rings ceased to rotate due to cracking/separation of zirconia wedge segments at the metal/zirconia connection points.

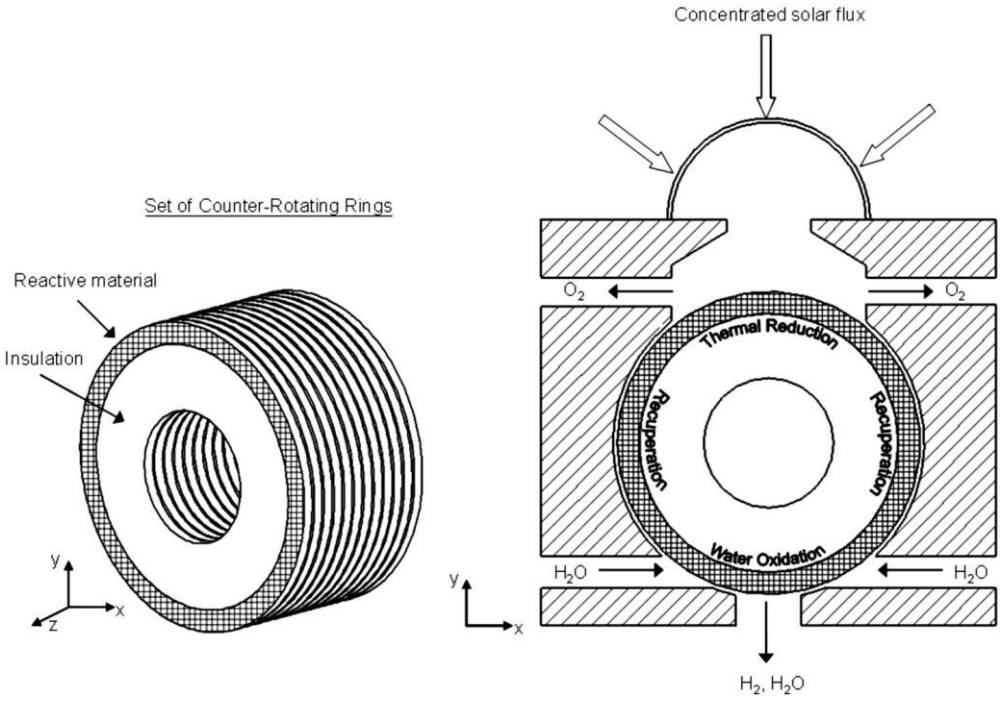

Figure 20: Schematic of the CR5 redox reactor

Source: (Diver, Miller et al. 2008)

The University of Minnesota rotating reactor

Researchers at the University of Minnesota have proposed another version of a rotating reactor (Lapp and Lipinski 2014). The basic idea involves heat recuperation from a rotating hollow cylinder of a porous reactive material to a counter-rotating inert solid cylinder via radiative heat transfer (Figure 21). The outer cylinder containing the reactive medium cycles between the high-temperature reduction and low-temperature oxidation zones, while the inner cylinder acts as an inert, heat-recuperating solid. Heat-transfer modelling predicted heat recovery effectiveness of more than 50% if thin cylinder walls and rotation periods of several minutes were employed. However, no actual on-sun experimental work using this concept has yet been reported.

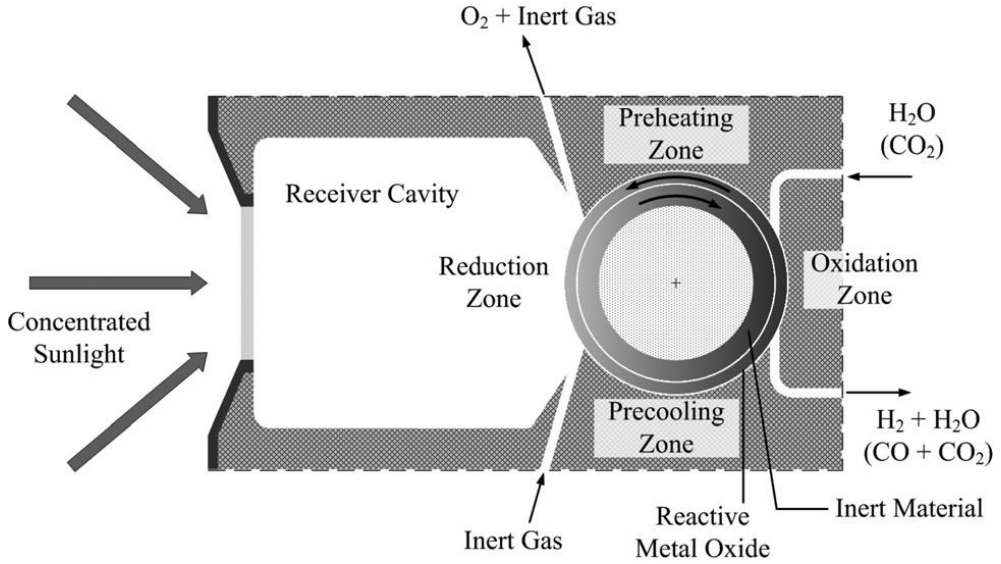

Figure 21: Schematic of the University of Minnesota University rotating redox reactor concept

Source: (Lapp and Lipinski 2014)

6.3 Thermal efficiency of metal oxide/redox cycles

The overall thermal efficiency of the metal oxide/redox route depends on many factors, such as the operating temperature, the extent of reduction and oxidation per cycle, and the efficiency of recuperation and use of high-temperature sensible heat. Although no cycle has yet achieved a thermal efficiency approaching that required for a practical process, several research groups have evaluated the influence of key process variables and operating strategies on the overall cycle thermal efficiency.

6.3.1 Thermal efficiency of the idealised Fe_3O_4/FeO cycle

The importance of both extent of reaction of the active material and the need for effective sensible heat recovery can be illustrated by the following analysis of data published by investigators from Sandia National Laboratories. The researchers exploring the thermal-to-chemical energy efficiency of an idealised Fe_3O_4/FeO cycle: perhaps the most challenging cycle in terms of the severity of its operating conditions (Diver, Miller et al. 2008). The basic heat flow data was taken from the paper and converted to SI units. The analysis was then extended to explore some of the sensitivities of the system. While this evaluation is based on an idealised iron oxide redox cycle, it can also be conducted for the other redox cycles considered in this report.

Figure 22 shows the basic heat flows for the idealised iron oxide cycle in which magnetite (Fe_3O_4) is reduced to wustite (FeO) in the high-temperature step. This requires 242.1 kJ of solar thermal input at 2300 K for the production of 1 mole of hydrogen, according to the thermodynamic calculations (Diver, Miller et al. 2008). The hydrogen has a HHV of 285.8 kJ.

The oxidation of FeO to Fe_3O_4 is exothermic, yielding 68.9 kJ of thermal energy. Heating the oxidised Fe_3O_4 from 700 K to 2300 K requires a further energy input of 497 kJ, while cooling the reduced FeO requires the removal of 394.8 kJ. Other heat inputs needed for the cycle are latent heat to evaporate the water (46.5 kJ) and sensible heat to produce superheated steam for introduction to the reactor (7.9 kJ). Finally, the sensible heat in the oxygen and hydrogen product streams, which amounts to 35.3 and 8.7 kJ, respectively, also needs to be removed.

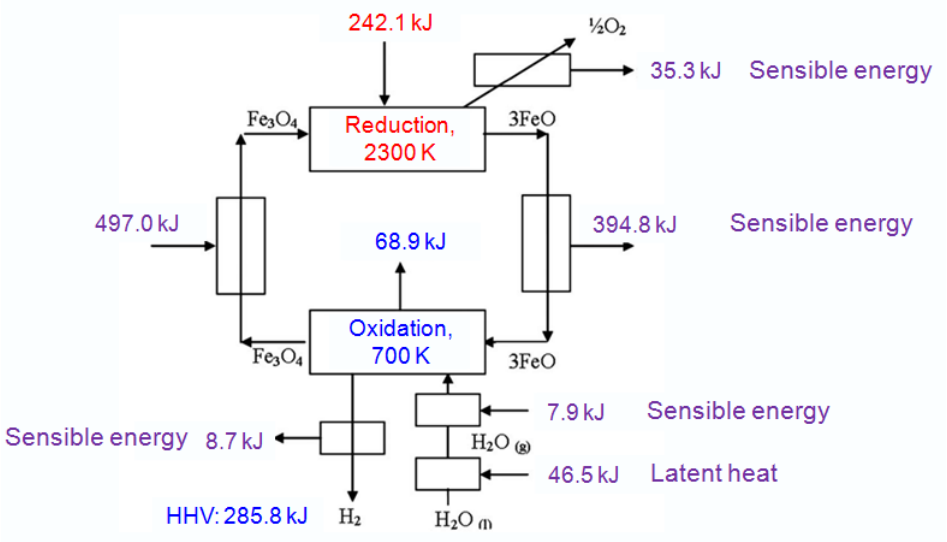

Figure 22: Basic heat flow diagram for an idealised thermochemical water-splitting cycle based on iron oxide

Figure 23 shows more clearly the thermal energy input streams to the cycle (in the red ovals). The total heat requirement is 793.5 kJ, while the stored chemical energy in the product hydrogen is 285.8 kJ. This suggests that an efficiency of 36.0% is possible, even without recuperating any of the thermal energy required for heating the active material to 2300 K. This would require complete reduction of the magnetite to wustite; that is, the material would need to be 100% active.

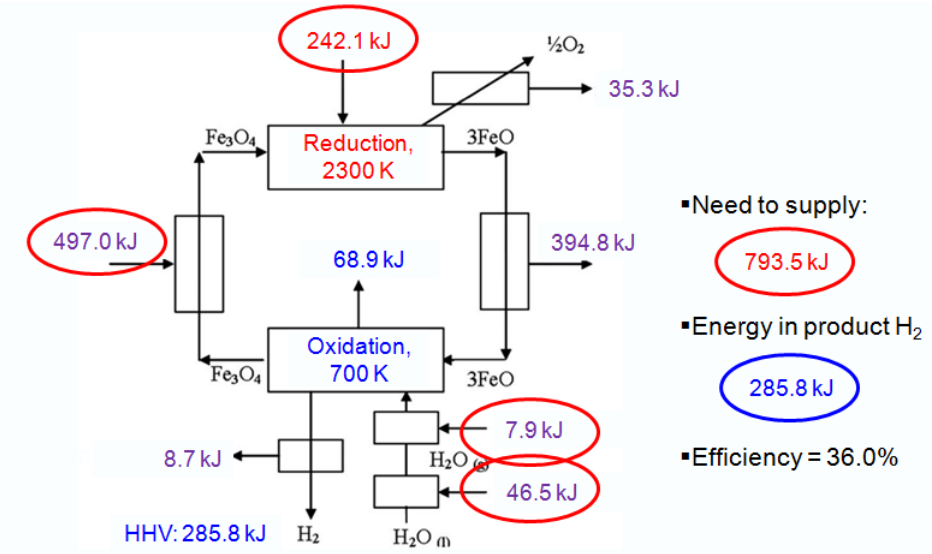

Figure 23: Energy inputs and overall thermal efficiency in an ideal cycle with complete oxidation and reduction of the active material

In practice, it is not possible to fully reduce or reoxidise all the active material in a thermochemical cycle. Diver et al. (2008) suggest that a more realistic figure for the amount of magnetite reduced is 35%. This means that 65% of the material is simply being cycled between the high and low temperatures, resulting in an extra demand for thermal energy to heat the material to 2300 K, and an extra cooling requirement to cool all the material back to 700 K. The heat flows for such a scenario are shown in Figure 24. This reduces the thermal efficiency of the cycle to 16.7%, which is below the performance considered to be required to make thermochemical hydrogen production more efficient than concentrating solar power plus alkaline electrolysis (target = 29%).

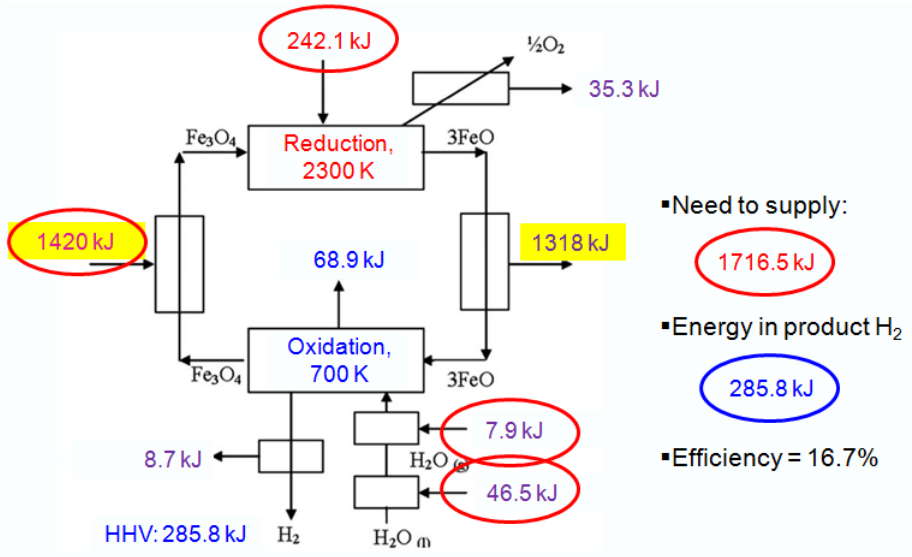

Figure 24: Energy inputs and overall thermal efficiency in an ideal cycle with 35% activity of the active material

Diver et al. (2008) suggest that recuperation is critical in these circumstances, and was one of the main considerations behind the counter-current rotating-ring design of the CR5 reactor. In this design, the reduced material exchanges heat by radiation with oxidised material on adjacent rings. However, this process requires a positive temperature difference over the entire rotation of the ring, and there is a pinch point in the process due to the melting points of the two iron oxide species: Fe_3O_4 (1870 K) and FeO (1650 K). This is shown in Figure 25, where an extra sensible energy input is required to maintain a positive temperature gradient throughout the rotation. The additional heat requirement was calculated by Diver et al. (2008) to be 67.1 kJ when converted to SI units.

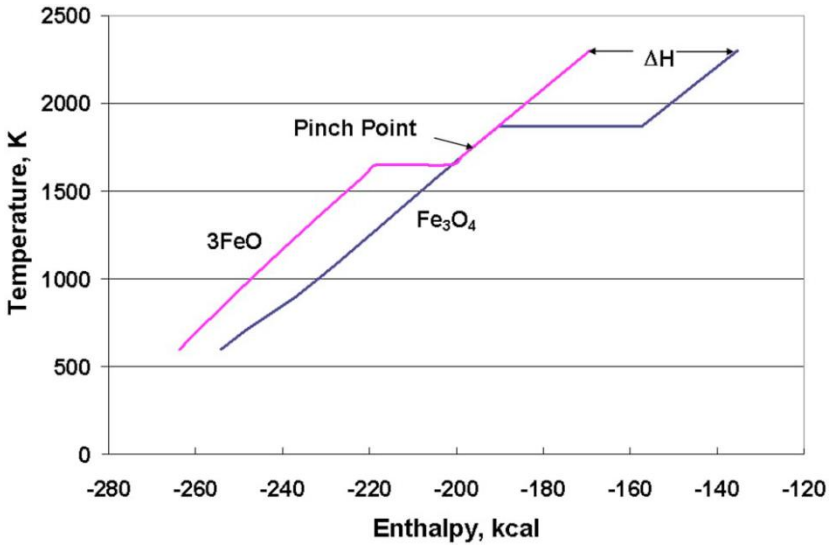

Figure 25: Pinch point diagram showing the requirement for an extra input of solar heat to maintain a temperature difference in the heat exchange process

Figure 26 shows the energy flows in a system in which all of the low-temperature heat inputs (<700 °C) are recovered from the sensible energy from the heat of reaction of the magnetite and the hydrogen product stream. There is an extra input of solar thermal energy (red ovals), and 430.1 kJ is recuperated from the high-temperature oxygen stream and the active material as it is cooled from 2300 K to 700 K. The energy flows (green ovals) are expected to be internally managed to provide preheating and water evaporation, using the heat of reaction from the oxidation reaction and the sensible heat in the product hydrogen.

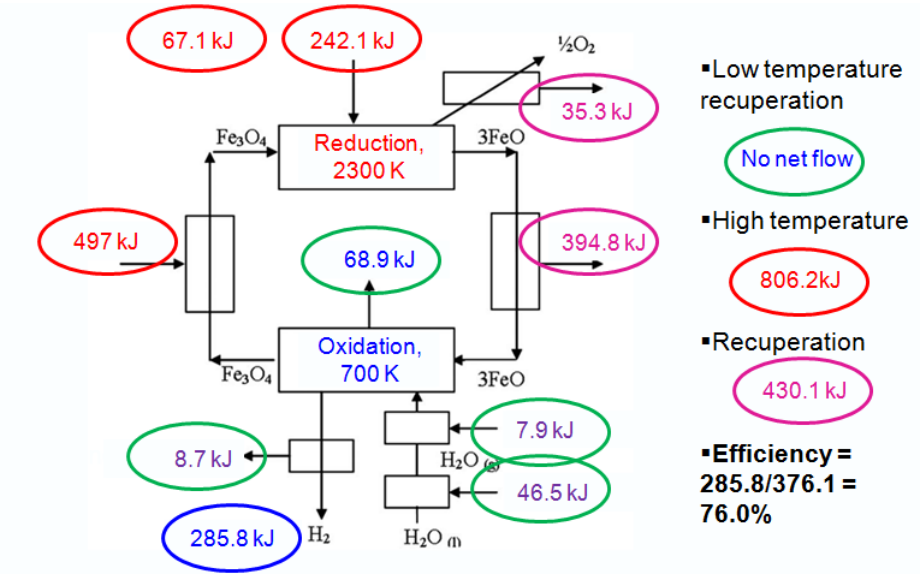

Figure 26: Energy flows in an ideal system with perfect recuperation and 100% activity of the redox material

Figure 27 shows the same scenario when only 35% of the redox material is active, but recuperation is 100% effective. While this significant increases the amount of energy to be recovered, there is no difference in the overall efficiency.

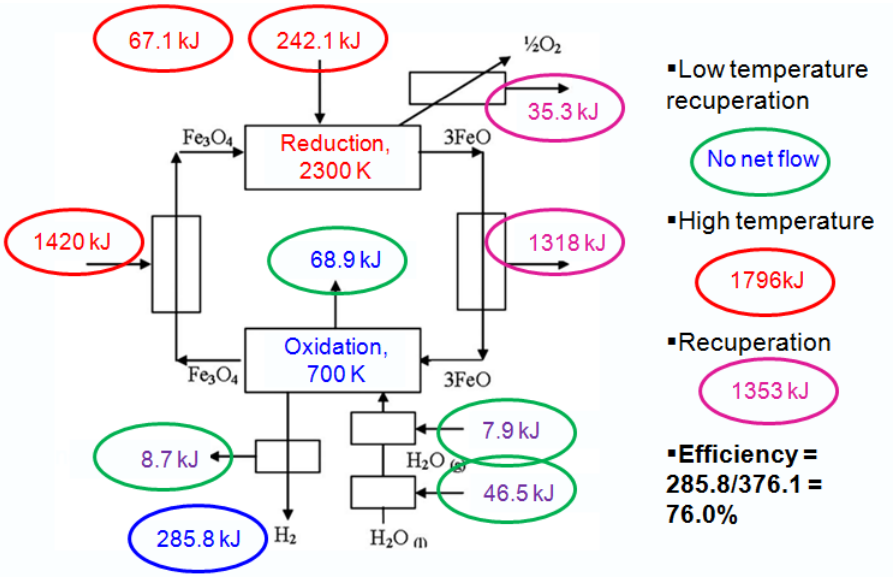

Figure 27: Energy flows in an ideal system with perfect recuperation and 35% activity of the redox material

Naturally, the amount of energy that can be recuperated is limited, and 100% efficiency would be impossible to attain. The following additional scenarios were considered:

- With 35% activity of the redox material and 80% efficiency in the high-temperature recuperation, the efficiency drops to 44.2%.
- With 5% activity of the redox material and 80% efficiency in the high-temperature recuperation, the efficiency drops to 12.2%.
- With 5% activity of the redox material, the recuperation efficiency would need to be 97% to attain an efficiency of 40%.

The above analysis clearly indicates the critical influence of both the amount of redox material that is active, and the efficiency with which the high-temperature energy can be recuperated, on the overall thermal-to-chemical efficiency of a thermochemical redox cycle such as this. This discussion is a somewhat extreme case, given the large difference between the reduction and oxidation temperatures for the active material. Most systems currently being studied have a significantly lower temperature difference: perhaps 200 to 400 K. This naturally reduces the amount of energy that must be recuperated. However, to limit the amount of sensible heat lost due to cycling inactive material through the temperature swings, it is still essential to maximise the amount of redox material participating in the redox reactions.

6.3.2 Thermal efficiency analyses for the ceria cycle

The solar-to-fuel efficiency ($E_{S\rightarrow F}$) has been defined by the ETH/PSI group (Furler, Scheffe et al. 2012) as:

$$\boldsymbol{E_{S\rightarrow F} = \left(\frac{r_{fuel} * \Delta H_{fuel}}{P_{solar} + r_{inert} * E_{inert}} \right) * 100} \quad (37)$$

where ΔH_{fuel} is the HHV of the fuel product (H_2 or syngas), r_{inert} is the total amount of fuel produced, and P_{solar} is the solar energy entering the reactor's cavity. The system-specific parasitic energy, $E_{penalty}$, consists of energy required for electricity and the production of inert gas (usually N_2 from air), or vacuum generation if this is used instead of inert gas. Note that the equation does not include the optical efficiency of the solar concentrating field, or any spillage of solar energy that does not enter the receiver aperture.

Thermodynamic analyses of the ceria cycle indicate the potential for reaching solar-to-fuel efficiencies of 20% in the absence of heat recuperation, and exceeding 30% by recovering the all of the sensible heat of the hot products (Chueh and Haile 2010; Lapp, Davidson et al. 2012; Scheffe and Steinfeld 2012).

Such solar-to-fuel efficiencies have not yet been approached in practice, with the values (as determined by equation 37) reported to date being less than 5%, and generally 0.7–3.5% (Chueh, Falter et al. 2010; Furler, Scheffe et al. 2012). However, these low figures are at least partly the result of the small-scale nature of the experiments, in which heat losses by all three modes (conduction, convection and radiation) would be disproportionately large, and that do not include sensible heat recuperation.

A techno-economic analysis for the production of methanol from H_2O and CO_2 via solar redox cycles indicates that with a solar-fuel efficiency of 20% and an overall efficiency from solar to methanol of 7.1%, the fuel price would be competitive with other renewable technologies for methanol production (Kim, Johnson et al. 2012).

Researchers at the University of Minnesota conducted a detailed thermodynamic analysis of the ceria cycle to demonstrate the importance of both solid and gas-phase heat recovery on the solar fuel-to-chemical efficiency (Lapp, Davidson et al. 2012). They analysed the effect of heat recovery from the metal oxide and the hot product gas on the efficiency of a hypothetical, dual-zone, solar thermochemical reactor used for ceria reduction and H_2O splitting. The system was assumed to

operate at atmospheric pressure, with nitrogen (separated from air) as a sweep gas to reduce the O_2 partial pressure.

In all cases, the Lapp et al. study assumed that complete reoxidation of the partially reduced ceria is achieved in a separate H_2O-splitting step, operated at 1073 K. This is the maximum temperature at which the available experimental data indicated that complete oxidation of the partially reduced ceria was possible. The reduction reactor was assumed to be located in an isothermal blackbody cavity receiver incurring re-radiation losses. The non-stoichiometry or reversible oxygen capacity, being dependent on both the reduction temperature and O_2 partial pressure, was investigated in the range of 0–0.25. Note that the higher end of this range far exceeds anything achieved to date in the laboratory.

The efficiency was very dependent on the solar concentration ratio, which was varied between 1,000 and 10,000 suns, since the higher this ratio the more efficient the solar absorption. For perfect heat recovery from both the gas and solid phases, solar-to-chemical efficiency (based on the solar energy entering the receiver) is limited only by the re-radiation losses through the cavity, ignoring any convective losses and those from the receiver external surface by conduction.

The peak efficiency, on a LHV basis without any heat recovery, varied between 1.7% and 5.1% over the above range of solar concentration ratios. At a concentration ratio of 3000, the maximum efficiency with no heat recovery was 3.7% at a reduction temperature of 1980 K. At the same reduction temperature, perfect heat recovery increased the efficiency to almost 40%.

In view of the large effect of the concentration ratio on efficiency, Lapp et al. recommended that this type of technology be used in conjunction with solar dish concentrators, rather than solar towers.

The O_2 partial pressure (P_{O2}) in the reduction reactor also has a large influence on overall efficiency. With increasing P_{O2}, the relative gain from gas-phase heat recovery decreases, due to lower volumes of heated gas from which to recover sensible heat. For example, increasing the gas heat recovery from 0 to 90% results in a sixfold increase in efficiency for $P_{O2} = 10^{-3}$ atm, versus a threefold increase for $P_{O2} = 10^{-2}$ atm.

Unlike gas-phase heat recovery, solid-phase heat recovery has greater potential for efficiency improvement with increasing P_{O2}, since increasing P_{O2} leads to more ceria being cycled in the reactor for a given solar input power. Hence, solid-phase heat recovery becomes more important. For $P_{O2} = 10^{-3}$ atm, increasing solid-phase heat recovery from 0 to 90% increases efficiency by a factor of 1.34, while at $P_{O2} = 10^{-2}$ atm, this factor is 1.66.

Efficiency can also be increased by improvements in the thermodynamic properties of the ceria: namely, an increase in the non-stoichiometry or reversible oxygen storage capacity. For example, if the reduction temperature is increased from 1850 to 2000 K, the non-stoichiometry of undoped ceria is claimed to increase from 0.025 to 0.059. At 2000 K, with 80% solid-phase heat recovery, advanced materials can only increase efficiency from 13.5 to 17%, while at 1850 K, advanced materials can increase efficiency from 11.9 to 19.5%: a higher maximum value due to decreased re-radiation losses and gas preheating.

Lapp et al. claimed that the same overall analyses were conducted for CO_2 splitting, and that cycle efficiencies matched those for H_2O splitting to within 0.2%.

6.4 Issues and challenges for non-volatile metal oxide/redox cycle for H_2O and/or CO_2 splitting

Challenges specific to non-volatile metal oxide cycles fall into three broad categories: the reactor, the working redox active materials, and systems-related considerations. Achieving commercial viability in a reasonable timeframe will require rapid and continuous advances to improve efficiency and durability, which will drive down anticipated cost and resource intensity. Several research groups have designed, built, and operated proof-of-concept prototypes, in which the intent has been to demonstrate the feasibility of the new approach, not necessarily create an early version of a commercial reactor design. Prototype reactors have produced H_2 from water and CO from CO_2 at measurable efficiencies, but need substantial performance improvements before they will be commercially interesting.

Non-volatile metal oxide reactor research focuses on three main areas:

- **New materials**: optimised thermodynamics, kinetics, transport (electron, ion, heat) properties, and structures – gas-surface, radiation-surface, physical properties
- **Solar reactor:** design for efficiency, sensible heat recuperation, ease of fabrication, ease of maintenance
- **Systems**: resolve issues of solar variability (diurnal, seasonal, and clouds), and 24/7/365 downstream, relatively steady, production of fuel and efficient separations.

The following issues and challenges are essentially common to all non-volatile metal oxide options:

- The efficiency that is realised in practice is a function of the extent of reaction, and the type of reactor in which the process is implemented. The possible extent of reaction is also limited by thermodynamics, such as the temperature and oxygen partial pressure, but may also be limited by factors such as heat and mass transfer. Mass transfer, in turn, is influenced by fundamental material properties, reactor configuration and material geometry. Beyond these considerations, a suitable thermochemical material will be stable to both physical and chemical degradation (e.g. erosion, volatilisation, sintering and formation of undesirable phases) over many thousands of cycles and hours of operation.
- Extremely high temperatures (1800 to >2000 K) are required for the reduction part of the cycle. This results in more costly (higher precision) solar field and containment materials, and large T^4 radiation (and possibly also convective) heat losses.
- The overall performance of a cycle is dependent on its reversible oxygen capacity: i.e. the difference in the oxygen non-stoichiometry between the reduction and oxidation steps. To maximise this parameter, very low O_2 partial pressures and very high reduction temperatures are needed. The former is achieved by either using large, energy-consuming vacuum pumps or large quantities of high-purity, costly inert sweep gas: most likely N_2 separated from air in any commercial application. The latter can result in excessive aperture radiation losses and the need for expensive materials of construction. The separation of O_2 from the sweep gas prior to its

recycle to the reduction step and the generation of a high vacuum are both problematic, energy-intensive processes.

- Hydrogen production is only at atmospheric (or even sub-atmospheric) pressure. Hence, there are high compression requirements for its ultimate end-use application (e.g. Fischer–Tropsch liquid fuels, ammonia or export to Japan as liquid hydrogen).
- Solids degradation (e.g. sintering) during the continual thermal cycling between reduction and oxidation temperatures is a serious issue. Partial evaporation and loss of metal redox material can also occur at extremely high reduction temperatures (e.g. in the ceria cycle).
- The kinetics of the oxidation step and the overall H_2 and/or syngas yields can be seriously limited by blinding/shrinking core chemical reaction issues.
- The input solar flux and thermal reduction kinetics need to be coupled in such a way that heat flux does not outpace that determined by the kinetics of the reduction step. Otherwise, the reduction temperature will increase beyond the desired level, and thereby increase the aperture radiation losses. The converse is the case if the solar flux is below that required by the kinetics (i.e. the net reduction level will decrease due to the reduced temperature).
- The importance of efficient sensible heat recovery on the overall cycle thermal efficiency is illustrated by the aforementioned idealised thermochemical analysis for the Fe_3O_4/FeO cycle, and the thermodynamic studies conducted on the ceria cycle. This shows that for the iron-based cycle operating at a reduction temperature of 2273 K and an oxidation temperature of 623 K, the maximum solar thermal-to-chemical efficiency that can be obtained is only 36%. However, if sensible heat is recovered from the cooling step and used to reheat the working oxide, the maximum possible solar-to-fuel efficiency is increased to 76%. This would overcome the major impediment to high-efficiency thermal recuperation between solids in efficient counter-current arrangements. While the above efficiencies will not even be approached in practice, this does highlight the need for effective thermal management and heat recuperation systems to be incorporated into the design of the receiver/reactor during scale-up.
- The solar-to-fuel thermal efficiencies achieved to date (a maximum of around 3.5% for the ceria cycle) are much lower than the generally recognised target of 20% for the redox option to be a potentially viable renewable means of generating hydrogen and/syngas. To some extent, this is the result of the small-scale experiments and the lack of heat recuperation. Major improvements in redox materials, reactor design and sensible heat recovery and use are required if this efficiency target is to be reached.
- Critical to future cost reduction is the ability to maximise conversion efficiency and thereby reduce the size of the solar field, which is likely to be the major cost component. Thermal management – including recuperation, storage and possible back-up power – is also very important.

The main challenge facing the metal oxide/redox option is the need for a material with much higher reversible oxygen storage capacity than current materials. This can best be illustrated by the following quote from Ermanoski (2015):

> ‘To illustrate the importance of oxide mass flow rates, consider the replacement of all coal-derived electricity in the United States (172 GW) with H_2. This scenario would require roughly

287 GW H_2 chemical flux (assuming a H_2-to-electricity efficiency of 60%) or a H_2 production rate of approximately 200 kg/s. For a reversible oxygen storage capacity of 0.03, the required ceria flow between the reduction and oxidation steps would be approximately 1.6 X 10^{11} kg/day. This value is much larger than the US coal consumption for electricity generation of approximately 2 X 10^9 kg/day. Even considering the differences between the long-range transport of coal and the internal oxide transport in a power tower type of structure, it is evident that low values of the reversible oxygen storage capacity have staggering solids transport implications when large scale H_2 production is considered, thus indicating the need for materials and operating conditions with much higher yields than ceria'.

While the non-stoichiometric perovskites have a reversible oxygen storage capacity some 5–10 times that of ceria, further development of redox materials is required for this option to become a viable means of H_2O and/or CO_2 splitting.

Overall, the main challenge facing the metal oxide/redox cycle route for H_2O/CO_2 splitting is finding cost-effective materials that can operate at lower reduction temperatures than current ferrite or ceria-based systems. These materials must have sufficient activity to minimise the above challenges and also achieve an annual solar-to-fuels energy efficiency of more than 20%, while being cheap to produce. Non-stoichiometric perovskite materials show some promise as effective redox materials, due to their amenability to doping and metal substitution.

7 Other redox (sulfur-based) cycles for H_2 production from H_20 splitting

Sulfur cycles were primarily developed for coupling with high-temperature heat from nuclear fission power plants. The main work has been carried out by General Atomics and Westinghouse in the United States, the European Joint Research Centre in Ispra, Italy and the Japan Atomic Energy Research Institute (now Japan Atomic Energy Agency).

Most of the processes are based on the thermal splitting of sulfuric acid into sulfur dioxide and oxygen. Even with efficient catalysts, this process requires temperatures above 850 °C. Since no very-high-temperature reactor is yet in operation, concentrated solar energy is the only available heat source that can be coupled to the cycles at a large scale. Note also that no solar plant has yet been coupled to a chemical process, although the hurdles to build one are considered to be lower than coupling to a very-high-temperature reactor.

A major advantage of the processes is their close relationship to sulfuric acid production. Although the high-temperature step – the decomposition of sulfuric acid – has currently only been demonstrated with a solar input at the 10-kW range, it is considered to be scalable.

7.1 Hybrid sulfur cycle (Westinghouse, ISPRA Mk 11)

The hybrid sulfur cycle (also known as the Westinghouse HyS Cycle) is a hybrid electrochemical–thermochemical cycle. Evaluations under the International Energy Agency Hydrogen Implementing Agreement's Task 25 'High-temperature processes for hydrogen production' and other parallel studies have ranked this cycle as the most promising of those currently under development. The original development efforts on the HyS cycle were focused on nuclear sources, since these were considered to be more economic than solar power for H_2 production. However, more recent work on this cycle has used concentrated solar energy as the heat source for sulfuric acid decomposition.

The cycle consists of the following steps: the thermal splitting of sulfuric acid into SO_3 and H_2O (Reaction 38), followed by thermal decomposition of SO_3 into SO_2 and O_2 (Reaction 39). After separating the SO_2 from O_2, the electrochemical oxidation of SO_2 with H_2O produces sulfuric acid and hydrogen (Reaction 40) to complete the overall water-splitting cycle and reactant regeneration.

$$H_2SO_4 \rightarrow H_2O + SO_3 \ > 723\ K \tag{38}$$

$$SO_3 \rightarrow SO_2 + \frac{1}{2}O_2 \ > 1123\ K\ with\ catalyst\ (> 1423\ K\ without) \tag{39}$$

$$2H_2O + SO_2 \rightarrow H_2SO_4 + H_2\ electrolysis, 353\ K \tag{40}$$

The process is a hybrid cycle, because it combines the thermal decomposition of sulfuric acid with the electrochemical oxidation of SO_2. The voltage needed for SO_2 electrolysis is only 0.17 V, much lower than the 1.23 V required for water electrolysis.

Catalysts are available for the SO_3 reduction at 1123 K; these are mainly based on iron oxide. The kinetics of the reaction are much faster if higher temperatures are available, but it is not yet known whether higher temperatures are economically more efficient than the catalysed reaction. Reactors used in laboratory tests have been made of glass or fused silica. Solar reactors are mostly constructed from ceramics such as silicon carbide, but steel has also been used (Noglik 2009).

Due to limited development support, the present size of available SO_2 electrolyser technology is limited to the 100-W range. However, the electrolysers show excellent efficiency and scale-up seems to be possible.

The ongoing European SOL2HY2 project aims to demonstrate all of the key steps in the HyS cycle, including the operation of a sulfuric acid decomposition reactor of several hundreds of kW-scale on a solar tower in 2016. Outotec, one of the major producers of sulfuric acid and sulfuric acid production technology, is a partner in this project. A brief summary of the project is given below.

7.2 The SOL2HY2 project

The three-year European SOL2HY2 project was initiated in June 2013. Its objectives were to develop materials for the challenging environments existing in the electrolyser, sulfuric acid decomposer and balance-of-plant components, and to develop optimum designs for the complete process, which must be tailored to specific solar input and plant site location. Solutions have been found for some of these challenges, but materials stability issues, costs and sustained operation of the complete solar-based HyS-plant still remain to be demonstrated.

Large-scale (400–800 MW) hydrogen production plant concepts based on the HyS cycle are unlikely to achieve H_2 costs below 3.0–3.5 €/kg, without further improvements in the technology. For smaller-scale plants, which might be more practical in the foreseeable future, the H_2 costs are likely to be even higher.

While the SOL2HY2 project recognises that the closed-loop solar HyS cycle remains the best long-term solution, the further development of the key components and subsystems is best conducted in a stage-wise manner. In this context, the research group decided to initially investigate the integration of solar energy with the Outotec® Open Cycle. This involves step (2) of the closed HyS cycle (Reaction 40 above), in which hydrogen and sulfuric acid are produced by SO_2-depolarised electrolysis (SDE). The SO_2 used in the process can be obtained from metallurgical smelting sulfur combustion and other industrial processes. Operation in the open cycle mode potentially allows short-term opportunities for smaller-scale co-production of hydrogen and sulfuric acid from sources of SO_2 destined for sulfuric acid production, without disrupting the supply of the acid. It also demonstrates one of the key steps in the closed-loop HyS cycle.

Ultimately, the aim of the project is to close the cycle by including the solar-driven sulfuric acid decomposition step (reactions 38 and 39), which the researchers plan to demonstrate in 2016 at the scale of several hundreds of kilowatts.

Key results obtained at mid-term (December 2014)

- Preparation of detailed process flow sheets and design for the entire cycle (including sulfuric acid decomposition) combined with thermodynamic and energy efficiency analyses. With maximum recovery and use of high-temperature heat from the sulfuric acid decomposition step, overall process thermal efficiencies of up to 30% appear to be feasible.
- The above task included the thermodynamic analysis of the SO_2–H_2SO_4–H_2O system as required to determine the maximum possible performance of the SDE step. These data were used to prepare simulation models for the controlled water transport and management of the electrolyser. A laboratory-scale, 100-cm^2 SDE cell and a small cell for membrane and catalyst characterisation were constructed and operated during this period.
- For SDE, a cost-effective option chosen for bipolar plates was gold-plated steel, which have been tested in 11 experimental SDE campaigns. The challenge of SO_2 cross-over as a parasitic reaction was observed, and the possibility of its minimisation by optimising catalyst load was demonstrated. To evaluate scaling-up effects, a five-cell SDE stack has been constructed and commissioning tests have begun.

In addition to the above work on the SDE step, the following activities were conducted on the SO_3 decomposition stage of the closed-loop HyS cycle:

- Relevant parameters of the model of the SO_3 decomposition chamber of the solar reactor were correlated with experimental results taken from the 10-kW_{th} solar reactor, which was operated in the DLR solar furnace. For a likely operating point of an industrial system (750 kW/m^2 direct normal irradiance and 0.45 $kg/s/m^2$ SO_3 mass flow rate), both the thermochemical efficiency and chemical conversion could be maximised. Additionally, the optimum reactor length of the scale-up system was identified, showing that the highest process efficiency can be achieved with a solar absorber having a length of about 1 m. Based on these findings, a computational fluid dynamics model of the solar receiver has been developed and used to support the process design work.
- Two designs were conducted for the porous materials inside the solar absorber/reactor. Various catalyst support structures were produced, and different catalysts supported on Al_2O_3 were tested. Prototypes of the sectioned solar absorber consisting of SiC foam structures were manufactured as proof of the feasibility of the design concept.
- Several catalysts have been prepared and tested under sulfuric acid decomposition conditions for up to 100 h each using daily thermal cycles. The most promising options have been selected for further analysis.
- Different cases for solar-to-heat configurations were evaluated for the Almeria site for January and July conditions (thermal power production, direct normal irradiance, and basic design option based on peak, annual average or minimum values). The main outputs considered were mirror field surface, thermal storage size, salt consumption, backup energy integration and thermal energy.

The SOL2HY2 research group claims that the project is on schedule to meet all major milestones and deliverables at the end of its duration (June 2016).

7.3 Sulfur–iodine cycle (General Atomics ISPRA Mark 16)

The second widely investigated sulfur-based process is the sulfur–iodine water-splitting cycle, also known as the ISPRA Mark 16 or General Atomics process (Brown 2003). Like the hybrid sulfur cycle, it was originally developed to split water using high-temperature heat from nuclear power plants. The three cycle steps are:

$$2H_2O + SO_2 + xI_2 \rightarrow H_2SO_4 + 2HI_x \; 300 - 400\; K \tag{41}$$

$$2HI_x \rightarrow xl_2 + H_2 \; 400 - 1000\; K \tag{42}$$

$$H_2SO_4 \rightarrow H_2O + SO_2 + \frac{1}{2}O_2 \; 1120 - 1200\; K \tag{43}$$

All three reactions are performed in separate sections of the plant, with the Bunsen reaction (reaction 41) and the sulfuric acid decomposition (reaction 43) run in parallel to avoid SO_2 storage (Figure 28).

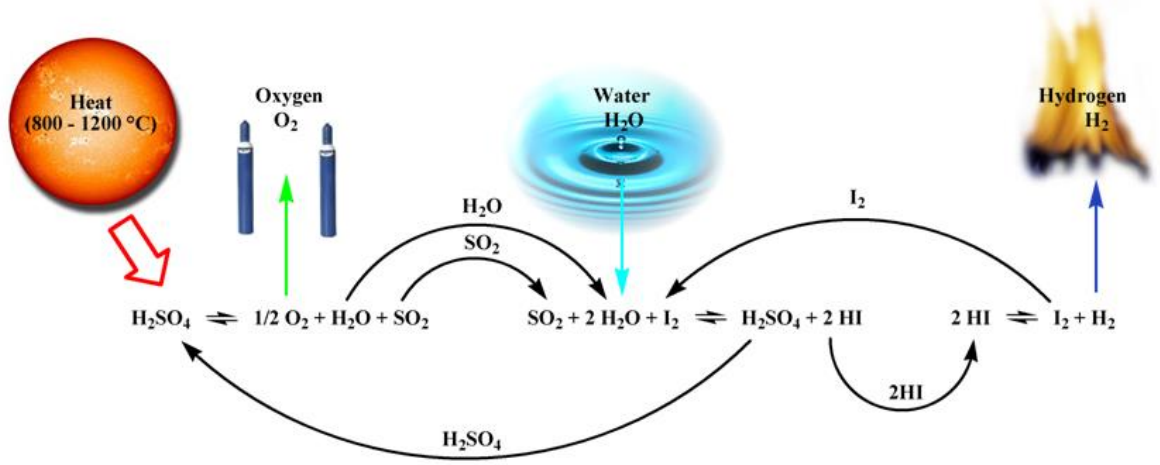

Figure 28: The sulfur–iodine water splitting process concept

General Atomics conducted an active research program on the sulfur–iodine process from the mid-1970s through the mid-1980s. The feasibility of the individual sections of the cycle was successfully demonstrated in a glass, quartz and Teflon laboratory-scale apparatus, while the sulfuric acid decomposition step was tested on the solar power tower of the Georgia Institute of Technology. The sulfuric acid splitting step was also demonstrated recently within the European project 'Hydrogen by Thermochemical Cycles' (HYTHEC) (Roeb 2005) and its successor, HyCycleS. The HyCycleS reactor is shown in Figure 29 in the solar furnace of DLR in Cologne, Germany (Roeb 2009).

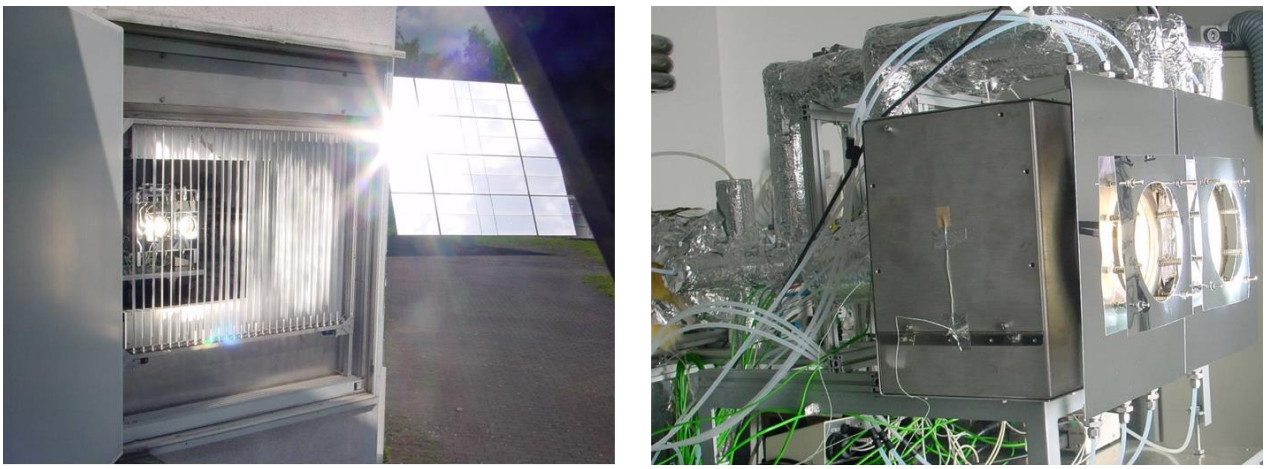

Figure 29: The HyCycleS solar reactor operating in DLR's solar furnace, Cologne, Germany

The decomposition of sulfuric acid and, in particular, hydroiodic acid (HI), reportedly causes severe corrosion problems. The experimental problems described and the less promising economic calculations led to General Atomics reducing the activities on the cycle by the 1980s. But in the 2000s, it was once again the focus of intensive research. An electrically heated pilot plant was set up in a joint venture involving General Atomics, Sandia National Laboratories, and the French Alternative Energies and Atomic Energy Commission (CEA) at the General Atomics site in San Diego, United States. The project is complete, but some of the problems described in the 1980s are still unsolved.

7.4 Issues and challenges for sulfur-based water-splitting cycles

Hybrid sulfur cycle

- Development of a low-cost method for separation of O_2 from SO_2 prior to SO_2 electrolysis.
- Scale-up of the SO_2 electrolysis step from the 100-W to the hundreds of kW scale.
- The challenges given below for the sulfur–iodine cycle in relation to sulfuric acid decomposition will also apply to the hybrid sulfur cycle when it is operated as a closed loop.

Sulfur–iodine cycle

- Identification/development of containment materials able to withstand the highly corrosive conditions in every step of the cycle.
- Development of robust, active iron-based catalysts for the sulfuric acid decomposition step. These catalysts need to maintain their activity over the thermal cycling conditions encountered under real solar conditions.
- Scale-up of the catalytic reactor for sulfuric acid decomposition and its efficient integration with high-temperature solar energy as the method of heat supply.
- Separation of the acids (HI and H_2SO_4) is problematic, and a method that is more effective and less costly than conventional distillation needs to be developed.

Finally, fully integrated operation of the complete cycle (including all key steps and balance of plant), using high-temperature solar energy as the heat source, has yet to be demonstrated at any scale for either cycle.

8 High-temperature steam and CO_2 electrolysis

The efficiency of the electrolytic production of hydrogen can be significantly improved via high-temperature electrolysis of steam. The conventional, low-temperature water electrolysis process for hydrogen production depends on the electrolytic conduction of an aqueous medium, such as alkaline or acid solutions. Most of the energy required for splitting water comes from the electrical energy input to the cell. However, by raising the temperature of the cell, an increasing amount of the energy for decomposing water can be thermal, according to the Second Law of Thermodynamics:

$$\Delta G = \Delta H - T\Delta S \tag{44}$$

and:

$$\Delta G = nFe \tag{45}$$

where ΔG is the free energy of water decomposition, ΔH is the enthalpy of water decomposition, ΔS is the entropy of water decomposition, T is the absolute temperature, e is the voltage of energy of the cell and n is the number of electron equivalents in producing a molecule of hydrogen.

High-temperature electrolysis, in which the feed stocks are in the gaseous or vapour phase, enables CO_2 to be split into CO and O_2. As shown in Figure 30, increasing the temperature significantly reduces electricity consumption in both cases. For example, in the case of steam electrolysis, as the steam temperature rises, the electrical energy requirement decreases as the thermal input increases in a linear fashion. (The total energy input required remains essentially constant.) Increasing the steam temperature from 100 °C (373 K) to 900 °C (1173 K) reduces the electrical energy requirement from around 238 kJ/mol to 180 kJ/mol, while the thermal energy increases from 15 kJ/mol to around 75 kJ/mol. The reduction in electricity requirement with increasing temperature is even more significant for CO_2 electrolysis.

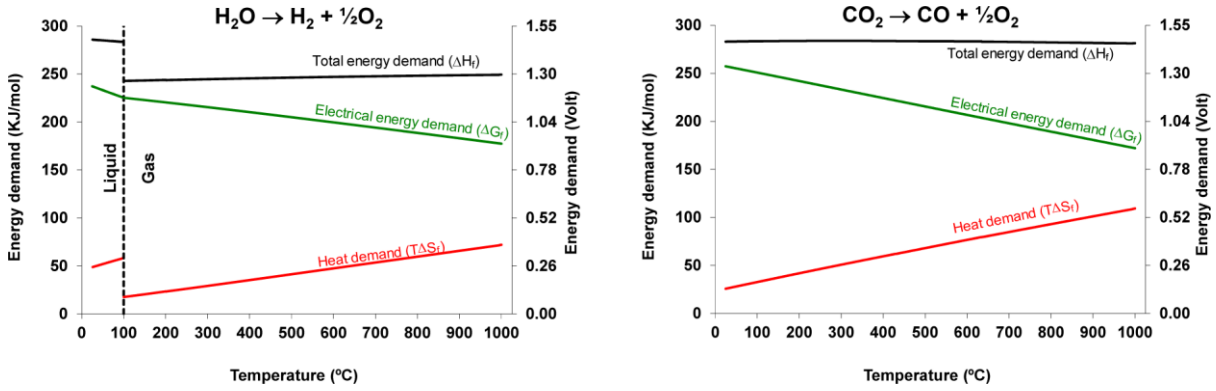

Figure 30: Thermodynamics of H_2O and CO_2 electrolysis at atmospheric pressure

Source: (Ebbesen, S. et al. 2014)

Electrolysis of both H_2O (steam) and CO_2 converts electric energy and heat into H_2 and CO according to the following:

$$H_2O + electric\ energy\ (\Delta G) + heat(T\Delta S) \rightarrow H_2 + \frac{1}{2}O_2 \quad (46)$$

$$CO_2 + electric\ energy\ (\Delta G) + heat(T\Delta S) \rightarrow CO + \frac{1}{2}O_2 \quad (47)$$

The high-temperature electrolysis route for hydrogen and/or syngas production is a purely renewable energy option, if both the heat requirement and the electricity is derived from solar energy or any other renewable resource, such as wind.

The above reactions can be conducted at high temperatures (923–1173 K) in solid oxide electrolysis cells (SOECs). The current status of SOEC technology for H_2O and/or CO_2 splitting has been reviewed in detail (Ebbesen, S. et al. 2014). Some of the key points/issues contained in that review are now briefly discussed.

Since both reactants are in the gas phase, the conduction must occur by ionic means, rather than electrolytic, as occurs in aqueous condensed systems such as conventional alkaline electrolysis. Suitable ionic conductors consist of a porous metal oxide ceramic, usually zirconium oxide (ZrO_2) stabilised with yttrium oxide (Y_2O_3). Electrodes are placed against a thin slab of gas-tight ZrO_2-(Y_2O_3). Typical electrode materials are nickel-cermet for the fuel electrode (cathode) and mixed oxides (perovskites) of lanthanum, strontium and cobalt for the O_2 electrode (anode).

For SOECs, the overall process for H_2O and CO_2 electrolysis is the same: steam or CO_2 is supplied on one side of the ionic conductor. On applying a direct current electrical field, hydrogen or CO form at the cathode, while oxygen ions (O^{2-}) migrate through the ionic conductor and form gaseous O_2 at the anode. In principle, the ionic conductors can be arrayed in various geometric configurations, such as in tubular or planar forms, to produce single cells that can be placed either in parallel or series circuitry to form a battery of cells. These in turn can be hooked up in a bank of batteries to form a large-scale reactor. The need to integrate the high-temperature electrolyser with concentrated solar energy as the heat source will dictate its final size and layout.

One of the critical components of such systems is the electrical connection between the single cell modules, also called the interconnection. Perovskites are often candidates for this; an example is $LaCrO_3$ doped with a divalent alkali earth metal (e.g. Mg, Ca). In high-temperature systems, the use of metallic materials for the interconnection is not possible, due to corrosion and oxidation of the surface at this temperature.

SOEC technology is not yet commercially available. Some of the key issues and challenges that need to be overcome to address this situation are listed below.

8.1 Issues and challenges for solarised high-temperature electrolysis of steam and CO_2

- The high-temperature electrolysis of steam was extensively researched during the 1980s. However, a major breakthrough for this potentially very interesting technology, in terms of using energy from water vapour, was never achieved. This was related to electrode degradation

issues, in particular the oxygen evolution electrodes. However, the rapid advances in solid oxide fuel cell technology may solve some of the previous problems with the SOEC.

- The co-electrolysis of H_2O and CO_2 is more complicated than simply the above two reactions 46 and 47, due to the WGS reaction ($CO + H_2O \rightarrow H_2 + CO$), which can occur in parallel with the electrolysis reaction.
- Electrolysis of CO_2 without the addition of H_2O in SOECs may lead to coke formation on the nickel-based fuel electrodes, since nickel is known to catalyse the dissociation of carbon-containing gases such as CO and CO_2.
- Operating SOECs at high current densities increases the production of H_2 and/or syngas, but with existing SOEC prototypes, significant degradation (increase in cell resistance) occurs at high current densities.
- Cell degradation is observed at both the fuel (cathode) and oxygen (anode) electrodes at high current densities. Weakening of the electrolyte–electrode interface at the oxygen electrode is caused by oxygen evolution and can lead to delamination. The exact degradation mechanism for the fuel electrode is yet to be determined.
- The optimum way of providing the thermal demand of SOECs by solar energy still needs to be determined. For example, it is not known whether this can be provided simply by preheating the H_2O/CO_2, or whether further thermal energy needs to be supplied to the cell itself to maintain the high operating temperature. It is also unknown whether there is scope for solar thermal energy here, or whether sufficient heat is developed by the cell's internal resistance.

References

Abanades, S. and G. Flamant (2005). Production of hydrogen by thermal methane splitting in a nozzle-type laboratory-scale solar reactor. *International Journal of Hydrogen Energy* **30**: 843–853.

Abanades, S. and G. Flamant (2006). Solar hydrogen production from the thermal splitting of methane in a high temperature solar chemical reator. *Solar Energy* **80**: 1321–1332.

Abanades, S. and G. Flamant (2008). Hydrogen production from solar thermal dissociation of methane in a high-temperature fluid-wall chemical reactor. *Chemical Engineering and Processing* **47**: 490–498.

Abanades, S. and H. Villafan-Vidales (2011). CO_2 and H_2O conversion to solar fuels via two-step solar thermochemical looping using iron oxide redox pair. *Chemical Engineering Journal* **175**: 368–375.

Adinberg, R., et al. (2004). Solar gasification of biomass: A molten salt pyrolysis study. *Journal of Solar Energy Engineering* **126**(3): 850–857.

Agrafiotis, C., et al. (2012). Hydrogen production via solar-aided water splitting thermochemical cycles: Combustion synthesis and preliminary evaluation of spinel redox-pair metals. *International Journal of Hydrogen Energy* **37**: 8964–8980.

Agrafiotis, C., et al. (2014). Solar thermal reforming of methane feedstocks for hydrogen and syngas production – a review. *Renewable & Sustainable Energy Reviews* **29**: 656–682.

Agrofiotis, C., et al. (2015). A review on solar thermal syngas production via redox pair-based water/carbon dioxide splitting thermochemical cycles. *Renewable & Sustainable Energy Reviews* **42**: 254–285.

Bhosale, R., et al. (2012). Thermochemical water splitting for hydrogen generation using sol-gel derived Mn-ferrite in a packed bed reactor. *International Journal of Hydrogen Energy* **32**: 2924–2934.

Brown, L. C., Besenbruch, G.E., Lentsch, R.D., Schultz, K.R., Funk, J.F., Pickard, P.S., Marshall, A.C., Showalter, S.K. (2003). High efficiency generation of hydrogen fuels using nuclear power, Final technical report for the period August 1, 1999 through September 30, 2002. General Atomics.

Chambon, M., et al. (2010). Solar thermochemical reduction of ZnO and SnO_2: Characterization of the recombination reaction with O_2. *Chemical engineering Science* **65**: 3671–3680.

Charvin, P., et al. (2011). Experimental study of SnO_2/SnO/Sn thermochemical systems of solar production of hydrogen. *AIChE Journal* **54**(10): 2759–2767.

Chueh, W., et al. (2010). High flux solar-driven thermochemical dissociation of carbon dioxide and water using non-stoichiometric ceria. *Science* **330**: 1797–1801.

Chueh, W. and S. Haile (2010). A thermochemical study of ceria: Exploiting an old material for new modes of energy conversion and carbon dioxide mitigation. *Philosophical Transactions of the Royal Society a–Mathematical Physical and Engineering Sciences* **368**(1923): 3269–3294.

Chueh, W. C., et al. (2010). High-flux solar-driven thermochemical dissociation of CO_2 and H_2O using nonstoichiometric ceria. *Science (New York, N.Y.)* **330**: 1797–1801.

Chueh, W. C. and S. M. Haile (2009). Ceria as a thermochemical reaction medium for selectively generating syngas or methane from H_2O and CO_2. *ChemSusChem* **2**(8): 735–739.

Coker, E., et al. (2012). Oxygen transport and isotopic exchange in iron oxide/YSZ thermochemically-active materials via splitting of C18O2 at high temperature studied by thermogravimetric analysis and ion mass spectrometry. *Journal of Materials Chemistry* **22**: 6726–6732.

Coker, E. N., et al. (2011). Ferrite–YSZ composites for solar thermochemical production of synthetic fuels: in operando characterization of CO_2 reduction. *Journal of Materials Chemistry* **21:** 10767–10776.

Dahl, J. K., et al. (2004). Solar-thermal dissociation of methane in a fluid-wall aerosol flow reactor. *International Journal of Hydrogen Energy* **29**: 725–736.

Dahl, J. K., et al. (2004). Sensitivity analysis of the rapid decomposition of methane in an aerosol flow reactor. *International Journal of Hydrogen Energy* **29**: 57–65.

Diver, R., et al. (2008). Solar thermochemical water-splitting ferrite-cycle heat engines. *Journal of Solar Energy Engineering* **130**(4): 041001.

Ebbesen, S. D., et al. (2014). High temperature electrolysis in alkaline cells, solid proton conducting cells and solide oxide cells. *Chemical Reviews* **114**: 10697–10734.

Epstein, M., et al. (2008). Towards the industrial solar carbothermal production of zinc. *Journal of Solar Energy Engineering* **130**(1): 014505.

Ermanoski, I. (2015). Maximising the efficiency of a two-step solar thermochemical cycle. *Energy Procedia* **69**: 1731–1740.

Ermanoski, I., et al. (2013). A new reactor concept for efficient solar-thermochemical fuel production. *Journal of Solar Energy Engineering* **135**(3): 031002.

Evdou, A., et al. (2008). Lanthanum-strontium perovskites as redox materials for hydrogen production. *International Journal of Hydrogen Energy* **33**: 5554–5564.

Flamant, G. (2010). The SOLHYCARB Project Project No. 019770: Final Publishable Executive Summary.

Frenso, F., et al. (2009). Solar hydrogen production by two-step thermochemical cycles: Evaluation of commercial ferrites. *International Journal of Hydrogen Energy* **34**: 2918–2924.

Fresno, F., et al. (2010). Comparative study of the activity of nickel ferrites for solar hydrogen production by two-step thermochemical cycles *International Journal of Hydrogen Energy* **35**: 8503–8510.

Furler, P., et al. (2012). Solar thermochemical CO_2 splitting utilizing a reticulated porous ceria redox system. *Energy & Fuels* **26**(11): 7051–7059.

Furler, P., et al. (2014). Thermochemical carbon dioxide splitting via redox cycling of ceria reticulated foam structures with dual-scale porosities. *Physical Chemistry Chemical Physics* **16**: 10503–10511.

Furler, P., et al. (2012). Syngas production by simultaneous splitting of water and carbon dioxide via ceria redox reactions in a high temperature solar reactor. *Energy & Environmental Science* **5**: 6098–6103.

Go, K., et al. (2008). Reaction kinetics of reduction and oxidation of metal oxides for hydrogen production. *International Journal of Hydrogen Energy* **33**: 5986–5995.

Gokon, N., et al. (2012). Steam gasification of coal cokes using fluidized bed reactor for solar thermochemical conversion. *SolarPACES 2012*. Marrakech, Morocco, 11–14 September 2012.

Gokon, N., et al. (2011). Ferrite-zirconia-coated foam device prepared by spin coating for solar thermochemical hydrogen production. *International Journal of Hydrogen Energy* **36**: 2014–2028.

Gokon, N., et al. (2011). Thermochemical two–step water splitting by internally circulating fluidised bed of nickel–ferrite particles: Successive reactions of thermal reduction and water decomposition. *International Journal of Hydrogen Energy* **36**: 4757–4767.

Gokon, N., et al. (2009). New solar water–splitting reactor with ferrite particles in an internally circulating fluidized bed. *Journal of Solar Energy Engineering* **131**(1): 011007.

Guo, P., et al. (2015). Fischer–Tropsch liquid fuel production by co-gasification of coal and biomass in a solar hybrid dual fluidized bed gasifier. *Energy Procedia* **69**: 1770–1779.

Guo, P., et al. (2015). Performance assessment of Fischer–Tropsch liquid fuels production by solar hybridized dual fluidized-bed gasification of lignite. *Energy & Fuels* **29**: 2738–2751.

Haltiwanger, J., et al. (2010). Renewable hydrogen from the Zn/ZnO solar thermochemical cycle: A cost and policy analysis. *Journal of Solar Energy Engineering* **132**(4): 041011.

Hathaway, B. J., et al. (2011). Solar gasification of biomass: Kinetics of pyrolysis and steam gasification in molten salt. *Journal of Solar Energy Engineering* **133**(2): 021011.

Hathaway, B. J., et al. (2014). Development of a molten salt reactor for solar gasification of biomass. *Energy Procedia* **49**: 1950–1959.

Hathaway, B. J., et al. (2014). Integration of solar gasification with conventional fuel production: The roles of storage and hybridization. *Journal of Solar Energy Engineering* **136**(1): 010906.

Hertwich, E. G. and X. M. Zhang (2009). Concentrating-solar biomass gasification process for a 3rd-generation biofuel. *Environmental Science & Technology* **43**: 4207–4212.

Hirsch, D. and A. Steinfeld (2004). Solar hydrogen production by thermal decomposition of natural gas using a vortex-flow reactor. *International Journal of Hydrogen Energy* **29**: 47–55.

Houaijia, A., et al. (2013). Analysis and improvement of a high-efficiency solar cavity reactor design for the two-step thermochemical cycle for solar production of hydrogen from water. *Solar Energy* **97**: 26–38.

Ishihara, H., et al. (2008). Two-step water-splitting at 1273–1623 K using yttria-stabilized zircona –iron oxide solid solution via co-precipitation and solid-state reaction. *Energy* **33**: 1788–1793.

Jiang, Q., et al. (2014). Thermochemical carbon dioxide splitting reaction with Cex M1-x O2-d (M = Sn, Hf, Zr, La, y and Sm) solid solutions. *Solar Energy* **99**: 55–66.

Kaneko, H., et al. (2004). Decomposition of Zn-ferrite for O_2 generation by concentrated solar radiation. *Solar Energy* **76**: 317–322.

Kaniyal, A., et al. (2013). Polygeneration of liquid fuels and electricity by the atmospheric pressure hybrid solar gasification of coal. *Energy & Fuels* **27**: 3538–3555.

Kaniyal, A. A., et al. (2013). Dynamic modeling of the co-production of liquid fuels and electricity from a hybrid solar gasifier with various fuel blends. *Energy & Fuels* **27**: 3556–3569.

Kawakami, S., et al. (2014). Thermochemical two-step water-splitting cycle using Ni-ferrite and ceria-coated foam devices by concentrated Xe-light radiation. *Energy Procedia* **49**: 1980–1989.

Kenarsari, S. and Y. Zheng (2014). Fast pyrolysis of biomass pellets using concentrated solar radiation: A numerical study. *Journal of Solar Energy Engineering* **136**(4): 041004.

Kim, J., et al. (2012). Fuel production from CO_2 using solar-thermal energy: System level analysis. *Energy & Environmental Science* **5**(9): 8417–8429.

Kodama, T. and N. Gokon (2007). Thermochemical cycles for high-temperature solar hydrogen production. *Chemical Reviews* **107**(10): 4048–4077.

Kodama, T., et al. (2008). Thermochemical two-step water splitting by ZrO_2-supported $Ni_x Fe_{3-x}O_4$ for solar hydrogen production. *Solar Energy* **82**: 73–79.

Kodama, T., et al. (2010). Coal coke gasification in a windowed solar chemical reactor for beam-down optics. *Journal of Solar Energy Engineering* **132**(4): 041004.

Kodama, T., et al. (2005). Thermochemical hydrogen production by a redox system of ZrO_2-supported Co(III)–ferrite. *Solar Energy* **78**: 623–631.

Kodama, T., et al. (2004). A two-step thermochemical water splitting by iron-oxide on stabilized zirconia. *Journal of Solar Energy Engineering* **128**(1): 3–7.

Kodama T., et al. (2002). Fluidized bed coal gasification with CO_2 under direct irradiation with concentrated visible light. *Energy & Fuels* **16**: 1264–1270.

Kogan, A., et al. (2007). Production of hydrogen and carbon by solar thermal methane splitting. IV. Preliminary simulation of a confined tornado flow configuration by computational fluid dynamics. *International Journal of Hydrogen Energy* **32**: 4800–4810.

Kogan, A. and M. Kogan (2002). The Tornado flow configuration – an effective method for screening of a solar reactor window. *Journal of Solar Energy Engineering* **124**: 206–214.

Kogan, A., et al. (2004). Production of hydrogen and carbon by solar thermal methane splitting. II. Room temperature simulation tests of seeded solar reactor. *International Journal of Hydrogen Energy* **29**: 1227–1236.

Kogan, A., et al. (2005). Production of hydrogen and carbon by solar thermal methane splitting. III. Fluidization, entrainment and seeding powder particles into a volumetric solar receiver. *International Journal of Hydrogen Energy* **30**: 35–43.

Kogan, M. and A. Kogan (2003). Production of hydrogen and carbon by solar thermal methane splitting. I. The unseeded reactor. *International Journal of Hydrogen Energy* **28**: 1187–1198.

Kostoglou, M., et al. (2014). Improved kinetic model for water splitting thermochemical cycles using nickel ferrite. *International Journal of Hydrogen Energy* **39**: 6317–6327.

Kruesi, M., et al. (2013). Solar-driven steam-based gasification of sugarcane bagasse in a combined drop-tube and fixed-bed reactor – Thermodynamic, kinetic, and experimental analyses. *Biomass and Bioenergy* **52**: 173–183.

Kruesi, M., et al. (2014). A two-zone solar-driven gasifier concept: Reactor design and experimental evaluation with bagasse particles. *Fuel* **117**: 680–687.

Lapp, J., et al. (2012). Efficiency of two-step solar thermochemical non-stoichiometric redox cycles with heat recovery. *Energy* **37**: 591–600.

Lapp, J. and W. Lipinski (2014). Transient three-dimensional heat transfer model of a solar thermochemical reactor for water- and carbon dioxide-splitting via nonstoichiometric ceria redox cycling. *Journal of Solar Energy Engineering* **136**(3): 031006.

Le Gal, A. and S. Abanades (2011). Catalytic investigation of ceria–zirconia solid solutions for solar hydrogen production. *International Journal of Hydrogen Energy* **36**: 4739–4748.

Le Gal, A., et al. (2011). Carbon dioxide and water splitting for thermochemical production of solar fuels using non-stoichiometric ceria and ceria/zirconia solid solutions. *Energy & Fuels* **25**: 4836–4845.

Leveque, G., et al. (2014). Characterisation of two-step tin-based redox system for thermochemical fuel production from solar-driven CO_2 and H_2O splitting cycles. *Industrial & Engineering Chemistry Research* **53**: 5668–5677.

Lichty, P., et al. (2010). Rapid high temperature solar thermal biomass gasification in a prototype cavity reactor. *Journal of Solar Energy Engineering* **132**(1): 011012.

Loentzou, S., et al. (2008). Aerosol spray pyrolysis synthesis of water-splitting ferrites for solar hydrogen production. *Granular Materials* **10**: 113–122.

Lorentzou, S., et al. (2014). Thermochemical CO_2 and CO_2/H_2O splitting over $NiFe_2O_4$ for solar fuels synthesis. *Energy Procedia* **49**: 1999–2008.

Loutzenhiser, P., et al. (2010). CO_2 splitting in an aerosol flow reactor via the two-step Zn/ZnO solar thermochemical cycle. *Chemical Engineering Science* **65**: 1855–1864.

Loutzenhiser, P., et al. (2010). Review of the two-step H_2O/CO_2-splitting solar thermochemical cycle based on Zn/ZnO redox reactions. *Materials* **3**: 4922–4938.

Loutzenhiser, P., et al. (2011). Concentrated solar energy for thermochemically producing liquid fuels from CO_2 and H_2O. *Journal of Metals* **63**(1): 32–34.

Loutzenhiser, P. G. and A. Steinfeld (2011). Solar syngas production from CO_2 and H_2O in a two-step thermochemical cycle via Zn/ZnO redox reactions: thermodynamic cycle analysis. *International Journal of Hydrogen Energy* **36**(19): 12141–12147.

Maag, G., et al. (2010). Heat transfer model and scale-up of an entrained-flow solar reactor for the thermal decomposition of methane. *International Journal of Hydrogen Energy* **35**: 13232–13241.

Maag, G. and A. Steinfeld (2010). Design of a 10 MW particle-flow reactor for syngas production by steam-gasification of carbonaceaous feedstock using concentrated solar energy. *Energy & Fuels* **24**: 6540–6547.

McDaniel, A., et al. (2013). Sr- and Mn-doped $LaAlO_{3-\delta}$ for solar thermochemical H_2 and CO production. *Energy & Environmental Science* **6**(8): 2424–2428.

Meier, A., et al. (1999). Soral thermal decomposition of hydrocarbons and carbon monoxide for the production of catalytic filamentous carbon. *Chemical Engineering Science* **54**: 3341–3348.

Melchior, T., et al. (2009). Solar-driven biochar gasification in a particle-flow reactor. *Chemical Engineering and Processing* **48**: 1279–1287.

Muhich, C., et al. (2013). Efficient generation of hydrogen by splitting water with an isothermal redox cycle. *Science* **341**: 540–542.

Müller, R., et al. (2003). Kinetic investigation on steam gasification of charcoal under direct high-flux irradiation. *Chemical Engineering Science* **58**: 5111–5119.

Nakamura, T. (1977). Hydrogen production from water utilizing solar heat at high temperatures. *Solar Energy* **19**(5): 467–475.

Ng, Y. and W. Lipinski (2012). Thermodynamic analyses of solar thermal gasification of coal for hybrid solar - fossil power and fuel production. *Energy* **44**: 720–731.

Noglik A., et al. (2009). Solar thermochemical generation of hydrogen: Development of a receiver reactor for the decomposition of sulfuric acid. *Journal of Solar Energy Engineering* **131**(1): 011003.

Paxman, D., et al. (2014). Initial experimental and theoretical investigation of solar molten media methane cracking for hydrogen production. *Energy Procedia* **49**: 2027–2036.

Perret, R. (2011). Solar Thermochemical Hydrogen Production Research (STCH) Thermochemical cycle selection and investment priority. *SANDIA REPORT SAND 2011*, SANDIA National Lab. May 2011: 117 pp.

Piatkowski, N., et al. (2009). Experimental investigation of a packed-bed solar reactor for the steam-gasification of carbonaceous feedstocks. *Fuel Processing Technology* **90**: 360–366.

Piatkowski, N., et al. (2011). Solar-driven gasification of carbonaceous feedstock–a review. *Energy & Environmental Science* **4**: 73–82.

Rodat, S., et al. (2009). Kinetic modelling of methane decomposition in a tubular solar reactor. *Chemical Engineering Journal* **146**: 120–127.

Roeb, M., et al. (2012). Materials-related aspects of thermochemical water and carbon dioxide splitting: A review. *Materials* **5**: 2015–2054.

Roeb, M., et al. (2009). Operational strategy of a two-step thermochemical process for solar hydrogen production. *International Journal of Hydrogen Energy* **34**: 4537–4545.

Roeb, M., et al. (2005). HYTHEC: Development of a dedicated solar receiver-reactor for the decomposition of sulphuric acid. In: *Proceedings of European Hydrogen Energy Conference EHEC 2005*, Zaragoza, Spain, pp. 22–25.

Roeb, M., et al. (2009). Experimental study on sulfur trioxide decomposition in a volumetric solar receiver-reactor. *International Journal of Energy Research* **33**: 799–812.

Roeb, M., et al. (2011). Test operation of a 100 kW pilot plant for solar hydrogen production from water on a solar tower. *Solar Energy* **85**(4): 634–644.

Romero, M. and A. Steinfeld (2012). Concentrating solar thermal power and thermochemical fuels. *Energy & Environmental Science* **5**: 9137–9674.

Saw, W., et al. (2015). Solar hybridized coal-to-liquids via gasification in Australia: Techno-economic assessment. *Energy Procedia* **69**: 1819–1827.

Scheffe, J., et al. (2011). Hydrogen production via chemical looping redox cycles using atomic layer deposition-synthesized iron oxide and cobalt ferrities. *Chemistry of Materials* **23**: 2030–2038.

Scheffe, J., et al. (2010). A spinel/hercynite water–splitting cycle. *International Journal of Hydrogen Energy* **35**: 3333–3340.

Scheffe, J., et al. (2013). Kinetics and mechanism of solar thermochemical hydrogen production by oxidation of a cobalt ferrite-zirconia compositie. *Energy & Environmental Science* **6**: 963–973.

Scheffe, J. and A. Steinfeld (2012). Thermodynamic analysis of cerium-based oxides for solar thermochemical fuel production. *Energy & Fuels* **26**: 1928–1936.

Scheffe, J., et al. (2013). Lanthanum-strontium-manganese perovskites as redox materials for solar thermal splitting of water and carbon dioxide. *Chemistry & Fuels* **27**: 4250–4257.

Sheu, E., et al. (2015). A review of solar methane reforming systems. *International Journal of Hydrogen Energy* **40**: 12929–12955.

Simakov, D. S. A., et al. (2015). Solar thermal catalytic reforming of natural gas: a review on chemistry, catalysis and system design. *Catalysis Science & Technology* **5**(4): 1991–2016.

Smestad, G. P. and A. Steinfeld (2012). Review: Photochemical and thermochemical production of solar fuels from H_2O and CO_2 using metal oxide catalysts. *Industrial & Engineering Chemistry Research* **51**: 11828–11840.

Spath, P. and W. Amos (2003). Using a concentrating solar reactor to produce hydrogen and carbon black via thermal decomposition of natural gas: Feasibility and economics. *Journal of Solar Energy Engineering* **125**(2): 159–164.

Stamatiou, A., et al. (2010). Solar syngas production via H_2O/CO_2-splitting thermochemical cycles with Zn/ZnO and FeO/Fe_3O_4 redox reactions. *Chemistry of Materials* **22**: 851–859.

Steinfeld, A., et al. (1997). Production of filamentous carbon and hydrogen by solarthermal catalytic cracking of methane. *Chemical Engineering Science* **52**: 3599–3603.

Sun, Y., et al. (2013). Investigation into the mechanism of $NiMg(Ca)_bAl_cO_x$ catalytic activity for production of solarised syngas from carbon dioxide reforming of methane. *Fuel* **105**: 551–558.

Sun, Y. and J. Edwards (2015). Solar-to-fuel energy conversion analysis of solarised mixed reforming of methane. *Energy Procedia* **69**: 1828–1837.

Sun, Y., et al. (2011). Thermodynamic analysis of mixed and dry reforming of methane for solar thermal applications. *Journal of Natural Gas Chemistry* **20**: 568–576.

Tamaura, Y., et al. (1995). Production of solar hydrogen by a novel two-step water-splitting solar thermochemical cycle. *Energy* **20**: 325–330.

Trommer, D., et al. (2004). Kinetic investigation of the thermal decomposition of CH_4 by direct irradiation of a vortex–flow laden with carbon particles. *International Journal of Hydrogen Energy* **29**: 627–633.

Trommer, D., et al. (2005). Hydrogen production by steam-gasification of petroleum coke using concentrated solar power–I. Thermodynamic and kinetic analyses. *International Journal of Hydrogen Energy* **30**(6): 605–618.

Venstrom, L., et al. (2012). The effects of morphology on the oxidation of ceria by water and carbon dioxide. *Journal of Solar Energy Engineering* **134**(1): 011005.

Vidal, T., et al. (2010). Solar gasification of petroleum coke. *18th World Hydrogen Energy Conference,* Essen, 16–21 May 2010.

Villasmil, W., et al. (2014). Pilot-scale demonstration of a 100 kW_{th} solar thermochemical plant for the thermal dissociation of ZnO. *Journal of Solar Energy Engineering* **136**(1): 011016.

von Zedtwitz, P. and A. Steinfeld (2003). The solar thermal gasification of coal – energy conversion efficiency and CO_2 mitigation potential. *Energy* **28**: 441–456.

Watson, L., et al. (2012). Modelling of a solar-powered super-critical water gasifier. *Proceedings of the 18th SolarPACES Conference,* Marrakech, Morocco, 11 –14 September, 2012. Available online at: http//sfg.anu.edu.au/publications/assets/inproc/watson-solarpaces-2012.pdf.

Wieckert, C., et al. (2007). A 300kW solar chemical pilot plant for the carbothermic production of zinc. *Journal of Solar Energy Engineering* **129**(2): 190–196.

Wieckert, C., et al. (2013). Syngas production by thermochemical gasification of carbonaceous waste materials in a 150 kW_{th} packed-bed solar reactor. *Energy Fuels* **27**: 4770–4776.

Xiao, L., et al. (2012). Advances in solar hydrogen production via two-step water-splitting thermochemical cycles based on metal redox reactions. *Renewable Energy* **41**: 1–12.

Z'Graggen, A. and A. Steinfeld (2009). Hydrogen production by steam-gasification of carbonaceous materials using concentrated solar energy–V. Reactor modelling, optimization, and scale-up. *International Journal of Hydrogen Energy* **33**: 5484–5492.

Z'Graggen, A., et al. (2008). Hydrogen production by steam-gasification of carbonaceous materials using concentrated solar energy–IV. Reactor experimentation with vacuum residue. *International Journal of Hydrogen Energy* **33**: 679–684.

Z'Graggen, A., et al. (2007). Hydrogen production by steam-gasification of petroleum coke using concentrated solar power–III. Reactor experimentation with slurry feeding. *International Journal of Hydrogen Energy* **32**: 992–996.

Z'Graggen, A. and A. steinfeld (2008). Hydrogen production by steam-gasification of carbonaceous materials using concentrated solar energy–V. Reactor modeling, optimization, and scale up. *International Journal of Hydrogen Energy* **33**: 5484–5492.

Zeng, K., et al. (2015). Solar pyrolysis of wood in a lab-scale reactor: Influence of temperature and sweep gas flow rate on products distribution. *Energy Procedia* **69**: 1849–1858.

Zeng, K., et al. (2014). High temperature flash pyrolysis of wood in a lab-scale solar reactor. *ASME 8th International Conference on Energy Sustainability*. Boston, Massachusetts, United States, 30 June – 2 July 2014.

Zvegilsky, D., et al. (2012). Pyrolysis and gasification of rice husks and the solar option. SolarPACES 2012, Conference of IEA SolarPACES program www.solarpaces.org, Marrakech, Morrocco, 11 –14 September 2012.

CONTACT US

t 1300 363 400
+61 3 9545 2176
e enquiries@csiro.au
w www.csiro.au

AT CSIRO WE SHAPE THE FUTURE

We do this by using science to solve real issues. Our research makes a difference to industry, people and the planet.

As Australia's national science agency we've been pushing the edge of what's possible for over 85 years. Today we have more than 5,000 talented people working out of 50-plus centres in Australia and internationally. Our people work closely with industry and communities to leave a lasting legacy. Collectively, our innovation and excellence places us in the top ten applied research agencies in the world.

WE ASK, WE SEEK AND WE SOLVE

FOR FURTHER INFORMATION

CSIRO Energy
Dr Jim Hinkley
t +61 2 4960 6128
e **jim.hinkley**@csiro.au
w www.csiro.au/energy

CSIRO Energy
Robbie McNaughton
t +61 2 4960 6048
e **Robbie.mcnaughton** @csiro.au
w www.csiro.au/energy